UNIVERSITY OF QUEBEC IN MONTREAL

CRUSTAL HEAT PRODUCTION :
IMPLICATIONS FOR GEONEUTRINO FLUX
AND HEATING OF THE CONTINENTAL LITHOSPHERE

THESIS PRESENTED

AS A PARTIAL REQUIREMENT

OF THE MASTERS OF EARTH SCIENCES

BY

LIDIA IAROTSKY

JUNE 2016

UNIVERSITÉ DU QUÉBEC À MONTRÉAL

PRODUCTION DE CHALEUR DE LA CROUTE : IMPLICATIONS POUR LE FLUX DE GÉONEUTRINOS ET LE CHAUFFAGE DE LA LITHOSPHÈRE CONTINENTALE

MÉMOIRE PRÉSENTÉ

COMME EXIGENCE PARTIELLE

DE LA MAÎTRISE EN SCIENCE DE LA TERRE

PAR

LIDIA IAROTSKY

JUIN 2016

ACKNOWLEDGMENTS

For your unlimited patience and wisdom, your priceless sense of humor and incredibly honest support I would like to thank you first and most Jean-Claude. You made everything about this possible and have shown more kindness over the past two years then I have see in my lifetime. I thank you for the opportunity to work with you, for your generosity and the happy memories I will keep. A especially want to thank you for making such a good humored place out of our working lab, where I could feel like I belong more then anywhere else. Thank you ! Tea time at 4 ?

Thanks to the bonkers office ! I will never forget the mad moments spent together. You are forever irreplaceable. Carolyne, you've been there for me all the way, you've helped me when i needed it, you consoled me, you made me laugh like few ever have, and for all that I am profoundly grateful. Fernando, you've been there for me more then you realize. Your unexpected and thought provoking ways gave me a new perspective on fundamental social concepts. Thank you for having enriched my grad life and life in general. Ignacio, I especially thank you for having been my parter in crime on so many occasions. You made me feel normal by been at my level of crazy. Thanks.

Thank you Fiona for you unique remarks and precious contribution to the lab spirit. Marie, thanks for the greatest moral support ever and for the out of the ordinary conversations. Petar, you make me smile all the time. Alessandro thanks for being there. Thank you Conny for moral support and Muay Thaï initiation and Arlette for great times.

A special thanks to chocolate, I wouldn't be here without you. Kim John Fridge and Doctor Francesco Fish, the geophysical experiment you brought even more "special" to an already extraordinary group.

Thank you, Claude Jaupart, for your time, contribution and generosity and for your special talent of turning any crazy situation into a serious conversation.

I would also like to thank Hanika Rizo, John Armitage, Pascal Audet, Andrew Schaef-

fer, Jonathan O'Neil, and Louise Hénault-Ethier for interesting conversations. Helene Bouquerel and Catherine Phaneuf thank you for our collaborations.

A special thanks to the GEOTOP crew. The congresses and conferences have given me additional insight on the diversity of Earth sciences. Thank you Nicole. I am grateful to NSERC that founded my research through a discovery grant to Jean-Claude Mareschal. I would also like to thank the faculty of science for additional support through "bourse d'excellence"

Thanks Lucille for our secret lunchs. Allison, Louis, Cesar, Matilde and François you made class time more fun. Thank you Elyse, Sophie and Marcello for an unforgettable GEOTOP congress. The British crew, Ian, Amy, Alister, Mitch and especially Laura Petrescu :).

Thank you Genevieve for telling me about Jean-Claude and for cheering me along the way. This all started thanks to you.

TABLE OF CONTENTS

LIST OF TABLES

LIST OF FIGURES

RÉSUMÉ

Le budget d'énergie de la Terre dépend de la production de chaleur et de son refroidissement séculaire. Le flux de chaleur est généralement mesuré dans les trous de forage dans le cadre de prospections minières et pétrolières limitant la couverture de données aux régions économiquement intéressantes. Pour toute autre région, des méthodes alternatives doivent être employées. CRUST1.0 est un modèle de la croûte terrestre qui a été utilisé pour estimer la production de chaleur de la croûte dans les continents. Nous avons cherché à améliorer les prédictions du modèle en ajustant les productions de chaleur des différentes couches constituants la croûte terrestre. Nos résultats montrent que l'hypothèse d'une production de chaleur uniforme pour chaque couche crustale n'est pas valide.

Le flux de géoneutrinos peut être directement déduit à partir de la production de chaleur par les éléments radioactifs. Nous avons testé la validité des prédictions faites grâce au modèle CRUST1.0 en le comparant au calcul basé sur les données de flux de chaleur. Le traitement différentié des couches crustales n'a pas amélioré le flux prédit. Nous avons également tenté une approche de calcul différente ainsi qu'un rééchantillonage dans le but d'augmenter la précision. Pour toutes ces tentatives, l'erreur peut atteindre 81 % par rapport aux valeurs calculées à partir des données de flux de chaleur dans l'Est canadien. Ceci montre que le modèle CRUST1.0 ne peut pas être utilisé pour prédire le flux de géoneutrinos provenant de la croûte.

La production de chaleur dans la croûte continentale détermine le régime et l'évolution thermique de la lithosphère. Une augmentation de la production de chaleur fait monter les températures lithosphériques alors que la différentiation des éléments radioactifs abaisse les profils de température. Nous avons étudié l'évolution thermique d'une croûte continentale archéenne lors de sa formation. La croissance continentale chauffe la lithosphère et fond la croûte terrestre. Lorsque la largeur de ceintures accrétées dépasse les 300 km et que l'épaisseur de la croûte est de 40 km ou plus, la température à la base de la croûte dépasse les 800°C pour une production de chaleur uniforme. Le métamorphisme et la fusion partielle produisent une croûte différentiée verticalement ce qui diminue l'effet du chauffage radioactif. Le chauffage de la lithosphère par les éléments radioactifs augmente avec leur profondeur.

Mots clés

Flux de Chaleur || Elements produisant de la chaleur || Budget énergétique || Terre silicatée || Nombre d'Urey || Refroidissement du noyau || Refroidissement du manteau || Cratons || Lithosphère || Production de chaleur de la croûte || Évolution de la croûte || Métamorphisme à haute température || Métamorphisme post-orogenique

ABSTRACT

Earth's energy budget includes secular cooling and heat production. Surface energy loss is measured by heat flow which can be determined in available boreholes usually drilled for economic purposes. This limits the data coverage to areas of interest for oil and mineral exploration. For regions of insufficient data coverage, heat flow must be estimated by alternative methods. CRUST1.0 is a global crustal model that has been used to estimate radiogenic heat production in stable continental regions. We have looked at various ways to improve the models by adjusting the heat production of the different crustal layers. Our analysis of this model shows that the assumption of laterally uniform heat production throughout the continental crust is not valid.

Crustal geoneutrino flux can be directly calculated from radiogenic heat production. We tested the CRUST1.0 models efficacy at predicting the geoneutrino flow by comparing them to predictions made with heat flow data. A layered crust does not improve the model predictions. We have also tried alternate calculation methods and rescaling. All failed at improving the model's predictions that are off by as much as 81% in Eastern Canada showing that using CRUST1.0 fails to predict the geoneutrino flux.

Heat production in the continental crust affects the lithosphere's thermal regime and evolution. Higher heat production increases temperatures, while differentiating the radioactive elements in the upper crust lowers the temperature. We investigated how the width and thickness of the continental crust affected its thermal structure in the Archean. We found that continental growth heats the lithosphere and can melt the crust. For accretionary belts, with a total width of over 300 km and a thickness of 40 km, the temperature at the base of a non differentiated crust exceeds 800 °C. The depth of a high heat producing layer augments the temperature increase this layer will generate. As a result the lower crust undergoes metamorphism and partial melts and the radioactive elements are redistributed into the upper crust thus cooling the lithosphere.

Keyword

Heat flow || Heat producing elements || Energy budget || Bulk silicate Earth || Urey number || Core cooling || Mantle cooling || Cratons || Lithosphere || Crustal heat production || Crustal evolution || High temperature metamorphism || Post orogenic metamorphism

GENERAL INTRODUCTION

The long term thermal evolution of the Earth is constrained by the present energy budget. Earth's total heat comes from two main sources. The first is the secular heat that was stored in the planet during its formation and early evolution. The second source is the heat generated by radioactive decay in the bulk silicate Earth (BSE) comprising both the crust and mantle. The continental crust is enriched in heat producing elements relative to the mantle. The main focus of this study is the distribution of heat producing elements in BSE and the thermal regime of the continental crust.

The amount of radiogenic heat produced in the Earth decreases exponentially with time following the radioactive decay law. Today's total heat loss is about 46 ± 3 TW out of which 19 ± 5 TW is accounted for by heat production and the remainder by secular cooling (Jaupart et al., 2014).

Convection is the most efficient cooling mechanism for an Earth-sized body. Hot and buoyant materials at the bottom of the mantle rise while cold dense materials at the surface sink. This generates large scale displacements in the silicate rocks of the mantle. This allows for a mixing of the materials throughout the mantle. The lithosphere can be defined as the upper boundary layer through which the heat transfer mechanism is conduction. The continental lithosphere does not take part in convection while the oceanic lithosphere forms at oceanic ridges and returns to the mantle at subduction zones. Today, continental crust is formed by accumulation of melts from the subducting oceanic lithosphere in back-arc environments. Radioactive elements such as Uranium, Thorium and Potassium are incompatible with mantle crystalline structures thus accumulating in the continental crust. This concentration of heat producing elements near the surface makes more efficient the evacuation of the heat produced. Although the mantle has a much larger mass ($\approx 67\%$ of Earth's mass for the mantle against $\approx 0.4\%$ for the crust) its total heat production is only slightly more than that of the crust.

The heat flow coming from the sea floor is accounted for by the cooling of the oceanic

lithosphere between the spreading centers and the subduction zones. The present rate of heat loss through the sea floor is 32±2 TW as estimated by Jaupart et al. (2015). For the continental crust, only half of the 14 TW heat loss comes from the mantle. The other half is from heat produced by radioactive decay. Globally, crustal heat production generates from 5.8 to 7.2 TW (Jaupart and Mareschal, 2015). Mantle heat flow is nearly constant under stable continental crust at $\approx$ 15 mW m^{-2} . The surface heat flow ranges from 15 to 75 mW m^{-2} in stable continental crust. In tectonically active regions such as rifts (like the East African rift) or continental collision (like the Himalayas) heat flow is much higher due to magma intrusions or thicker crust.

Heat is propagated from the upper mantle to the surface by conduction. According to Fourier's law, the heat flux Q is defined as follows :

$$Q = -\lambda \frac{\partial T}{\partial z} \tag{1}$$

where λ is the thermal conductivity, T is temperature and z is depth. Thermal conductivity is an intrinsic property of the rocks. In stable continental crust, thermal steady state can be assumed. In steady state and without heat production heat flux would be constant through the lithosphere.

The radioactive elements concentrated in the crust produce heat which is then evacuated by conduction near the Earth's surface. The heat flux measured at the surface is the sum of the mantle heat flow and the total crustal heat production which can be expressed as follows :

$$Q_0 = Q_m + \int_0^{z_m} H(z)dz \tag{2}$$

where Q_0 and Q_m are the heat flux at the surface and at the Moho respectively. $H(z)$ is the heat production rate as a function of depth, and z_m is Moho depth.

There are many reasons to study heat production in the continental crust. First and foremost, heat production is one of the components that determines how temperature varies

with depth in the continental crust. Integrating Fourier's law to obtain the temperature we find :

$$T(z) = T_0 + \int_0^z \frac{1}{\lambda} Q(z')dz' \tag{3}$$

where the heat flow with depth $Q(z)$ is determined by equation 2 where we integrate over z'' up to a given depth z'.

$$T(z) = T_0 + \int_0^z \frac{1}{\lambda} \left[Q_0 - \int_0^{z'} H(z'')dz'' \right] dz' \tag{4}$$

Temperature depends on the vertical distribution of the radioactive elements in the enriched crust. It controls melting, metamorphic processes and mechanical properties.

The study of continental heat flow can also improve our understanding of the global energy budget and gives us some constraints on Earth's thermal reconstruction. During the course of my Masters, we were interested in two problems : How to best estimate crustal heat production in steady state continental crust ? What are the implications of crustal heat production for the thermal regime during continental accretion ?

First, heat flow can be determined from measurements of temperature profiles in bore-holes or it can be estimated by using a global model derived from seismic data. From the bore hole data, one can get precise estimate of the local surface heat flux. The first method is always preferred but unfortunately it has not been possible to make heat flow measurements all over the Earth's surface, thus the interest of complementing the data by using the second method. We have compared the estimates from seismic models to the heat flow data and tried to adjust the parameters (heat production for the different layers of the seismic model) to reduce the differences with the data where available.

In the second chapter, the outcome from our models are compared with results from different other studies in a more general context including the present day comprehension of mechanisms of heat loss and partition of heat sources between the continental crust and mantle. Earths secular and radiogenic heat production are discussed as a part of Earth's heat

budget. The CRUST models serve to estimate the continental crustal heat and neutrino production. The mantle heat and neutrino contributions to the surface flux are discussed afterwards.

Then, we looked at the thermal regimes of the crust during craton formation. Long belts of crustal material accrete together to form continents. We calculate the temperature profile for accretion belts of various widths and thicknesses. These profiles inform us about partial melts and other temperature controlled phenomena.

In the last chapter, the calculations made above are compared with large data sets on heat flow and heat production. Herein, we discus crustal stratification estimates and heat production in a number of geological provinces.

1

Calculating crustal heat production and geo-neutrino flux in stable continents.

1.1 Global Crustal Model

In this section, we illustrate the tests that we made with the CRUST1.0 model to estimate surface heat flow and geoneutrino flux. CRUST1.0 is a global crustal model based on seismic data and crustal type and age. Excluding ice and water, the crust is divided in six layers, three for the sediments and three for crystalline crust. The Earth is divided in cells of 1° latitude per 1° longitude and the model gives a thickness and physical properties for each crustal layer in every cell.

We shall calculate for each cell the crustal heat production and surface heat flux and compare the result with heat flux measurements. The motivation for this approach is that if the model matches well with the available data, it can be used with a certain confidence to estimate heat flow in thermally equilibrated areas where data are unavailable. The objective is to find the heat production rates that will provide a good fit.

1.2 Comparing Heat Flow

In steady state the surface heat flux is the sum of the mantle heat flux and the total crustal heat production. We attribute a heat production rate to each crustal layer and integrate over crustal thickness to obtain the component of the surface heat flow contributed by crustal heat production. We attributed heat production rate to all sedimentary layers adding an average mantle heat flow Q_m gives us the surface heat flux that can be compared with measured heat flux as shown in equation 2 (page 2).

$$Q_0 = Q_m + \sum_{1}^{6} A_i \Delta z_i \tag{1.1}$$

Where A_i and Δz_i are the heat production rate and thickness of the crustal layer i.

The heat flow data are unevenly distributed. To compare with the model, we averaged the data points over 1°x1° cells thus also reducing the weight of anomalous individual measurements. We can then compare all cells with data to cells from the model in stable continental areas where transient thermal perturbations are negligible.

We tried different heat production rates for the different crustal layers. As a first approximation, we tried a global crustal average for the heat production of 0.89 μW m^{-3} , as calculated by Rudnick and Gao (2014). We then made different attempts with a differentiated crust. In the first attempt, we used the heat production rates for crustal layers from Rudnick and Gao (2014) and 0.9 μW m^{-3} for sediments. The results follow more closely the crustal thickness maps than the heat production maps.

We also varied the heat production rates to find the set of A_i that minimizes the root mean square (RMS) difference with the dat1. This gave the optimized model. We calculated the optimal set of parameters separately for each region of analysis. This yielded the maps 1.3c for the global optimization and 1.5c for Eastern Canada's optimization. The optimal values obtained for both global and regional scales are listed in table 1.1 where we assumed

a constant heat production in all sedimentary layers.

Finally, we tried to use the average concentrations of heat producing element in the different layers of the crust using concentrations from Huang et al. (2013). The heat production is calculated by adding the individual contributions of thorium, uranium and potassium using the following formula :

$$H = 10^{11}(9.52[U] + 2.56[Th] + 3.48[K]) \tag{1.2}$$

where [U] and [Th] are the uranium and thorium concentration in ppm and [K] is the potassium concentration in %. This gives heat production per unit mass, that is expressed in W kg^{-1}. Using an average crustal density of 2700 kg m^{-3} , we obtain the heat production rate per unit volume A in μW m^{-3} .

$$A = 0.257[U] + 0.069[Th] + 0.094[K] \tag{1.3}$$

To obtain the heat production per unit volume for each crustal layer we multiply by layer density divided by 2700 kg m^{-3} .

1.2.1 Global Analysis

Figure 1.3 illustrates the results from different sets of heat production per unit volume. We are comparing it with the continental heat flux interpolated data map from the figure 4.5. It is easy to see that even if the error is minimal (c), the lateral variations in the data are still significantly larger than what the model can account for.

There are many notable differences, the most obvious one is that the heat flux data are on average much higher that heat flux from the models. As discussed in section 1.3.1 one might think that this is due to biased sampling : for example, boreholes have often been drilled for geothermal exploration.

But averaging the points over cells of the same dimensions as the model reduces significantly the weight of those data points as can be observed in figure 1.2. Then there are the contrasts that are much greater in the data than in any of the model. The high heat flow regions that have a higher surface flux than the models are not in equilibrium and will not be discussed further. The low heat flux areas, specifically the shields have a lower flow than any of the models because their heat production is very low even though the crust is thick. In other words, continental shields and low heat flow regions are not visible because the model assumes incorrectly a constant heat production in each layer. On a large scale, all the models exhibit the same patterns as the crustal thickness map shown in Figure 4.4 rather than those of heat flow data.

1.2.2 Regional Analysis

We then tested the model on a regional scale over Eastern Canada where there are many heat flow data.the region has two distinct crust types : the Shield and the Appalachians. Looking at the interpolated data map of figure 2.4 one can see that the northern older regions are characterized by very low heat production. The highest heat production is in the southeasternmost corner of Canada : the Appalachians. Several small scale areas of high heat production can also be observed. As in the global analysis, for the purpose of comparison, all data points have been averaged on cells identical to those of the model and shown in figure 1.4.

The difference between the Shield and the Appalachians is not seen in any of the tests and the calculated heat flux is directly proportional to crustal thickness. Because the crustal thickness of the Appalachians is close to that of the shield, see figure 1.6 one can not distinguish one from the other if the heat production is uniform throughout the entire crust. The Rudnick and Gao (2014) heat production rates generates a model that suggests a higher heat production on average in the Appalachians than in the Shield, but the contrasts in heat production are much larger for the data maps especially in central Quebec. We have minimized the root mean square difference to obtain the optimal model. Some of the low

heat production zones are better represented but the high heat production remains significantly higher in the data. On the other hand, the model resulting from concentration of heat producing element of Huang et al. (2013) attributes well for the high heat producing areas notably the Appalachian orogen but fails in the older Shield areas with very low heat production.

In the data, variations of over 35mW m^{-2} in the surface heat flux can occur over less than 100 km ($\approx$ 1 cell) which is never seen in the models that are very smooth in comparison. The variations in all models are spread out over large distances and show no abrupt changes comparable to those in the data.

We have also compared the model crustal thickness to that from seismic data. Looking at the two maps of crustal thickness in Eastern Canada one can see that the crustal thickness is accurate in that region. Therefore the discrepancy in heat productions is not due to an error in predicted crustal thickness but only due to the calculation method. We have concluded that assuming a constant heat production within each layer of the crust is not valid. Thus the heat production is higher in the Appalachian not because the highest heat producing layer is thicker than in the Shield but because the concentration of heat producing elements is higher within the same layers. A similar conclusion applies to the Shield for low heat production. It is also more natural for small scale high heat flow anomalies to coincide with a large increase in concentrations rather than abrupt thickening of a layer.

If crustal thickness is not the issue when modeling heat production, then the only remaining parameter is the heat production rate. Each value used represents an average for a given crustal layer. Even if the average is accurate, the heat production rates will still vary laterally within the layer over large and small scales. The only way to get additional information on these variations is by heat flow measurements. This is not due to a shortcoming of CRUST1.0 which contains no information on heat production, but to the wrong assumption made by users of the model that crustal composition is uniform laterally.

1.2.3 Conclusion

Both the global and regional analysis show large discrepancies emerging in areas of low heat production characteristic of continental shields. In the multilayered models, the Appalachians can barely be distinguished from the shield and the amplitude of the difference in heat productions is significantly less in the model than in the heat production determined from the heat flow measurements. This shows the obvious lack of lateral variability of scale and amplitude in the CRUST1.0 models that can not account for lateral changes in concentrations of heat producing elements. The model assumes that the heat production rate remains constant within each crustal layer which cannot show the lateral variations in heat flow that have been observed.

1.3 Estimating Crustal Geoneutrino Flux

As described in Fiorentini et al. (2005) disintegration of each radiogenic element produces heat and neutrinos in known amounts. We can thus deduce geoneutrino flux from heat flow provided that we know the ratios of the concentrations in Heat producing elements. Assuming a perfectly spherical geometry of Earth and integrating over it's volume, the total geoneutrino flux at any point is obtained by :

$$\Phi_i(\vec{r}) = \frac{1}{4\pi} \int_V \frac{A_i(\vec{r'})\rho(\vec{r'})}{|\vec{r'} - \vec{r}|^2} dV', \tag{1.4}$$

where A_i is the luminosity (number of anti-neutrinos per unit time produced inside Earth) per unit mass for isotopes ^{238}U and ^{232}Th, ρ is the local density. $\vec{r'}$ and $\vec{r}$ are the location of the source and the observation point, respectively. Here we only consider isotopes ^{238}U and ^{232}Th because both ^{40}K and ^{235}U produce neutrinos below the 1.8 MeV threshold of detection in liquid scintillatior (Fiorentini et al., 2005). But, given the elemental abundances ratios that are better known, one can deduce the amount of ^{40}K and ^{235}U once the absolute abundance of ^{238}U and ^{232}Th are measured.

Because we are only interested in calculating the crustal component of the neutrino flux Φ in terms of heat production H from the crust, we integrate only over the volume of Earth's crust.

$$\Phi(\theta,\phi) = \frac{\gamma a^2}{4\pi} \int_0^{z_m} dz' \int_0^{2\pi} d\phi' \int_0^{\pi} d\cos\theta' \, \frac{H(z',\theta',\phi')}{R_{pp'}^2}, \tag{1.5}$$

where the factor γ is the conversion factor of crustal radioactivity to neutrino production rate, a is the radius of the Earth, θ and ϕ are, respectively, the colatitude and longitude at the observation point, z the depth, z_m the Moho depth, $R_{pp'}$ is the distance between the source (p') and the observation point (p) and H is the crustal heat production. Here the unchanging factor γ assumes a constant mass ratio of the heat producing elements. For Th/U = 4 and K/U =12,000, we obtain $\gamma = 0.65 \times 10^{12}$ J^{-1}. Neutrino Flux is expressed in terrestrial neutrino units (TNU). Where one TNU corresponds to one event recorded per year of exposure in a detector of 10^{32} protons.

To calculate the global neutrino flux, we calculated the flux from equation 1.5 for each of CRUST1.0 model cells. We separated the near and the far field regions. For two cells that are far apart, we make a point source approximation. $R_{pp'}$ is the distance between the centers of both cells. For neighboring cells, the point approximation is not valid, but we can neglect Earths curvature when we integrate over all $R_{pp'}$. We compared two different calculation methods for this in subsection 1.3.2.

Because of the geoneutrino radial flux and Earth's geometry one needs to have a heat flow value for each cell off the model to get an accurate estimate of the crustal geoneutrino flux. Because many cells do not contain heat flow data, we extrapolated the data where possible. In areas where the crust is not in thermal equilibrium and heat production cannot be estimated from heat flow, we used heat flow estimates from the CRUST1.0 model. For cells in continental stable crust where heat production is calculated with confidence we can approximate the difference in geoneutrino flux from heat production estimated with the

CRUST1.0 model and from the calculated heat flux.

We subdivided the world map in three crustal categories, oceanic, active and stable continental crusts. We consider as oceanic, all the cells that have an oceanic crustal age. The distinction between stable and active crustal areas are based on heat flow and crustal thickness. We consider as active the continental crust thinner than 25 km or thicker than 60 km and/or regions with heat flux higher than 65 mW m^{-2} . This classification is illustrated in figure 1.7 where the areas in green are the only ones where heat flow data can be used for estimating neutrino flux.

From this comparison, we get an estimate of the magnitude of the error made by the model using CRUST1.0 alone to predict neutrino flux.

1.3.1 Varying Heat Production

The neutrino flux maps are much smoother than the heat production ones. The intensity of the neutrino flux is inversely proportional to the square of the distance as shown in equation 1.5, while the heat flux is proportional to z/R^3.

For the far field, we are using a point source approximation so we can only use one heat production per cell of the model. We have looked at the effect of changing the average crustal heat production on the scale of the difference it will produce with the model using heat flow data where available. We subtracted the neutrino flux calculated using only CRUST1.0 estimated heat flux from the one using data where available in stable crust for each of the difference maps in figure 1.8. The differences are in TNU units. We use TNUs in this section to compare with the neutrino detection resolution in TNUs.

In the previous section we have seen that the model does not account well for the regions with low concentrations of heat producing elements in the crust that often are found in Shields. Therefore we expect to overestimate the neutrino production in those areas. In figure 1.8a the global average heat production is estimated at 0.67 μW m^{-3} the

CRUST1.0 deduced model seems to underestimate the data deduced one unlike what we would expect. The following figure 1.8b assumes a 0.75 μW m^{-3} of global heat production average and what shows well here is that all the areas where the neutrino difference is very positive, are near the stable to active crust boundary. In other words the areas where the crust is stable but the neutrino flux modeled with data are higher that the ones coming from CRUST1.0. This shows that the heat production rate of those areas is underestimated. The only areas where the heat flow is higher than in the model are in active crustal zones. This is coherent with the continental heat production estimates of 0.79 to 0.95μW m^{-3} by Jaupart and Mareschal (2014). Both figure 1.8c with an average heat production of 0.83 μW m^{-3} and figure 1.8d with 0.90 μW m^{-3} are within that range and show significantly smaller areas with positive error and a more of the expected negative error.

In the last figure 1.8e, we have calculated the crustal average heat production for each cell assuming concentrations for each layer from Huang et al. (2013). The resulting difference map is very similar to the results from figure 1.8d with 0.90 μW m^{-3} , showing small differences in the Canadian and Baltic Shields but larger ones in Asia.

1.3.2 Varying Calculation Method Used for the Model

We have calculated the neutrino flux using two different methods. The first one that we call global, uses a cylindrical approximation to integrate over the volume of a crustal column in the near field. The second method that we call local, performs a two dimensional integration over the surface of the cell and multiplies by crustal thickness in the near field.

The results based on data (figures 1.9a and 1.9b) display greater variation than the ones based on crustal thickness (figures 1.9c and 1.9d). The differences between the data and crustal thickness based models (figures 1.9e and 1.9f) are as high as 25 TNUs for both calculation methods. This is an error larger than the absolute value of the flux in the northern Quebec region. In the surroundings of the Sudbury Neutrino Observatory (SNO) the error is low. The very old northern Quebec craton core is where the error is largest.

Figure 1.10 shows the north to south gradient to be due to the cylindrical approximation and the size variation of cells with latitude. Comparing the two calculation methods in figure 1.10, we note that the difference is less than 1 TNU over most of the region. This implies that the error of the cylindrical approximation is small. The calculation method does not affect the results of the model when predicting the neutrino flux.

1.3.3 Varying the Sampling Square Size

We also looked at the effect of rescaling the size over which we integrate to have a better accuracy in the neutrino flux. Instead of using the 1° latitude per 1° longitude division we tried dividing the Earth in 0.5° per 0.5° and 0.25° per 0.25° sized cells.

The increased "accuracy" has no effect on the model. Increase in precision of calculation does not show on the smoothed (figures 1.11) highlighting once again the systematic error in the models use.

1.3.4 Power Spectra

We have compared the power spectra of the heat flow and crustal thickness for the North American continent. Both data sets were placed on a $1^o \times 1\ ^o$to calculate the power spectra over the same range of wavenumbers. Unfortunately both data sets do not have sufficient spatial resolution to make a comparison over a large range of wavenumbers. The comparison shows that crustal thickness is smoother than the heat flow field. The spectral slope $(dlog(P)/dlog(k))$ of the crustal thickness power spectrum (2.3) is larger than that of the heat flow (1.5) resulting in a smoother field. Partly, this is because small scale features on the Moho cannot be resolved by seismic data. But, this is also an artifact due to the elimination in the crustal model of differences in thickness between cells that have the same geological type. The heat flow integrates heat production vertically and horizontally over a cone whose radius increases with depth, also resulting in smoothing of the field but not in annihilation of the shorter wavelength. Over North America, heat flow and crustal

thickness are not correlated (r=0.15). Worldwide, the correlation between heat flow and crustal thickness is even slightly negative (r=-0.1) (Mareschal and Jaupart, 2013).

1.3.5 Conclusion

Regardless of heat production values used, the models using CRUST1.0 predictions are off by more than 25 TNUs in continental Shields. The error remains as great with improved calculation methods and accuracy. CRUST1.0 can not be used to accuratly predict neutrino flux. This is developed in the following chapter as a part of larger discussion on heat flow.

Table 1.1 Heat production per unit volume assigned to each crustal layer for the different attempts.

	Model	Average Heat Productions per Unit Volume (μW m^{-3}) sedimentary	upper crust	middle crust	lower crust
(a)	Single-layered	0.89 †			
(b)	1st Multilayered	0.9	1.6†	0.96†	0.18†
(c)	Optimized				
	Global	1.5	1.4	0.8	0.6
	Estern Canada	1.5	1.4	0.2	0.1
(d)	Concentrations‡	0.98	1.67	0.78	0.19

† Rudnick and Gao (2014)

‡ Huang et al. (2013)

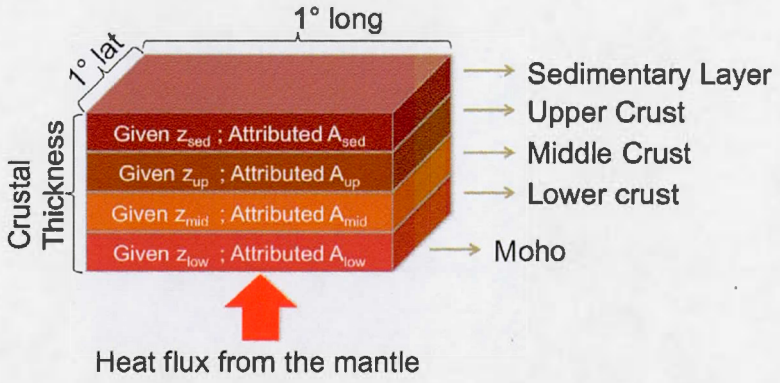

Figure 1.1 An illustration of the structure of the CRUST1.0 model. For each cell a thickness is given for every layer. To deduce heat flux, we attribute heat production rates to all crustal layers.

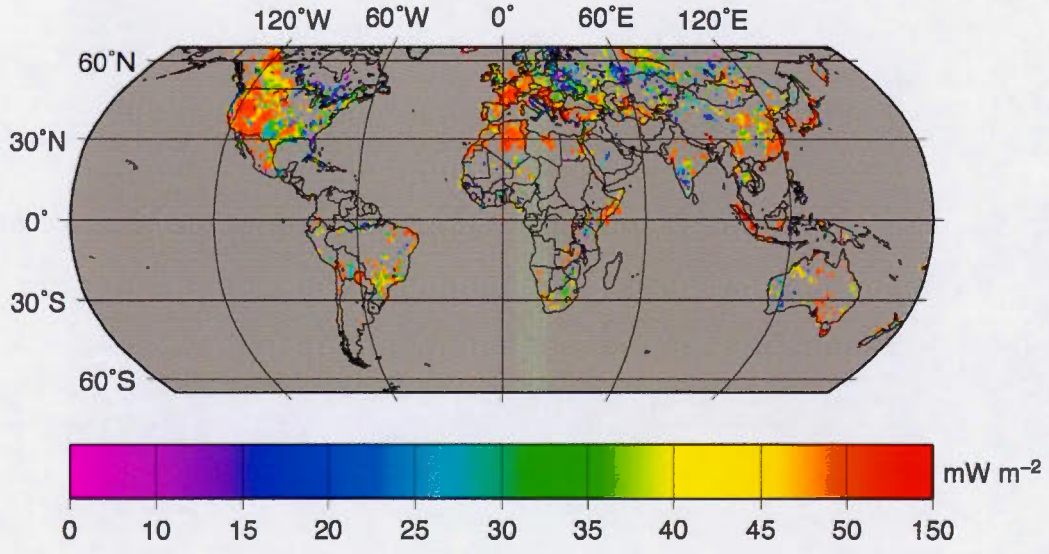

Figure 1.2 Globally calculated heat production from borehole data of heat flux averaged over 1° x 1° cells supposing a constant mantle flow of 15mW m^{-2}

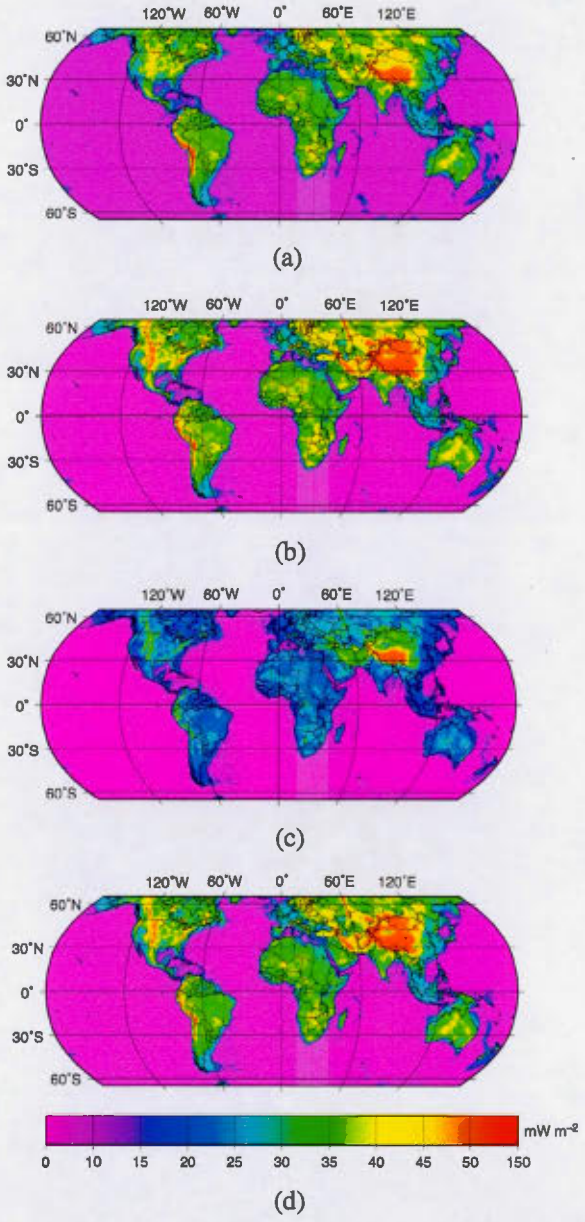

Figure 1.3 Four attempts to estimate heat flux on a global scale where (a) is obtained using a crustal average heat production of 0.89 estimated by Rudnick and Gao (2014) (b), (c) and (d) are using a differentiated crustal heat production with the heat production rate of each crustal layer is that estimated by Rudnick and Gao (2014) in (b) optimized to reduce the average difference with the data in (c) and is deduced from estimated concentrations of heat producing elements by Huang et al. (2013) in (d) the heat production rate values for each model are shown in table 1.1

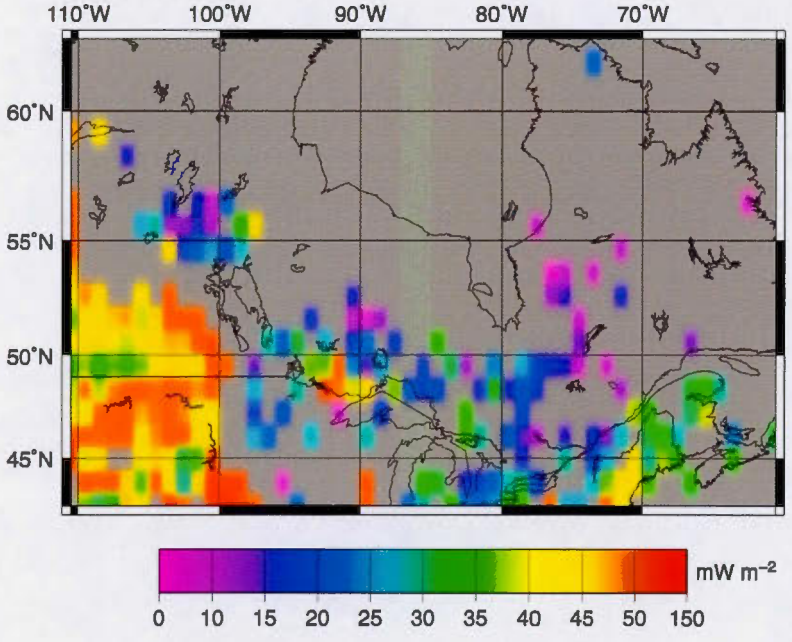

Figure 1.4 Eastern Canada calculated heat production from heat flux data averaged over 1° x 1° cells supposing a constant mantle flux of 15mW m^{-2}

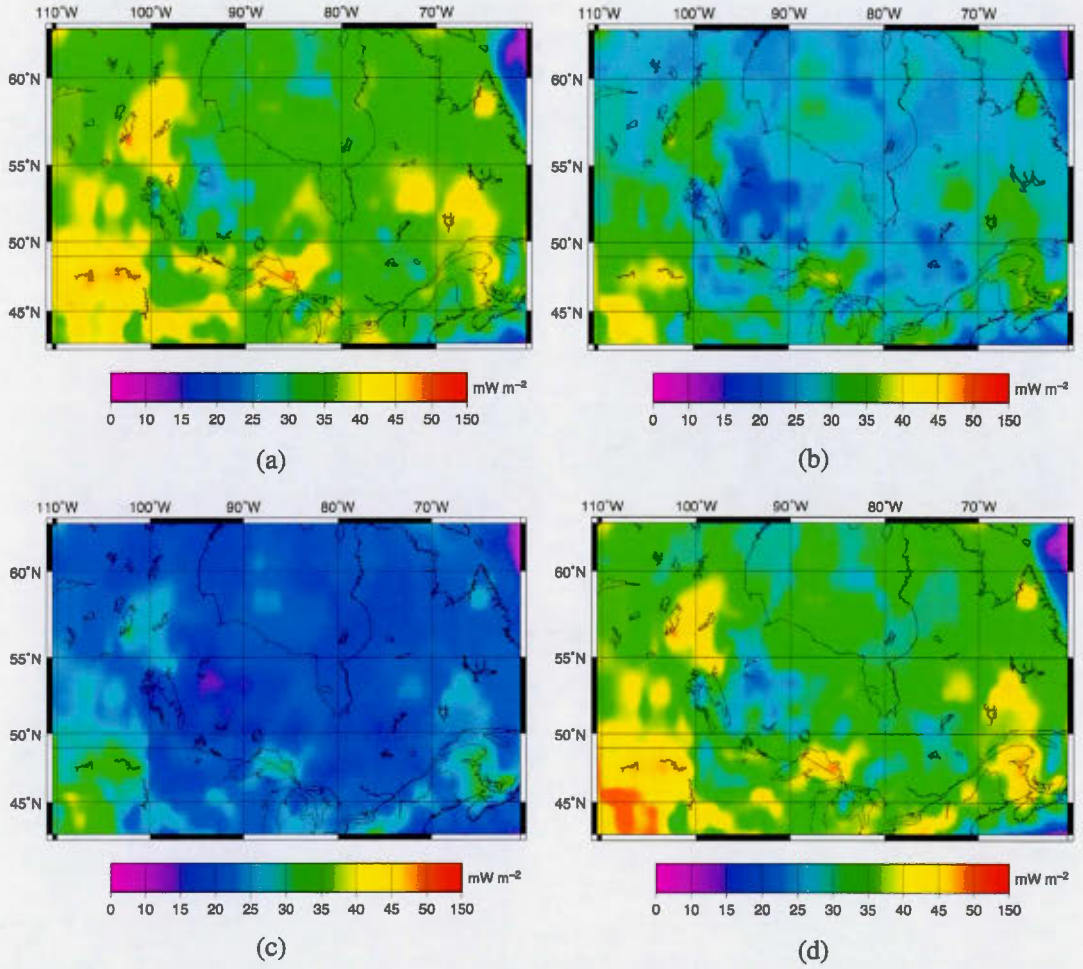

Figure 1.5 Four attempts to estimate heat flux on a regional scale where (a) is obtained using a crustal average heat production of 0.89 mW m^{-2} estimated by Rudnick and Gao (2014) (b), (c) and (d) are using a differentiated crustal heat production with the heat production rate estimated by Rudnick and Gao (2014) in (b) optimized to reduce the difference with the data in (c) from estimated concentrations of heat producing elements by Huang et al. (2013) in (d). The heat production values for each attempt are shown in table 1.1.The figures have been smoothed.

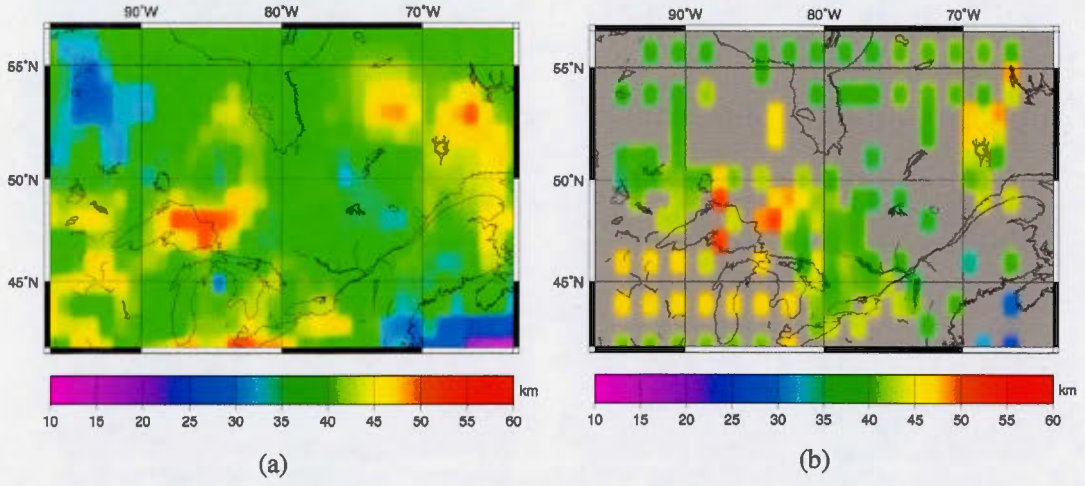

Figure 1.6 Eastern Canada crustal thickness according to the CRUST1.0 model in (a) and according to data (F. Darbyshire, pers. comm) in (b)

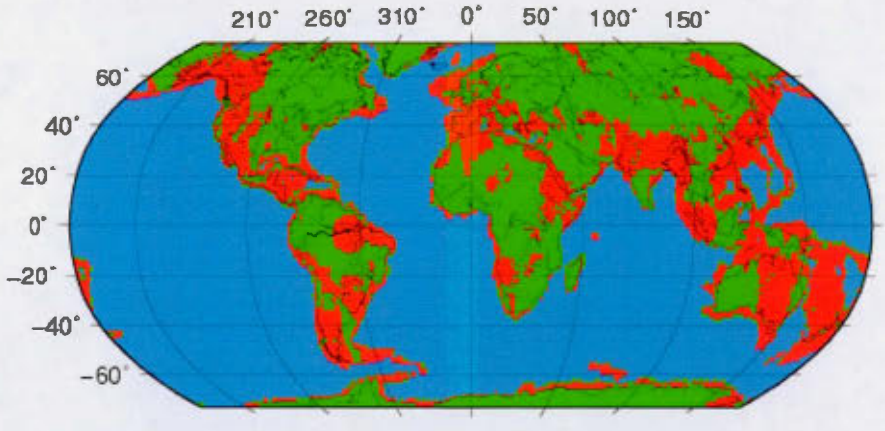

Figure 1.7 Active vs steady state cells for our calculations. The cells are BLUE for oceanic crust, GREEN for stable continental crust, and RED for active continental crust. Stable continental crust is defined as having a heat flow below 65 mW m^{-2} and crustal thickness between 25 and 60 km.

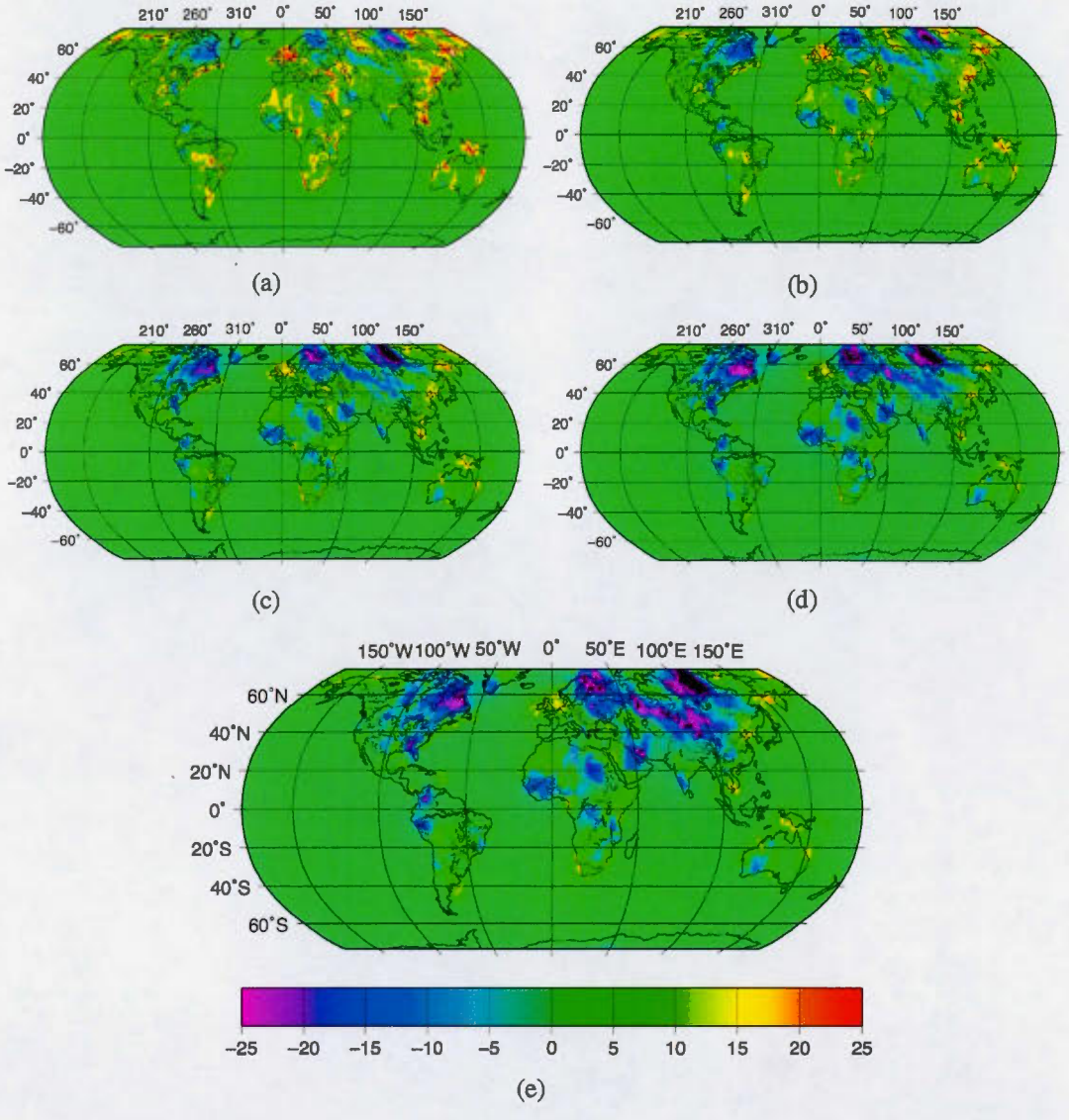

Figure 1.8 Difference between the models using the heat flow data and the ones using heat productions estimated with CRUST1.0 model in TNUs. In each case we used a different heat production for the crust. (a) average hp = 0.67 μW m^{-3} (b)average hp = 0.75 μW m^{-3} (c) average hp = 0.83 μW m^{-3} (d) average hp = 0.90 μW m^{-3} (e) using Huang et al. (2013) concentration values as discussed in previous section.

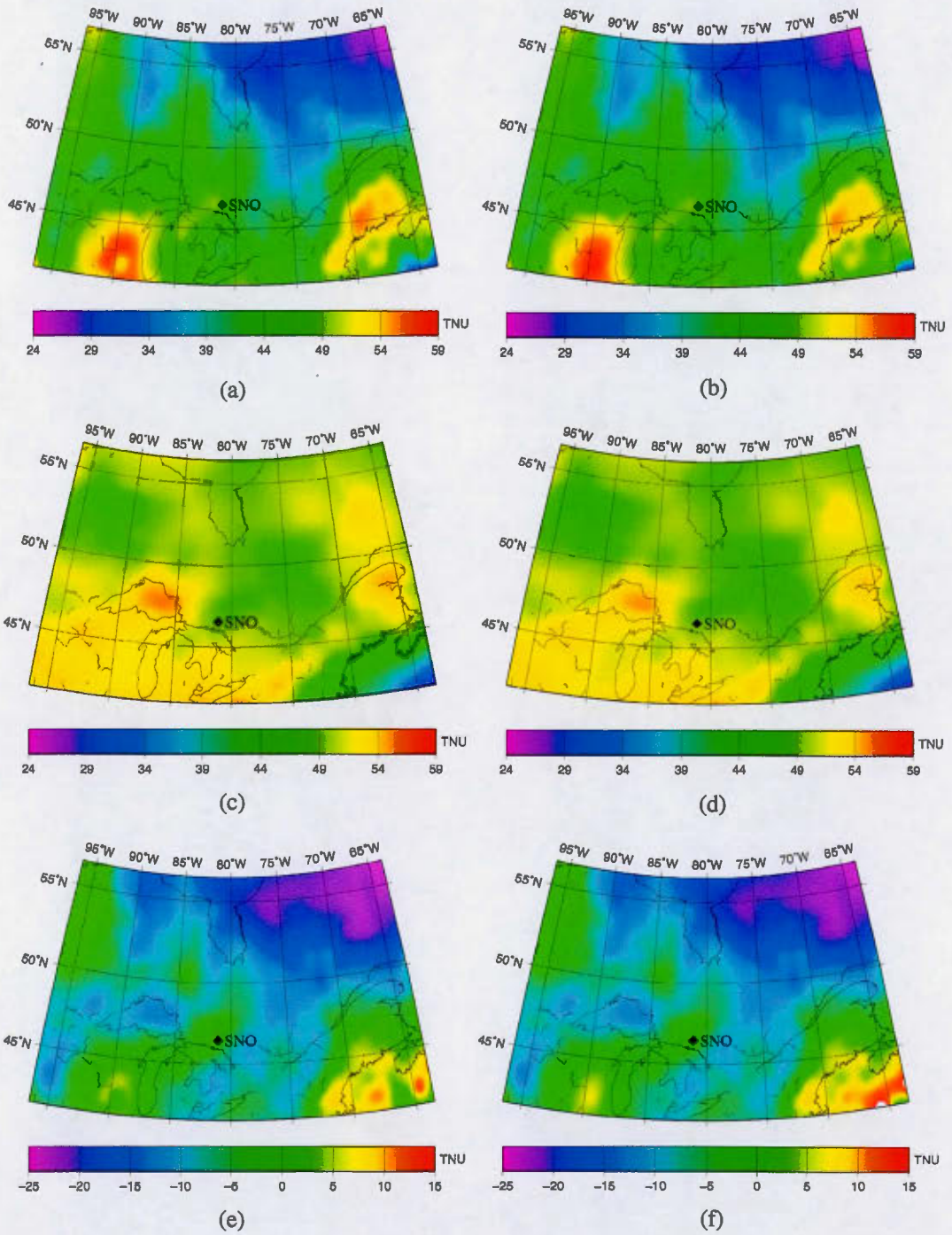

Figure 1.9 Comparing local to global calculation methods. All the figure on the right hand side are produced with the global model. The ones one the left are from the local model. In the first row, we presented the models using heat flow data where available, in the second one, the model using only CRUST1.0 values and in the last row, we have subtracted the second row from the first.

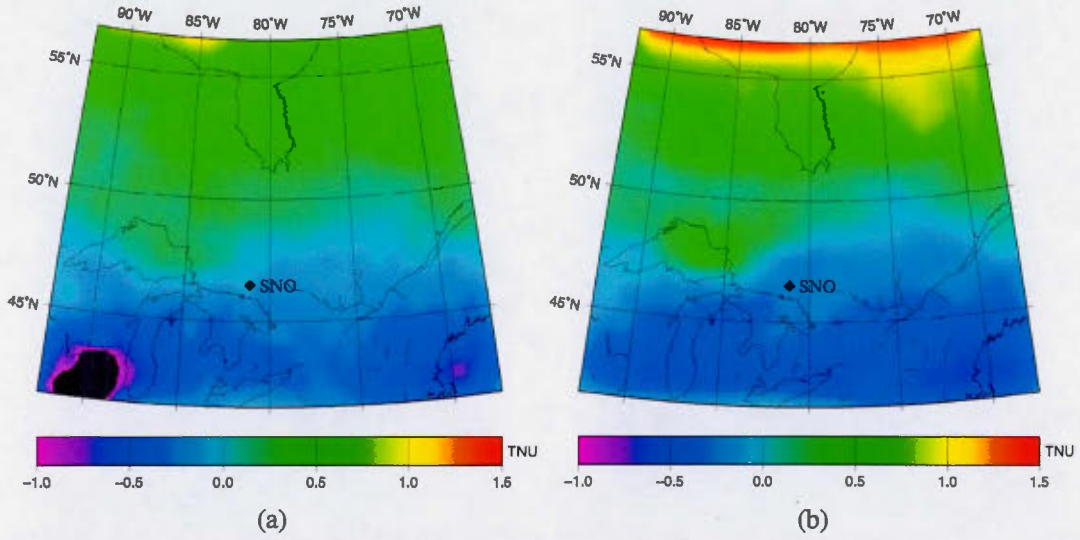

Figure 1.10 We have compared the two models by subtracting the local model from the global one for both the data deduced maps in (a) and the CRUST1.0 deduced one in (b).

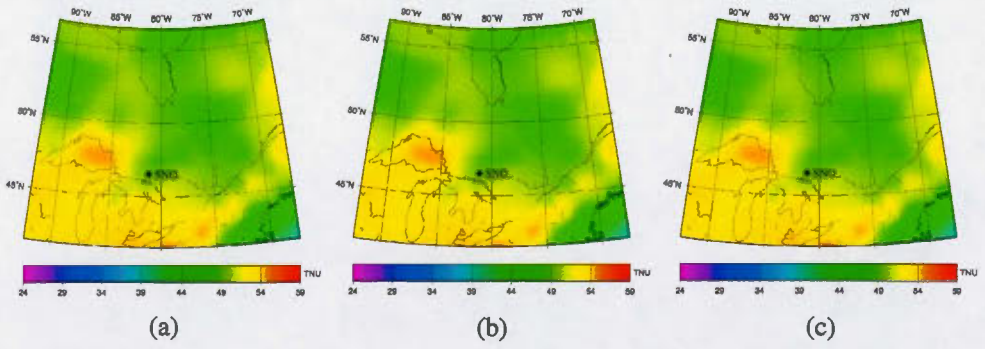

Figure 1.11 Effect of rescaling the cell size on the calculation accuracy. (a) the crustal model with a cell of 1° square ; (b) resized to 0.5 ° and in (c) resized to 0.25 °.

2

The Earth's Heat Budget, Crustal Radioactivity and Mantle Geoneutrinos

Jean-Claude Mareschal

GEOTOP, University of Quebec at Montreal, POB 8888, sta. downtown, Montreal, H3C3P8, Canada – mareschal.jean-claude@uqam.ca

Claude Jaupart

Institut de Physique du Globe de Paris, 1, rue Jussieu - 75238 Paris cedex 05, France – jaupart@ipgp.fr

Lidia Iarotsky

GEOTOP, University of Quebec at Montreal, POB 8888, sta. downtown, Montreal, H3C3P8, Canada – iarotsky.lidia@courrier.uqam.ca

Mareschal, J.C., Jaupart C., Iarotsky L., 2016. The Earth's Heat Budget, Crustal Radioactivity and Mantle Geoneutrinos, In : Ludhova, L. (Ed.), Geoneutrinos. ISBN 978-83-944520-1-8

Abstract

Studies of the Earth's thermal evolution have progressed slowly because of the fundamental difficulty of dealing with a highly heterogeneous system that continuously changes its upper boundary conditions and internal distribution of heat sources. Here, we review current understanding on the mechanisms of heat loss and on the partition of heat sources between the continents and the convecting mantle. We evaluate the various items, including the core heat loss, in the energy budget of our planet with emphasis on the methods used to determine them and their uncertainties. The total energy loss of the Earth 46 ± 3TW is well established by heat flow measurements in the continents and well-tested physical models for cooling of the sea floor. This energy loss is balanced by heat production of radioactive elements in the crust and in the mantle and by secular cooling of the mantle and core. The amount of heat due to radioactive decay in the continental crust can be determined quite accurately (i.e., within $\pm$ 10%) and accounts for a fraction of the Earth's total heat generation that may be as large as 50%. In contrast, heat generation in the Earth's mantle is poorly constrained, which limits our understanding of the Earth's convective engine. For geologists, the main challenge is not to determine the Earth's secular cooling rate because it can be determined directly from ancient lava samples, but to understand the physical controls on plate tectonics and continental growth, which act to deplete the Earth's mantle in heat producing elements. On land, heat flux measurements record the total crustal heat production without knowledge of all the rock types present including those of lower crustal horizons that are beyond the geologist's reach. Geoneutrino observations and measurements of the Earth's surface heat flux are both needed to narrow down the uncertainties on the breakdown of the energy budget. They complement each other in the interpretation of the geoneutrino signal at observatories located on land where the crustal contribution is much larger than the mantle one and must be determined independently.

Keyword

Heat flow || Heat producing elements || Energy budget || Bulk silicate Earth || Urey

number || Core cooling || Mantle cooling

2.1 Introduction

Secular cooling has always been a central issue in the Earth Sciences because our planet's present state and geological activity result from more than four billion years of evolution. In the 19th century, advances in the theory of heat conduction and in thermodynamics were immediately applied to questions regarding the internal structure and thermal evolution of the Earth. When Fourier first published his *Théorie Analytique de la Chaleur*, he realized that the temperature inside the Earth had to be very high and he thought that the Earth had retained most of the heat from its formation (Fourier, 1820, 1824). Lord Kelvin reached the same conclusion with his famous calculation of the age of our planet (Thomson, 1864). His result was not consistent with geological evidence. The strong controversy that ensued is exemplary of the divide still to be bridged between physicists and geologists. At the time of Fourier and Kelvin, the Earth's temperature gradient was estimated to be in the range 20-30 K km^{-1}, which is surprisingly accurate. From this value, Kelvin deduced that our planet was not much older than 100 My. His calculation rested on the assumptions that the Earth is cooling by conduction and that there are no sources of heat inside it, which are not valid. He might not have followed this approach if he had paid more attention to the variability of surface heat flux. Even in his days, temperature measurements in deep mine shafts and galleries showed that the heat flux varies by large amounts at Earth's surface, which is not consistent with a uniform cooling model for the planet. From our present-day perspective, the most serious flaws of Kelvin's model are that it relied on a value for the temperature gradient in continents and that it did not account for the fundamental differences that exist between oceans and continents. We know now that heat generated locally by the decay of uranium and thorium in the crust is by far the largest contribution to the continental heat flux. The Earth is losing most of its heat through the sea floor and it is in the oceans that the hypothesis of a static planet cooling by conduction was invalidated in the most spectacular manner. As we shall see, the fundamental dichotomy of the mecha-

nisms of heat loss in continents and oceans has hampered progress in part because it took a long time to secure reliable measurements at sea and in part because heat flux measurements on land had to be complemented by determinations of radiogenic heat production in crustal rocks.

The discovery of radioactivity by Becquerel in 1896 completely changed our understanding of the Earth's energy budget. The importance of long-lived radioactive elements was rapidly appreciated (Strutt, 1906; Joly, 1909; Holmes, 1915a,b). Attention was soon focussed on the distribution of heat producing elements within the Earth and only much later turned to the issue of heat transport by convection. With almost no evidence for the early Earth's thermal state, some authors even entertained the notion that the Earth had been heating because of radioactivity (Holmes, 1931). Although it is now clear that this is not so, the contribution of secular cooling to the energy budget remains very poorly constrained. Another consequence of the discovery of radioactivity is that the heat released in rocks by the decay of uranium, thorium and potassium can be compared with the heat flux and used to constrain the composition of the Earth. Three years before the discovery by seismology of the Mohorovicic discontinuity separating the crust and the mantle, Strutt (1906) used this method to conclude that the Earth's crust could not be thicker than 60km.

These studies set the course of research on surface heat flow and on the cooling of the Earth very early on. Heat flow studies provide the strongest constraints on the total heat loss of the Earth but, except for heat production in the continental crust, they can not resolve the other components of the energy budget (mantle and core cooling, mantle heat production). It is hoped that geoneutrino observations will provide a direct measurement of the concentration of uranium and thorium in the Earth's mantle, lead to better constraints on mantle heat production, and reduce the uncertainty on the secular cooling of the core and mantle. Geoneutrino and heat flow studies complement one another in another important area. In continental observatories, the neutrino flux is dominated by the local crustal radioactivity. Accounting for this contribution is a major challenge because of the extremely heterogeneous structure of the Earth's crust at all scales and the difficulty in relating

a geophysical model of crustal structure to the amount of radioactive elements. The surface heat flux directly records the total crustal heat production beneath the measurement site, from which one can infer uranium and thorium contents with little error.

In this chapter, we begin by reviewing the present understanding of Earth's secular evolution and the debates on the mantle processes that have shaped the Earth. We then briefly summarize how the total heat loss of the Earth has been calculated. Outstanding questions on how the tectonic regime of our planet has evolved are best tackled from a thermal perspective and rely on an analysis of the secular evolution of mantle convection, which requires a breakdown of the energy budget of the Earth's mantle. We show that uncertainties on the main items of this budget are crippling and discuss how geoneutrino studies could help. Turning to crustal heat production, we demonstrate how the total crustal neutrino flux can be determined directly from heat flux measurements in stable continents. In a final section, we discuss different ways to calculate the crustal geoneutrino signal with applications to the Sudbury neutrino observatory, Canada, and the proposed site at Lena in Finland.

2.2 The Secular Cooling and Evolution of Earth

2.2.1 Initial Conditions

Initial conditions are required for thermal calculations but, more importantly, provide the most natural perspective to evaluate how the Earth's current dynamic regime has superseded previous ones. There is no doubt today that our planet started from very high initial temperatures. The earliest phases of its existence were marked by several independent processes which all released large amounts of energy. The end of accretion probably saw a giant impact which led to the formation of the Moon and heated the planet by as much as 7000 K, such that parts of the Earth were vaporized (Cameron, 2001; Canup, 2004) . This makes irrelevant the question of whether the Earth was melted from impacts during the accretion sequence. Following accretion, large quantities of iron sank through the Earth's

mantle and accumulated in the Earth's core, a process that converts gravitational potential energy into heat. As dense iron phases moved downwards through a silicate matrix, viscous dissipation may have raised the temperature of the planet by as much as 1700 K (Flasar and Birch, 1973).

Both the giant impact and core formation resulted in temperatures that were high enough for the entire Earth to be molten. This led to a so-called "magma ocean" phase of short duration ($\approx$ 10 My) when the molten mantle cooled and solidified rapidly due to its low viscosity (Solomatov and Stevenson, 1993; Abe, 1993, 1997). In this part of its evolution, the Earth went through two rheological transitions, from pure liquid to slurry (solids suspended in a liquid) and from slurry to mush (interconnected solid phase forming a compacting matrix). One further transition may have been required to steer it to its current convection regime with melting that is limited to the upper parts of upwelling currents, which has been called "sub-solidus". In this regime, the diverging surface flow generated by upwellings involves solid plates that descend into the mantle in a process called subduction. The Earth has the additional complexity of melting in subduction zones. This occurs because the crust and parts of the shallow mantle get hydrated in contact with seawater during their residence at the surface. Hydration acts to lower solidus temperatures and allows melting in subduction zones that are colder than the average mantle. For geologists, this process is all the more important because it is responsible for the generation of continental crustal material and, by way of consequence, of the continents themselves. Subduction is therefore a key geological process as well as an efficient cooling mechanism. When it started in Earth history is a fundamental question that has been and remains vigorously debated.

In equilibrium conditions, the solid fraction depends on temperature and the rheological transitions described above occur at specific thresholds. In a planet with large variations of internal pressure, temperatures are keyed to an isentrope and "potential temperature" refers to temperature at the surface pressure. On Earth, the slope of an isentrope is less than those of the solidus and liquidus, and the solid fraction along an isentrope is constrained to

be less than the surface value. The slurry-to-mush transition occurs when the solid phase forms a continuous network and controls the rheology. In principle, this occurs at a solid fraction that depends on the shape and size distribution of the fragments as well as on the geometrical packing arrangement. For simplicity, it will be fixed at a solid fraction of 0.64, which corresponds to the random close packing of identical spheres. Allowing for a $\pm$ 15% variation of the critical solid fraction and experimental uncertainties, the slurry-to-mush rheological transition occurs at a potential temperature of 1800 $\pm$ 100 K for a mantle composed of dry pyrolite (Herzberg and Zhang, 1996; Litasov and Ohtani, 2002). With such an average potential temperature, the Earth would be capped with a slurry layer thicker than 40 km. Note that, in a convecting system, active upwellings are hotter than average and would therefore generate slurry patches extending over a larger thickness. The current convection regime with rigid surface plates is not possible for a slurry, but it may require a larger solid fraction than the critical value for the slurry to mush transition. This issue has not been resolved yet and we shall discuss it again using a different kind of evidence. In the fully molten and slurry regimes, the mantle viscosity is controlled by that of the melt phase, so that the vigorous convection that ensues cools the planet rapidly. Here, we are concerned with convection in a solid mantle and therefore take an initial potential temperature of 1800 $\pm$ 100 K. The time at which this initial condition must be set is debatable because it depends on external processes. After accretion, a phase of heavy meteorite bombardment did not add much mass to the Earth but led to pervasive resurfacing. According to theoretical calculations, the meteorite flux had dropped to small values by 4 Ga and this can be taken as the initial time. This time coincides with the age of the oldest rocks found on Earth. Note that a few ancient rocks contain individual minerals that are older than this, called zircons. Zircons are able to withstand high temperature as well as large stresses and provide us with a record of primitive conditions that is difficult to interpret with certainty but that is very valuable nevertheless.

2.2.2 Growth of the Continents and Depletion of the Earth's Mantle in Heat-Producing Elements

It would be a serious error to consider the secular cooling of the Earth from a purely thermal perspective, because the processes involved are not limited to heat loss through the surface and internal heat production due to radioactive decay. The Earth, however, evolves in more complicated, and more interesting, ways. With time, mantle melting and melt separation have led to the formation and accumulation of buoyant continental crust at the surface. What makes this process particularly significant is that radioactive elements with large atomic radii such as uranium and thorium get strongly partitioned into the melt phase. Thus, during a sequence of melting and fractional crystallization, these elements remain in the steadily shrinking melt residue, leading to a final rock that is markedly enriched relative to the initial one. Uranium and thorium concentrations in the continental crust are on average higher than in the mantle by two orders of magnitude ! The growth of continents has thus led to depletion of heat sources in the Earth's mantle, thereby fundamentally altering the logic of the mantle energy balance.

To grasp the implications of this, we now discuss how the interior temperature of a planet depends on where its heat sources lie. We consider the simple problem of a system in thermal equilibrium, such that it evacuates all the heat that is released by steady internal sources. In the case of the Earth and its heat producing elements, such sources decay and get concentrated in the continental crust at the mantle expense, implying complex transient thermal conditions that cannot be reduced to a few simple equations. A planet may maintain a uniform distribution of heat sources in its mantle through convective stirring but it may also concentrate them in a cold upper layer which is too rigid to be involved in convective motions. These two cases differ markedly in their internal temperatures. We consider two mechanisms, convection in a fluid with viscosity μ over thickness h and conduction in a rigid crust enriched in radioactive elements over thickness d_c. The respective rates of heat generation are noted H_{conv} and H_{cond}. The total amount of heat generated is the same in both cases, so that $H_{conv}h = H_{cond}d_c$. For clarity, we consider that no heat is brought into

either the convecting mantle or the rigid crust from below. Thus, the surface heat flux is the same in both cases, and is equal to $Q = H_{conv}h = H_{cond}d_c$. The temperature differences between the surface and the Earth's interior in the two cases are (Davaille and Jaupart, 1993) :

$$\Delta T_{conv} = C_Q^{-3/4}\left(\frac{H_{conv}h}{\lambda}\right)^{3/4}\left(\frac{\kappa\mu}{\rho_o g\alpha}\right)^{1/4} \tag{2.1}$$

$$\Delta T_{cond} = \frac{H_{cond}d_c^2}{2\lambda} \tag{2.2}$$

where C_Q is the (dimensionless) constant in the local heat flux scaling law, λ the thermal conductivity, κ the thermal diffusivity, ρ the density, g the acceleration of gravity, α the thermal expansion coefficient. These two temperatures differ by large amounts. Their ratio is :

$$\frac{\Delta T_{cond}}{\Delta T_{conv}} = \frac{C_Q^{3/4}}{2}\frac{d_c}{h}\left(\frac{\rho_o g\alpha H_{conv}h^5}{\lambda\kappa\mu}\right)^{1/4} = \frac{C_Q^{3/4}}{2}\frac{d_c}{h}Ra_H^{1/4} \tag{2.3}$$

where Ra_H is the Rayleigh number for internal heating and where the proportionality constant is $C_Q^{3/4}/2 \approx 0.2$. In the Earth, $d_c \approx 30$ km and $h \approx 3000$ km, and hence $d_c/h \approx 10^{-2}$. This result shows that it takes very large Rayleigh numbers, *i.e.* extremely vigourous convection, for ΔT_{cond} to be larger than ΔT_{conv}. In practice, this requires $Ra_H > 5 \times 10^{10}$, which was only possible in early stages of Earth's evolution. For reference, this Rayleigh number is about 10^9 today, so that $\Delta T_{cond}/\Delta T_{conv} \approx 0.4$. In other words, conduction in a thin enriched crust evacuates internal heat with an internal temperature that is lower than that of a vigorously convecting system. This simple calculation shows why growing a rigid radioactive crust at the top is an efficient cooling mechanism.

2.2.3 The Secular Cooling Rate of the Earth

The thermal history of the Earth's mantle can be reconstructed empirically by analyzing ancient magmas and lavas that have survived. In a multi-component system, melting occurs over a finite temperature interval and generates liquids of different compositions de-

pending on temperature (Putirka, 2005; Herzberg et al., 2007). For the Earth's mantle, the melting interval stretches over a wide range of potential temperature ($\approx$ 600 K), allowing geologists to study the thermal evolution of our planet with some precision. One caveat is that one must pay attention to the geodynamic conditions of melting. In the Earth, magmas are generated in different settings, some of which depend on local factors that are not relevant to the planet as a whole. In a convecting system that is powered by internal heat sources only, there are no active upwellings such as plumes and motions are entirely driven by cooling from above. In such conditions, the flow consists of focussed downwellings separated by a large-scale diffuse return flow. The latter accounts for most of the volume and is therefore representative of the average temperature. In the Earth, convection is also propelled by heating from the core, which is responsible for a small number of plumes with positive thermal anomalies. Magmas from large shield volcanoes such as Hawaii are generated in mantle that is hotter than average and must be excluded from this analysis. For similar reasons, one must also exclude magmas from subduction zones, which are colder than the average mantle by amounts that depend on a host of parameters. To study the average mantle, one must restrict oneself to passive upwellings such as mid-ocean ridges. Herzberg et al. (2010) have thus used petrological data from oceanic basalts to determine how the Earth's mantle temperature has changed with time (Figure 2.1). This secular evolution may be compared to that of the volume of continental crust, which has also changed with time. One must note that the mantle temperature started to decrease in measurable amounts when more than 50% of the volume of continental crust had been extracted from the mantle, at *ca.* 3 Ga.

One can complement the geological data at old ages with determinations of today's mantle temperature from a number of independent methods summarized in Jaupart et al. (2014). These methods include constraints from the depths of seismic discontinuities and phase transitions in the solid mantle as well as from the cooling behaviour of the oceanic lithosphere away from mid-ocean ridges (McKenzie et al., 2005). One finds a range of 1600-1700 K for today's mantle potential temperature. It appears that the cooling rate has

changed with time. For ages older than about 2.5 Ga, there is no discernable trend in the data and the temperature remains in a 1850±50 K range (Figure 2.1). Interestingly, this is close to the threshold temperature for plate tectonics and sub-solidus convection that has been discussed above. Both geological data and physical constraints on the thermal structure of the early Earth indicate that the cooling rate has increased as the planet got older. They also indicate that the total temperature decrease over 3 Ga is only about 200 K, corresponding to an average cooling rate of about 70 K Gy^{-1}. This number can be compared to the present-day cooling rate derived from the Earth's heat budget that will be developed in the next section.

2.3 The Present Heat Loss of the Earth

The heat flux map of the Earth (Figure 2.2) summarizes our understanding of the present Earth energy loss. The map combines two very different types of information : (1) in the continents and on their margins, it interpolates between heat flux data points, (2) in the oceans it uses a plate cooling model to predict the heat flux as a function of sea floor age. One can note the contrast between the oceanic heat flow which is high near the ridges and decreases smoothly toward the old sea floor, and the continental heat flow which is lower and exhibits variations at all the scales represented on the map. In stable continental regions, these variations are related to crustal heat production.

The total heat loss of the Earth is obtained by integrating the heat flux over the entire surface. We shall briefly summarize how it is done in practice and refer to the article by Jaupart et al. (2014) for more details.

2.3.1 Continental Heat Flow

Two difficulties arise when calculating the heat loss through the surface of the continents. One is the very uneven distribution of heat flux measurements with most of the data located in Eurasia and North America, much less data in the southern hemisphere, and

practically none in Greenland and Antarctica. Determining the heat flux on land requires the measurement of the temperature gradient in deep (i.e, >300m) holes and of thermal conductivity of core rock samples. These measurements are time consuming and, because of the drilling cost, they are almost always performed in holes of opportunity (usually drilled for mineral exploration). The other difficulty stems from the bias in the sampling because many measurements were made for geothermal exploration in high heat flow regions. In order to properly calculate the mean continental heat flux, we must weigh the heat flux values by the area sampled. Following such a procedure, the area weighted average continental heat flux is 66mW m^{-2} (vs 80mW m^{-2} for the average of all heat flux values). The total heat loss through the continents, obtained by multiplying the mean continental heat flux by the total area of the continents and their margins, is 14TW. An identical value is obtained when binning the heat flux data by geological age and integrating over the age distribution of the continental crust (Pollack et al., 1993; Davies and Davies, 2010).

2.3.2 Oceanic Heat Flow

After it was recognized that the sea floor forms at the midoceanic ridges and cools as it moves away from the ridge, simple thermal models have been used to explain oceanic heat flux data (McKenzie, 1967; Oxburgh and Turcotte, 1968; Sclater and Francheteau, 1970). Models differ in their boundary conditions but they all predict that for young sea floor ages, heat flux decrease as the inverse square root of age. Plate models that fix a boundary condition (usually constant temperature) at some depth predict that heat flux becomes constant at an age fixed by the depth of the lower boundary. Oceanic heat flux measurements exhibit a lot of dispersion, particularly near the mid-oceanic ridges. When data are binned by age, there is a trend of decreasing heat flux with age of the sea floor (Stein and Stein, 1994) but, for young ages, heat flux is lower than predicted by plate cooling models. As shown by Figure 2.2, the heat flux measured on sea floor older than 80 Ma tends to fluctuate around a constant value $\approx$48mW m^{-2} (Lister et al., 1990). Heat flux measurements record only the conductive transport of heat and do not account for heat transported by convection. It

has been recognized that near the midoceanic ridges, hydrothermal circulation takes place and can account for the discrepancy between the plate cooling model and the heat flux measurements (Lister, 1977). This hypothesis has been thoroughly tested by measurement campaigns that show that, in regions where hydrothermal circulation has been shut down, the data follow exactly the prediction of the cooling model. The function $Q(\tau)$ that fits best the heat flux data for ages $\tau < 80$My is given by :

$$Q(\tau) = C_Q \tau^{-1/2} \tag{2.4}$$

with τ sea floor age and $C_Q = 490 \pm 20$mW m^{-2} My$^{-1/2}$. For sea floor older than 80Ma, heat flux that fluctuates around 48mW m^{-2} can be considered constant (Lister et al., 1990).

Sea floor bathymetry can also be calculated by combining an isostatic equilibrium condition with plate density derived from the cooling plate model. The prediction that depth of the sea floor increases with $\sqrt{\tau}$ has been verified for all ages <80Ma.

$$h(\tau) = h_0 + C_h \tau^{1/2} \tag{2.5}$$

with $h_0 = 2600 \pm 20$m and $C_h = 345 \pm 3$m My$^{-1/2}$. Bathymetry data, which are much less noisy than heat flux, record the total cooling of the oceanic lithosphere since its formation, and provide the strongest confirmation of the plate cooling model.

In order to determine the total oceanic heat loss, we integrate the heat flux times surface area over all ages using the areal distribution of sea floor ages. The distribution of sea floor ages has been very well determined from studies of the marine magnetic anomalies (Müller et al., 2008). There are few ages higher than 180Ma and the areal distribution appears to decrease linearly with age τ, such that the areal distribution can be approximated by :

$$\frac{dA}{d\tau} = C_A(1 - \tau/180) \tag{2.6}$$

where τ is age in Ma In order to account for the total area covered by the oceans including

the marginal basins ($300 \times 10^6 \text{km}^2$) the accretion rate $C_A = 3.4\ \text{km}^2\ \text{y}^{-1}$.

Integrating separately sea floor younger and older than 80 Ma gives :

$$\begin{aligned} Q_{80-} &= \int_0^{80} C_Q \tau^{-1/2} C_A (1 - \tau/180) d\tau = 24.3\ \text{TW} \\ Q_{80+} &= 48\text{mW m}^{-2} \times \int_{80}^{180} C_A (1 - \tau/180) d\tau = 4.4\ \text{TW} \\ Q_{oceans} &= 29 \pm 1\ \text{TW} \end{aligned} \tag{2.7}$$

Hotspots bring additional heat to the oceanic plates. This heat is not accounted for by the plate cooling model and should be added to the heat loss. The additional heat flux is barely detectable from heat flow measurements, but it can be estimated from the volume of the swells of the sea floor : it amounts to 2-4TW (Davies, 1988; Davies and Richards, 1992).

The total heat loss at the Earth surface includes continental heat losses 14TW, cooling of the sea floor, 29TW, and heat from the hot spots, 3TW, for a total of 46TW.

Recent estimates of the total heat loss differ by less than 10% although they are based on slightly different approaches (Table 2.1). The two most recent values are slightly higher than the previous ones because they include the contribution of the hotspots that had been neglected in antecedent studies.

2.4 The Main Sources of Energy

Part of the Earth's heat comes from radioactive heat production in the continental crust which has been estimated by multiple and extensive sampling, (see Table 2.2 and Rudnick and Fountain, 1995; Rudnick and Gao, 2003; Jaupart and Mareschal, 2014). Heat production in the lithospheric mantle beneath the continents is believed to be very small (Michaut et al., 2007), and contributes < 0.5TW to the heat budget. The total power of the continental lithosphere is estimated to be 7 ± 1TW, leaving 39 TW for the total heat flow at the

surface of the mantle. Three main components balance the mantle energy loss : radiogenic heat production in the mantle, heat flow from the core, and secular cooling of the mantle. Other sources (tidal dissipation, gravitational settling, changes in gravitational potential energy due to thermal contraction) contribute less than 1TW (Jaupart et al., 2014).

2.4.1 Heat Producing Elements in Bulk Silicate Earth

We shall not discuss geochemical and cosmochemical models to estimate mantle radioactivity that are covered by Engel and McDonough in another chapter of this book. Such models refer to the composition of the bulk silicate Earth (BSE) which include the crust and mantle. Several estimates of heat producing elements concentrations in BSE are given in Table 2.3. With these estimates ranging between 3.4 and 5.1 pW/kg and the mass of BSE (4.043×10^{24}kg), the total radiogenic power ranges between 13.6 and 20.4TW (Table 2.3). The radiogenic power of the mantle is obtained by subtracting the contribution of the continental crust from BSE.

2.4.1.1 Mantle Heat Production : Urey Ratio

Removing the heat producing elements that have been stored in the continental crust leaves a total heat production between 6.6 and 13.4 TW for the mantle. Whether the Earth is heating up or cooling with time is determined by the ratio of the total heat production to the heat loss. This ratio has been called the Urey ratio. Because the crustal heat production does not contribute to mantle convection, it must be excluded from the definition of the Urey ratio. The convective Urey ratio is thus defined as the ratio of the total radiogenic heat production of the mantle to the convective heat loss (e.g., Christensen, 1985; Korenaga, 2008). For the range of total heat production in BSE, the present value of the convective Urey ratio is comprised between 0.15 and 0.35. The implications of such a low value for thermal history models of the Earth have been debated at length. With very little internal heat production to balance the heat loss, the cooling rate of the Earth should lead to much higher mantle temperatures in the Archean for which there is little or no geological

evidence (Burke and Kidd, 1978; England and Bickle, 1984). Simple parameterized thermal models with low Urey ratio indeed imply rapid cooling of the mantle and lead to an Archean thermal catastrophe (Christensen, 1985). Different solutions have been proposed to avoid the Archean catastrophe including time changes in the scaling laws for the convective heat loss (Korenaga, 2003), but their ability to capture the complex characteristics of plate tectonics has been questioned (Jaupart et al., 2014).

2.4.2 Heat Flow from the Core

Mass exchanges between the core and mantle are insignificant but as the core cools down energy is transferred to the mantle. Because the core is much less viscous than the mantle, it is essentially the efficiency of mantle convection (determined by mantle viscosity) that controls the energy flux across the CMB. One constraint is that the core has sustained a geodynamo during most if not all of Earth's history and that the core heat flow must be consistent with thermodynamic requirements for a geodynamo. Assuming that all the heat of mantle plumes comes from the core provides another constraint (Davies, 1993), but it turned out to be a weak and not very useful lower bound to the core heat loss (Labrosse, 2002). The geodynamo can be attributed with confidence to convective motions in the liquid outer core, implying that the core heat flux must be larger than the heat flux which is conducted along the core isentrope. The core isentrope is now well constrained but the thermal conductivity value is not. Calculations and laboratory measurements have suggested a high thermal conductivity value for the outer core at CMB pressure and temperature (λ = 85-140W m^{-1} K^{-1} depending on core composition) (Pozzo et al., 2012; Gomi et al., 2013). With such values, the conductive heat flux along the core isentrope must be > 70mW m^{-2} , which is difficult to reconcile with the heat budget of the Earth, as discussed below. Recently, Zhang et al. (2015) have criticized some of the theoretical assumptions made by Pozzo et al. (2012) and have argued that their conductivity values are too high. Unfortunately, their calculations are valid for pure crystalline iron and cannot predict values for the outer core, because it is made of melt that contains light elements. We can only

conclude that these important topics deserve further study and consider for the sake of argument the total range of conductivity values that have been proposed by various authors, 46-150W m^{-1} K^{-1}. The core heat loss is thus within a range of 5-17 TW.

2.4.3 Balancing the Budget : Secular Cooling of the Mantle

Having established constraints on the mantle heat production and on the heat flow from the core, we can determine a range of values for secular cooling of the mantle. With an average value of 1200 W kg^{-1} K^{-1} for the specific heat of the mantle, 1TW represents cooling by 6K Gy^{-1}. Using the mean values for mantle heat production and core heat loss, we obtain a central value of 16TW for mantle cooling with a range of 4-27TW. This implies that the mantle temperature has decreased by 250K since the end of the Archean at 2.5Ga, which is close to the upper bound deduced from the petrological, geological and physical constraints discussed above (see section 2). The present energy budget provides only a snapshot that we cannot extrapolate too far back in time. It should only be viewed as a constraint that thermal evolution models must satisfy. These results are consistent with low Urey number thermal evolution models implying sluggish convection.

Figure 2.3 shows our best estimates of the terms in the present energy budget of the mantle (Table 2.4). This breakdown of the budget is significantly different from those proposed by Davies (1999) and by Stacey and Davis (2008) (Table 2.5). Both these authors have assumed a low heat flux from the core which they assumed equal to the heat flow from the hotspots. They made up for the deficit by increasing the total radioactive heat production and added that of the crust to that of BSE. Their total radiogenic heating power of 28TW is higher than the highest estimates from geochemistry. This only points out the need for a direct measure of mantle radiogenic power.

2.5 Determining U and Th in the Mantle with Geoneutrinos

Geoneutrino studies could address three main questions : What is the present total mass of U and Th in the mantle from which we could infer the mantle radioactivity and the convective Urey ratio ? What is the vertical distribution of heat producing elements in the mantle ? Are there lateral variations in the HPE distribution in the mantle ? But at this time the question is : How can we best address these questions ?

The flux of neutrino observed at distance r from a point source decreases as r^{-2}. Because the neutrino detectors measure the total flux of neutrinos through the detector, not the flux in the vertical direction, even for a spherically symmetric Earth, integrating the neutrino flux over the Earth surface does not allow to determine the total heat production. For a detector located at the surface of a spherically symmetric Earth, the neutrino flux Φ_i from radioelement i is obtained as :

$$\begin{aligned}\Phi_i &= \int_0^{2\pi} d\phi \int_{-1}^{1} d\cos\theta \int_0^{a} \frac{N_i(r) r^2 dr}{4\pi(a^2 - 2ar\cos\theta + r^2)} \\ &= \frac{a}{2}\int_0^1 N_i(u) \log\left(\frac{1+u}{1-u}\right) u du\end{aligned} \tag{2.8}$$

with $u = r/a$, a is the Earth's radius, and $N_i(r)$ is the volumetric activity for radio-elements ^{232}Th or ^{238}U at distance r from the Earth center. The equation 2.8 shows how the neutrino flux depends on the radial distribution of the radioactive sources and that it is more affected by the shallow than by the deep ones. For example, assuming the same total mass of radioactive elements, the flux is $\approx$10% lower if the upper mantle is depleted by a factor of 3 relative to the lower mantle.

In principle (and in practice) gravity studies can always determine the total mass of the sources. The total mass of the Earth can be determined to a very good approximation from one single gravity measurement. This is not so for neutrino studies because it is the total flux, and not its vertical component, that is measured. On the other hand, we get no new information by measuring gravity at different levels but we would obtain more

information if only we could measure the neutrino flux at different levels. Alternatively, should directional information be obtained, we could calculate the vertical component of the neutrino flux and thus the total amount of U and Th in the Earth.

The function $N(r)$ cannot be determined from the neutrino flux measured at the Earth surface, but some constraints could be obtained by using *a priori* information. How much information can be extracted from one single observation could be addressed rigorously as an inverse geophysical problem (e.g., Tarantola, 1987; Menke, 2012). With directional information available, the variations of the neutrino flux with inclination can be inverted to determine U and Th distribution with depth (Mareschal et al., 2012).

Another difference between gravity and geoneutrino studies, a further difficulty for the latter, comes from the fact that a large number of radioactive elements are stored in the Earth's crust, while almost all the mass of the Earth resides in its mantle and core. Therefore the geoneutrino signal in continental observatories is dominated by the crust. The deployment of geoneutrino observatories on the sea floor would allow the measurement of a neutrino flux that originates in the mantle (Dye et al., 2006; Dye, 2009). Moving the sea floor observatory to different locations might also allow the resolution of lateral variations in radioelement concentrations in the lower mantle (Šrámek et al., 2013).

2.6 Crustal Contribution to Geoneutrino Flux in Continents

So far, geoneutrino observations have been made with detectors located in deep underground laboratories on the continents, Kamland in Japan, and Borexino in Italy (Kamland collaboration, 2005, 2011, 2013; Borexino collaboration group, 2010, 2013, and chapters by Watanabe and by Zavatarelli in this volume). The still preliminary results are all the more impressive that the observatories are located at the worst possible sites where the contribution of the crust to the geoneutrino signal is most difficult to calculate. Observations will soon start at the upgraded Sudbury neutrino observatory (SNO+) (see chapter by Chen in this volume). The JUNO observatory in China should become operational in

2020 (see chapter by Ran and Jun) and plans are being made for a European observatory possibly to be sited at Pyhäsalmi, Finland (Wurm et al., 2012).

2.6.1 Variations in Surface Heat Flux and Crustal Heat Production in Stable Continents

For the purpose of this discussion we define stable continental regions as those where the lithosphere has reached thermal steady state, i.e. transient perturbations have decayed and the lithosphere is in conductive equilibrium. In practice, this is achieved more than 200My after the last tectonic perturbation. Considering the vertical flow of heat across the lithosphere, we have that in steady state :

$$Q_0 = Q_b + \int_0^L H(z)dz \tag{2.9}$$

where Q_0 is the surface heat flux, Q_b the heat flux at the base of the lithosphere, $H(z)$ the heat production rate, and L is the thickness of the lithosphere. Horizontal variations in the heat flux at the base of the lithosphere are attenuated by heat diffusion and are negligible at the surface. Vertical variations in heat production are more important than horizontal ones and the terms in equation 2.9 should be seen as horizontally averaged over a distance comparable to the thickness of the lithosphere. Heat production is much lower in the lithospheric mantle than in the crust (Russell et al., 2001; Michaut et al., 2007) and it is common to consider that

$$Q_0 = Q_m + \int_0^{z_m} H(z)dz \tag{2.10}$$

where Q_m is the heat flux across the Moho, and z_m is the crustal thickness. Because mantle heat production rate is small, and variations in basal heat flux are attenuated when they reach the base of the crust, variations in Q_m are expected to be small and variations in Q_0 are essentially due to differences in crustal heat production rate. The depth of crustal heat sources is constrained by the horizontal scale of heat flux variations. If Q_m could be determined, the bulk crustal heat production could directly be calculated from the surface

heat flux.

2.6.2 Determining the Moho Heat Flux

An obvious constraint on Q_m is that it must be less than the lowest value of the surface heat flux. Surface heat flux values on the order of 18-20mW m^{-2} have been reported from different Shield areas, which gives an absolute upper bound. Accounting for the lowest possible heat production in crustal rocks gives an even lower upper bound for Q_m.

Table 2.7 shows minimum and maximum values of the regional averages of the surface heat flux in different shield areas. The table emphasizes two points : one is that, in some shields, the minimum values are very low implying that Q_m is in 11-15mW m^{-2} range; the second is that the range of the crustal contribution (the difference between lowest and highest values) is 25-30mW m^{-2} .

Different methods have been used to narrow down the range of Q_m. In different regions of the world, an entire section of the crust including the deep crust has been exposed at the surface either by thrusting along a crustal ramp (e.g. the Kapuskasing structural zone, in the Superior Province, Canada), or by the rebound of the crust following a meteoritic impact (e.g., the Vredefort structure in the Kaapvaal craton, South Africa). In such regions, the total crustal heat production can be determined by sampling the different crustal levels exposed at the surface. In some Provinces, such as the Grenville Province in Canada, tectonic processes have brought up and exposed different crustal levels at the surface. In these regions, extensive sampling of the rocks at the surface is equivalent to vertical sampling and yields the vertically averaged heat production. Subtracting average crustal heat production from surface averaged heat flux yields Q_m (Pinet et al., 1991). Table 2.8 summarizes estimates of Q_m in Shield areas obtained by different methods.

2.6.3 Distribution of Heat Producing Elements in the Crust

2.6.3.1 Horizontal Variations

In contrast to the oceanic heat flux, the variations in continental heat flux do not follow a well organized and predictable pattern, as demonstrated by the heat flow map of Eastern Canada (Figure 2.4). Short wavelength variations are superposed to a long wavelength contrast between the stable eastern and the active western parts of the continent. These are not due to errors but to variations in the crustal heat production which take place at different scales. There are variations with crustal age, but there are large variations within each of the age groups (Table 2.6). For example, there are marked differences of the mean heat flux between the different belts that form the Trans-Hudson orogen, in northern Manitoba and Saskatchewan, Canada (Mareschal et al., 2005). These differences are due to variable crustal composition and reflect the diverse mechanisms of formation of these belts. In the Abitibi terrane, in Quebec, a long wavelength (300km) trend has been identified that could be related to the presence of two distinct volcanic zones in this subprovince (Pinet et al., 1991; ?). In stable continents, short wavelength positive anomalies are associated with shallow granites and felsic intrusions enriched in heat producing elements (?).

2.6.3.2 Vertical Variations

From the surface heat flux Q_0 and crustal thickness z_m, we can calculate the average crustal heat production : $(Q_0 - Q_m)/z_m$. Heat production measured on samples of surface rocks $< H_0 >$ is usually higher because crustal differentiation results in enrichment of the upper crust at the expense of the lower. Following Perry et al. (2006), this enrichment can be quantified with a differentiation index DI :

$$DI = \frac{< H_0 \times z_m >}{Q_0 - Q_m} \tag{2.11}$$

The depth scale of the enrichment can be estimated by comparing province-wide average heat flux and heat production. For the different provinces of the Canadian Shield, the linear relationship between averaged heat flux and heat production has a slope of 10km, indicating that the upper 10km are enriched relative to the entire crust.

2.6.4 Estimating the Crustal Geoneutrino Signal

Following the approach of Fiorentini et al. (2005), Huang et al. (2013) have constructed a reference model to predict the geoneutrino flux at any point of the Earth surface. They have superposed the neutrino flux from a layered mantle to that of the crust derived from the global crustal *model* CRUST2.0 from Mooney et al. (1998) with values of U and Th concentrations assigned to the various crustal layers. This reference model provides a useful starting point for interpreting geoneutrino observations. However, it may be of little practical use unless it has the required spatial resolution and accuracy. One serious problem is that the reference model is based on CRUST2.0 which is a notoriously bad *model.* Although CRUST2.0 used a compilation of seismic data, it is a *model.* A "characteristic" crustal column, consisting of 7 layers with different composition and physical properties has been established for each geological type (based on age and tectonic setting) and is assigned to each cell depending on its geology. CRUST2.0 provides a detailed crustal column for $2^o \times 2^o$ cells, which is not constrained by geophysical measurements but only inferred from the geological type. It is a gross oversimplification because it does not account for the heterogeneity of the continental crust. Globally, it fails to predict accurately the global gravity field (Tenzer et al., 2009). In Canada, a comparison between CRUST2.0 and data constrained crustal thicknesses showed a root mean square (RMS) difference of 20% (Perry et al., 2002). CRUST2.0 has been superseded by CRUST1.0 which provides similar information, but on a $1^o \times 1^o$ grid (http ://igppweb.ucsd.edu/ gabi/crust1.html). We have compared the crustal thickness of CRUST1.0 with real data from seismic studies in Ontario and Quebec and found that they differ by up to 30%. For Ontario and Quebec, the RMS difference between seismically measured and CRUST1.0 predicted crustal thicknesses is

3.9km. The error seems systematic with the mean crustal thickness from CRUST1.0 being 1.5km less than observed, possibly because Archean crustal thickness is underestimated by CRUST1.0.

It is unlikely that the reference geoneutrino flux model will be tested for more than 3 or 4 observatories in the foreseeable future, but the crustal heat production of the model with can be compared with the observed surface heat flux in stable continental regions. It is expected that the surface heat flux predicted by crustal models can only be less accurate than the estimates of crustal thickness because, the heat flux is affected by the variations in crustal thickness within a crustal type as well as variations in crustal heat production (Mareschal and Jaupart, 2004). We have compared "model predicted heat flux" with data in a stable continental region, the Canadian Shield. We calculated the mean surface heat flux in all the cells where data are available and compared it with the heat flux predicted by the CRUST1.0 crustal column (Figure 2.5). Differences between the model based estimates and the data are as large as 45% even though we tried to adjust the heat production for the different layers of the model in order to minimize these differences. One must also note that after subtracting the mantle heat flux, the relative differences between model predictions and data are even larger and reach up to 100%. The RMS difference between measured heat flux and the values predicted by CRUST1.0 is 10 mW m^{-2} in a region where the crustal component of the surface heat flux is $\approx$25mW m^{-2}, which represents a 40% error in the crustal radioactivity.

As discussed above, the geoneutrino flux differs from the gravity or heat flux fields because it is the total field that is measured, and not its vertical component. In practice, this implies that, even if their sources are identical, the geoneutrino and heat flux fields have a very different character with the long wavelengths variations being amplified in the geoneutrino flux relative to the heat flux (see Appendix in section 2).

2.6.4.1 North America and the Sudbury Neutrino Observatory

The Sudbury neutrino observatory (SNO) is located in the Creighton mine on the southern rim of the Sudbury structure which straddles the boundary between the Archean Superior Province and its PaleoProterozoic margin, the Southern Province. The structure, which is the result of a meteoritic impact at 1.8 Ga, can be described as a basin with the impact melt sheet, the Sudbury igneous complex (SIC), at the base covered by different sedimentary formations (Grieve et al., 1991; Boerner et al., 2000, and references therein). The basin owes its present elliptical shape to tectonic deformation most likely during the Grenville orogeny at 1.1Ga. The north south shortening was accompanied by thrusting of the southern part of the basin over the northern segment. The Sudbury structure is rich in mineral deposits and has been the target of intense mineral exploration activity with thousands of holes drilled almost exclusively in the Sudbury igneous complex along the rim of the structure and in offshoot dikes. The availability of so many holes offers a good opportunity to study the surface heat flux and the distribution of heat producing elements in the crust near Sudbury. Based on the limited data set available to them, Perry et al. (2009) pointed out that the high crustal radioactivity in the Sudbury region would enhance the crustal geoneutrino flux. New heat flow data have been collected and the Sudbury structure is now completely encircled by 18 heat flow sites that are located on its rims or immediately outside. Figure 2.6 shows the total crustal heat production for the Sudbury region inferred from the heat flux measurements. The crustal heat production varies between 27 and 46mW m^{-2}, with all values higher than the mean for the Superior Province. The mean crustal heat production in Sudbury is 35 mW m^{-2} compared to 24 mW m^{-2} for the entire Superior Province, $\approx$ 40% higher than the average Superior Province. The mean heat production of core samples collected at 12 heat flow sites is 1.35μW m^{-3}, which is $\approx$ 70% higher than the average surface heat production of the Superior Province (0.8μW m^{-3}) (Phaneuf and Mareschal, 2014). The regional field is constrained by heat flux data at Sturgeon Lake, 80km east of Sudbury, and at East Bull Lake and Elliot Lake, 80 and 120km to the west. In the Sudbury basin the variations in heat flux occur over relatively short dis-

tances (<20km) implying that they are due to local enrichment in heat producing elements in the upper crust near SNO.

A first order estimate of the effect of such enrichment on the geoneutrino flux could be obtained by considering that the enriched region is contained in a vertical cylinder with heat production H, thickness d and radius R. The local enrichment in heat producing element causes an increase in neutrino flux at the center, $\Delta\Phi$, can be calculated with the equation (Perry et al., 2009) :

$$\Delta\Phi = \frac{\gamma H d}{2}\left(\frac{1}{2}\log(1+\frac{R^2}{d^2})+\frac{R}{d}tan^{-1}(\frac{d}{R})\right) \tag{2.12}$$

where γ is the ratio of neutrino luminosity to heat production (for given U/Th and U/K ratios). Figure 2.7 shows the increase in neutrino flux at the center of a circular region where heat flux is higher than background as a function the radius of the cylinder. This is a crude approximation but it provides an estimate of the magnitude of the expected variations in neutrino flux. One can see that for a 25% change in the crustal heat production, which is small, over a region two crustal thicknesses in width, the neutrino flux increases by more than 10%. This estimate of the effect of enhanced crustal radioactivity in the Sudbury basin can be improved by considering detailed models of the structure (Figure 2.8). As discussed in the appendix, the main issue is that of the long wavelength variations that are still poorly constrained. This points to the difficulty of estimating the crustal geoneutrino flux in continental regions with the required precision. Even though there are now many heat flux data in the Sudbury basin, large uncertainties remain on crustal heat production at the regional scale. The highest heat flux values are found southwest of the structure at sites that are located in the Southern Province, where some sedimentary rock core samples have heat production $>3\mu$W m^{-3} . There are only a few heat flux measurements in the Southern Province, but they are all higher than the average Canadian Shield, possibly because the sedimentary rocks were derived from the enriched upper layer of the Superior Province. It is also noteworthy that there are Uranium deposits in the Southern Province including several mines in the Elliott Lake district. The effect of a large mass of U at such a distance

is negligible at SNO, but that of high radioactivity throughout the Southern Province is not. The heat production of the crust of the southern Province is one of the questions that need to be answered before the crustal geoneutrino flux can be determined for Sudbury. Other include the composition of the crust in the Superior Province north of the structure. Very high heat production values have been measured near the Cartier batholith NW of the structure (Schneider et al., 1987; Meldrum et al., 1997). Although airborne radiometric surveys underestimate the crustal radioactivity, they also indicate increased heat production W and NW of the structure (Phaneuf and Mareschal, 2014).

2.6.4.2 Estimating the Geoneutrino Flux in Eastern North America

To demonstrate the impact of the selection of a crustal radioactivity model, we have compared two different approaches to calculate the geoneutrino flux in eastern North America. We first followed the methods of Huang et al. (2013) who used the crustal structure model CRUST1.0 and assigned to each of the main crustal layers the values of radioactivity that they have estimated. Alternatively, we have calculated the crustal radioactivity from the heat flow data in regions where the lithosphere is in thermal equilibrium, thus excluding the tectonically active provinces where we used the crustal model. Details of the procedure can be found in ?Iarotsky et al. (2015b). The geoneutrino flux is measured in Terrestrial Neutrino Unit (TNU) without oscillation and for 100% efficiency. One TNU is the flux corresponding to one event per year in a 10^{32} protons detector. The map derived from the crustal model (Figure 2.9) shows only small variations in the geoneutrino flux over most of eastern Canada. In contrast, the flux calculated from heat flow (Figure 2.10) is much more variable with very low neutrino flux in the north east where crustal heat production is low (?) and high flux toward the Appalachian Province. The RMS difference between the values predicted by the two models is 10.2 TNU, compared with signals on the order of 40 TNU. These differences are relatively less than for the surface heat flux because of the smoothing effects discussed above. The standard deviation of the geoneutrino flux derived from the crustal model is 3.2 TNU, while that for the heat flow model is 7.7 TNU. This

shows that the crustal model ignores the large variations in crustal composition that are well recorded by the surface heat flux. By an extraordinary coincidence though, the difference between the two models is quite small (<3TNU) near Sudbury where the neutrino observatory is located.

2.6.4.3 The Baltic Shield and Proposed Lena Observatory

In several regions, all the available measurements indicate that the mean surface heat flux is extremely low (Table 2.9) and suggest that, because of the low crustal heat production, these regions are the most suitable for a land geoneutrino observatory if we want to minimize the crustal geoneutrino signal. The construction of an observatory at the Pyhäsalmi mine, in Finland, has been under consideration (Wurm et al., 2012). Although the reference geoneutrino flux map of Huang et al. (2013) does not show this, the heat flow map suggests that Finland may offer one of the best possible sites for geoneutrino observations. The surface heat flux is very low in the Archean provinces of the Baltic Shield (Kukkonen, 1989), with regional averages dropping to 15mW m^{-2} and the total crustal heat production being among the lowest measured in the world (Table 2.7). Near the Pyhäsalmi mine, the total crustal heat production is $\approx$ 20mW m^{-2}, about half that of the Sudbury region. This can be seen in the world heat flux map (Jaupart and Mareschal, 2008) but it is not reflected at all in the reference geoneutrino flux map of Huang et al. (2013) because the crust is thick in the Baltic Shield. We have calculated the neutrino flux for the Baltic Shield using both the crustal structure model and the heat flux data. The map of neutrino flux based on the crustal model (Figure 2.11) shows a relatively high flux ($\approx$50TNU) with little variability over the entire region. The map based on the heat flux data shows low geoneutrino flux ($\leq$30TNU) over most of the region with a trend of increasing values toward the south west. The Pyhäsalmi mine is located in the transition zone with a predicted neutrino flux of $\approx$35TNU. This is 20TNU lower than estimated from the crustal model. One obvious conclusion can be drawn from these comparisons in the Canadian and Baltic Shield . It will be necessary to elaborate very well constrained crustal heat production

models to extract useful information from geoneutrino observations.

2.7 Conclusions

Geoneutrino observations provide an opportunity to directly measure the radioactivity of the Earth's deep interior, and thus yield important information on the global energy budget and the thermal evolution of the Earth.

Because the total number of neutrino observatories will remain limited, there is a need to devise the best strategy to extract the maximum information possible from geoneutrino observations. In that regard, heat flow studies could prove extremely useful. Heat flow studies have revealed the very low concentrations of heat producing elements in the oceanic lithosphere, which is a key argument today for building a deep sea geoneutrino observatory.

So far, the continental sites that host underground neutrino observatories have been selected only for reasons of opportunity. From the heat flow perspective, none of these sites is ideally situated : Kamland and Borexino are located in tectonically active regions, which makes it impossible to determine precisely the total crustal heat production. In that regard, the location of SNO is better because it is in a tectonically stable region where the total crustal radioactivity can be determined from heat flow measurements. Unfortunately the Sudbury observatory is located in a region of high crustal heat production whose spatial extent remains insufficiently documented, which leaves a large uncertainty on the crustal contribution to the geoneutrino flux. Crustal models based on geophysical data will be useful provided that they are tested and calibrated against heat flux data, at least in stable continents.

Were low heat flow to be considered a selection criterion for future observatories, a good case could be made for the proposed Lena site, or possibly for sites in the Siberian craton, or near James Bay, in northern Ontario and Quebec.

Appendix : Neutrino and Heat Flux in Spectral Domains

The crustal heat flux field in three dimensions can be written as :

$$Q(x,y) = \int_{-\infty}^{\infty} dx' \int_{-\infty}^{\infty} dy' \int_{0}^{z_m} dz' \frac{z' H(x',y',z')}{((x-x')^2+(y-y')^2+z'^2)^{3/2}} \tag{2.13}$$

with $H(x,y,z)$ the crustal heat production. The neutrino flux field is :

$$\Phi(x,y) = \int_{-\infty}^{\infty} dx' \int_{-\infty}^{\infty} dy' \int_{0}^{z_m} dz' \frac{\gamma H(x',y',z')}{((x-x')^2+(y-y')^2+z'^2)} \tag{2.14}$$

where γ is the ratio of neutrino luminosity to heat production. To emphasize the difference between the two fluxes, we can look at the convolutions in transform domain. For sources at depth z, the 2-D Fourier transform of the heat flux Green's function is found as :

$$G_Q(k_1,k_2,z) = \int_{-\infty}^{\infty} dx \int_{-\infty}^{\infty} dy \exp(i(k_1 x + k_2 y) \frac{z}{(x^2+y^2+z^2)^{3/2}} = \exp(-|k|z) \tag{2.15}$$

with $|k| = (k_1^2+k_2^2)^{1/2}$. The transform of the neutrino flux Green's function is :

$$G_n(k_1,k_2,z) = \int_{-\infty}^{\infty} dx \int_{-\infty}^{\infty} dy \exp(i(k_1 x + k_2 y) \frac{1}{(x^2+y^2+z^2)} = K_0(|k|z) \tag{2.16}$$

where K_0 is the modified Bessel function. We see that the ratio of the spectra is :

$$\frac{G_n(k_1,k_2,z)}{G_Q(k_1,k_2,z)} = \frac{K_0(|k|z)}{\exp(-|k|z)} \tag{2.17}$$

The point is that for $|k| \to 0$, the ratio becomes arbitrarily large (although the inverse transform of the modified Bessel function still converges). The spectrum of the neutrino flux is dominated by very long wavelength (i.e., small wavenumbers) variations relative to the spectrum of the heat flux. We can also see how one could directly derive the crustal neutrino flux from the heat production in Fourier transform domain. The same type of relationship could be established on the sphere using spherical harmonics.

If the heat sources distribution can be expressed in cylindrical coordinates, the Fourier transform is replaced by the Bessel (or Hankel) transform. The Bessel transform of the heat flux Green's function is :

$$G_Q(\lambda, z) = \exp(-z\lambda) \tag{2.18}$$

where the transform variable λ can be viewed as the "wavenumber". The Bessel transform of the neutrino flux is

$$G_n(\lambda, z) = K_0(z\lambda) \tag{2.19}$$

where K_0 is the modified Bessel function, with $K_0(\lambda) \to \infty$ for $\lambda \to 0$ but the integral $\int K_0(\lambda)\lambda d\lambda$ converges. We obtain the same relationship as in the Fourier domain. We note again that the low "wavenumber" part of the neutrino spectrum is amplified by a factor $K_0(\lambda z) \times \exp(\lambda z)$ relative to the heat flux.

Acknowledgements

Thanks to Livia Ludhova for comments on a preliminary version of this paper and to Jun Korenaga for a constructive review. We are grateful to Catherine Phaneuf, John Armitage, Hélène Bouquerel, Carolyne Pickler and many others who have helped with field measurements in and around Sudbury.

Table 2.1 Estimates of the continental and oceanic heat flux and global heat loss

	continental mW m^{-2}	Oceanic mW m^{-2}	Total TW
Williams and von Herzen (1974)	61	93	43
Davies (1980)	55	95	41
Sclater et al. (1980)	57	99	42
Pollack et al. (1993)	65	101	44
Jaupart et al. (2014)†	65	94	46
Davies and Davies (2010)	71	105	47

† The average oceanic heat flux does not include the contribution of hotspots. The total heat loss estimate includes 3TW from oceanic hotspots.

Table 2.2 Some estimates of bulk continental crust heat production $< A >$, of the crustal component of heat flux for a 41km thick crust $< Q_c >$, and of the total heat production of the continental crust

$< A >$ μW m^{-3}	$< Q_c >$ mW m^{-2}	TW	Reference
0.74-0.86	30-35	6.4-7.4	Allègre et al. (1988) ; O'Nions et al. (1979)
0.83	34	7.1	Furukawa and Shinjoe (1997)
0.92	38	8.0	Weaver and Tarney (1984)
0.58	24	5.0	Taylor and McLennan (1995)
2.31	54	11.3	Shaw et al. (1986)
1.25	51	11.1	Wedepohl (1995)
0.93	38	8.0	Rudnick and Fountain (1995)
0.70	29	6.1	McLennan and Taylor (1996)
0.55-0.68	23-29	4.8-6.1	Gupta et al. (1991)
0.94	39	8.2	Nicolaysen et al. (1981), Jones (1988)
0.84-1.15	34-47	7.1-9.8	Gao et al. (1998)
0.70	29	6.1	Jaupart et al. (1998)
0.79-0.99	32-40	6.8-8.2	Jaupart and Mareschal (2014)

Table 2.3 Radio-element concentration and heat production in meteorites, in the Bulk Silicate Earth, in Earth mantle and crust

	U (ppm)	Th (ppm)	K (ppm)	A* (pW kg^{-1})
CI Chondrites				
Palme and O'Neill (2003)	0.008	0.030	544	3.5
McDonough and Sun (1995)	0.007	0.029	550	3.4
EH Chondrites				
Wasson and Kallemeyn (1988)	0.009	0.030	/	
Bulk Silicate Earth				
From CI Chondrites				
Javoy (1999)	0.020	0.069	270	4.6
From EH Chondrites				
Kaminski and Javoy (2013) †	0.018 ± 0.001	0.060 ± 0.003	217 ± 11 ‡	4.0 ± 0.2
From Chondrites and Lherzolites trends				
Hart and Zindler (1986)	0.021	0.079	264	4.9
From Elemental Ratios and Refractory Lithophile Elements abundances				
McDonough and Sun (1995)	$0.020 \pm 20\%$	$0.079 \pm 15\%$	$240 \pm 20\%$	4.8 ± 0.8
Palme and O'Neill (2003)	$0.022 \pm 15\%$	$0.083 \pm 15\%$	$261 \pm 15\%$	5.1 ± 0.8
Lyubetskaya and Korenaga (2007)	$.017 \pm 0.003$	$.063 \pm 0.011$	190 ± 40	3.9 ± 0.7
Jackson and Jellinek (2013)	0.014 ± 0.003	0.055 ± 0.011	166 ± 30	3.4 ± 0.5
Depleted MORB source				
Workman and Hart (2005)	0.0032	0.0079	25	0.59
Average MORB mantle source				
Su (2000); Langmuir et al. (2005)	0.013	0.040	160	2.8
Peridotites	0.006	0.02	100	1.5
Continental crust				
Rudnick and Gao (2003)	1.3	5.6	$1.5\ 10^4$	330
Jaupart and Mareschal (2014)	/	/	/	293 - 352

† U and Th values deduced from the Ca concentration and the chondritic U/Ca and Th/Ca ratios. ‡ calculated from the U value and $K/U = 12{,}000$.

Table 2.4 Mantle energy budget, preferred value and range. The distribution in the range is barely known for most cases and the preferred value is simply the middle one. The cooling rate is computed assuming $C_P = 1200 \mathrm{JK}^{-1}\mathrm{kg}^{-1}$.

	TW	TW
Oceanic Heat Loss ($300 \times 10^6 \mathrm{km}^2$)	32	30 - 34
Continental Heat Loss ($210 \times 10^6 \mathrm{km}^2$)	14	13 - 15
Total Surface Heat Loss ($510 \times 10^6 \mathrm{km}^2$)	46	43 - 49
Radioactive sources (mantle+crust)	18	13 - 21
Continental heat production (crust + lith. mantle)	8	7 - 8
Heat flux from convecting mantle	38	35 - 41
Radioactive heat sources (convecting mantle)	11	5 -14
Heat from core	11	5 - 17†
Tidal dissipation in solid earth	0.1	
Gravitational energy (differentiation of crust)	0.3	
Total input	22	14 - 31
Net loss (mantle cooling)	16	4 - 23
Present cooling rate, K Gy^{-1}	106	27–180
Present Urey ratio‡	0.29	0.12–0.40

† This range includes estimates from core thermodynamics and inference from the perovskite–post-perovskite phase diagram.

‡ Urey ratio for the convecting mantle, leaving out crustal heat sources from both the heat loss and heat production.

Table 2.5 Various estimates of the global budget

	Stacey and Davis (2008)	Davies (1999)	Jaupart et al. (2014)
Total heat loss	44	41	46
Continental heat production	8	5	8
Upper mantle		1.3	
Lower mantle		11-27	
Mantle heat production	20	12-28‡	11
Latent heat -Core differentiation	1.2	<1	
Mantle differentiation	0.6	0.3	0.2
Gravitational (Thermal contraction)	3.1		
Tidal dissipation		0.1	0.1
Core heat loss	3.5	5	11
Mantle cooling	8	9†	16
Present Urey ratio	0.64	0.3 – 0.68	0.12–0.49

† Mantle cooling is fixed

‡ Lower mantle heat production is variable and calculated to fit the mantle cooling rate.

Table 2.6 Estimates of bulk continental crust heat production from heat flow data (Jaupart and Mareschal, 2014)

Age group	A^a μW m^{-3}	Q_C^b mW m^{-2}	% Area [c]
Archean	0.56-0.73	23-30	9
Proterozoic	0.73-0.90	30-37	56
Phanerozoic	0.95-1.21	39-50	35
Total Continents	0.79-0.99	32-40	100

[a] range of heat production in μW m^{-3}
[b] range of the crustal heat flux component in mW m^{-2}
[c] Fraction of total continental surface, from Model 2 in Rudnick and Fountain (1995)

Table 2.7 Regional variations of the heat flux in different cratons. Minimum and maximum values obtained by averaging over 200km×200km windows

	minimum	maximun
	mW m^{-2}	
Superior Province	22	48
Trans Hudson Orogen	22	50
Australia	34	54
Baltic Shield	15	39
Siberian Shield	18	46

Table 2.8 Various estimates of the heat flux at Moho in stable continental regions (Jaupart et al., 2014)

location	heat flux ($mW\ m^{-2}$)	reference
Norwegian Shield	11 †	(Swanberg et al., 1974; Pinet and Jaupart, 1987)
Baltic Shield	7-15 ‡	(Kukkonen and Peltonen, 1999)
Siberian craton	10-12 †	(Duchkov, 1991)
Dharwar craton (India)	11 †	(Roy and Rao, 2000)
Kapuskasing (Canadian Shield)	11-13 †	(Ashwal et al., 1987; Pinet et al., 1991)
Grenville (Canadian Shield)	13 †	(Pinet et al., 1991)
Abitibi (Canadian Shield)	10-14 †	(Guillou et al., 1994)
Trans-Hudson orogen (Canadian Shield)	11-16 †∗	(Rolandone et al., 2002)
Slave province (Canada)	12-24 ‡	(Russell et al., 2001)
Vredefort (South Africa)	18 †	(Nicolaysen et al., 1981)
Kalahari craton (South Africa)	17-25 ‡	(Rudnick and Nyblade, 1999)

† Estimated from surface heat flux and crustal heat production

∗ Estimated from condition of no melting in the lower crust at the time of stabilization

‡ Estimated from geothermobarometry on mantle xenoliths

Table 2.9 Low heat flow regions in the world. $< Q >$ is the mean surface heat flux, $< H >$ the mean surface heat production

Region	Province	Age Gy	$< Q >$ (mW m^{-2})	$< H >$ (μW m^{-3})	Reference
Lynn Lake Belt	THO (Canada)	1.8	22	0.7	Mareschal et al. (2005)
Voisey Bay	Nain Plutonic Suite (Canada)	1.4	22	0.7	Mareschal et al. (2000)
	Baltic Shield	2.5	22-28		Kukkonen and Joehlet (1996)
	Siberian Shield	2.5	21	-	Duchkov (1991)
Niger	West Africa Shield		17-22	-	Chapman and Pollack (1974)
Tagil-Magnitogorsk	Urals	0.4	25	0.3	Kukkonen et al. (1997)

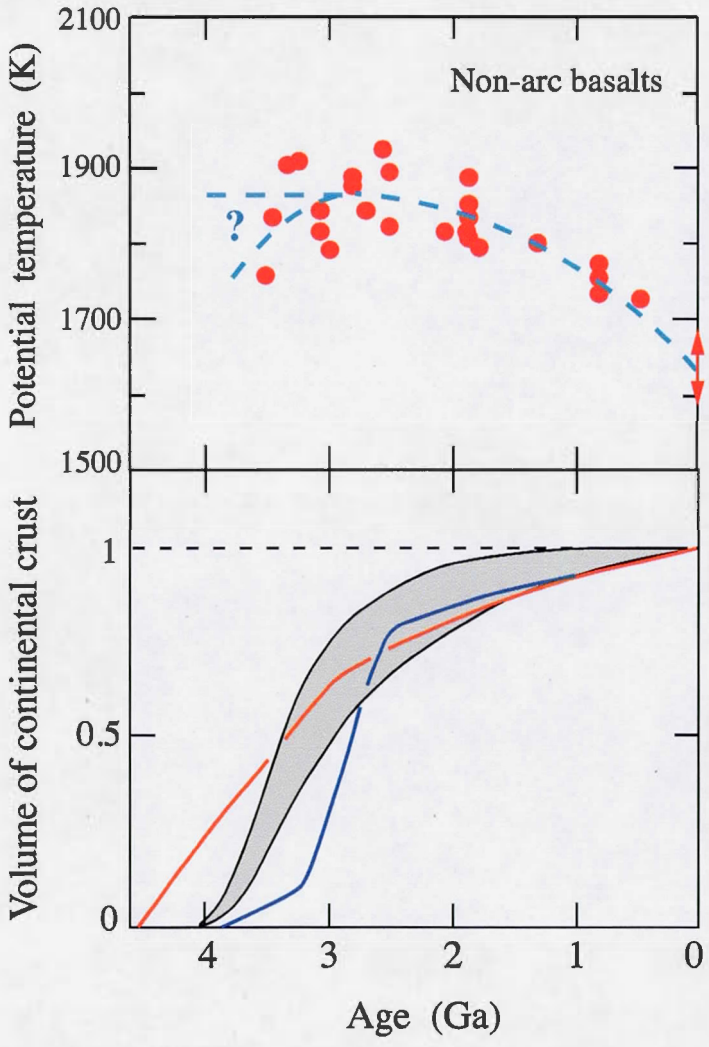

Figure 2.1 Two variables that illustrate the secular evolution of the Earth. (Top) Potential temperature of the bulk mantle, based on petrological data, as a function of age, but plotted forward in time, from Herzberg et al. (2010). The vertical arrow at zero age indicates the temperature range obtained by completely different methods, from Jaupart and Mareschal (2011). Dashed curves indicate possible trends through noisy data. These data suggest that temperature did not change appreciably between *ca.* 3.5 and 2.5 Ga. (Bottom) Volume of continental crust normalized to the present-day value as a function of age from various sources. Shaded domain from Pujol et al. (2011), red curve from Dhuime et al. (2012) and dark blue curve from Taylor and McLennan (1995). Note that temperature begins to go down when the rate of continental growth is small.

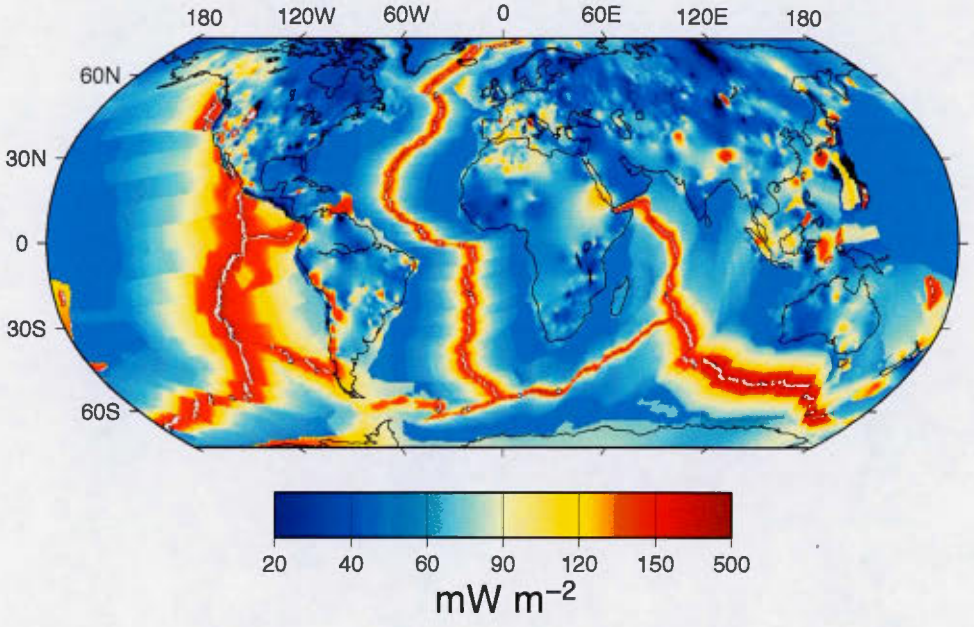

Figure 2.2 World heat flow map combining continental heat flux measurements in the continents and plate cooling model for the oceans.

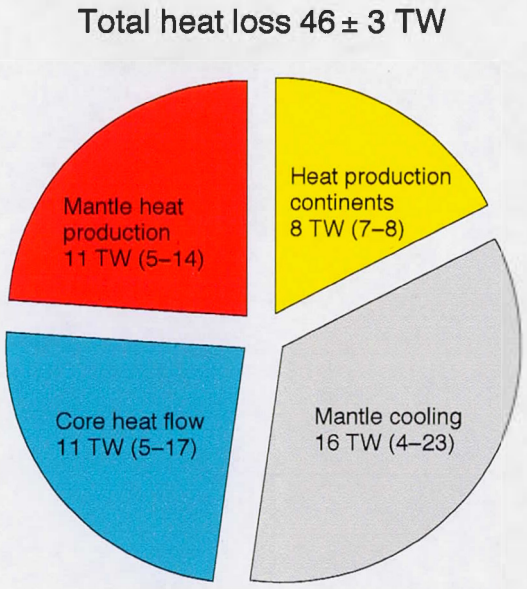

Figure 2.3 Breakdown of the present energy budget of Earth from Jaupart et al. (2014). Note that the mantle cooling component is estimated by subtracting the other components from the surface heat flow, resulting in a large uncertainty.

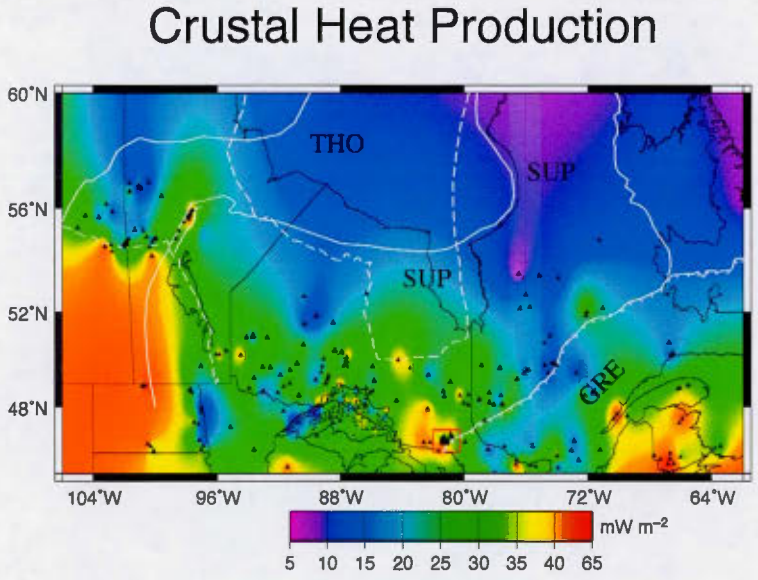

Figure 2.4 Crustal heat production map of the southeastern Canadian Shield. Total crustal heat production was calculated by subtracting constant 15mW m^{-2} value of Moho heat flux from measured surface heat flux. White lines mark boundaries of geological provinces (SUP : Superior, THO : Trans Hudson Orogen, GRE : Grenville, APP : Appalachians). The dashed white lines mark the limits of Paleozoic sedimentary cover. The red box is the Sudury region enlarged in Figure 2.6.

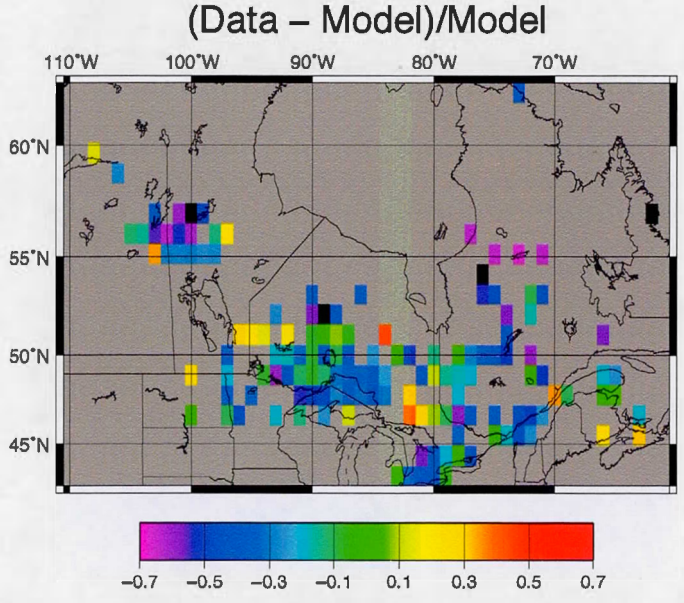

Figure 2.5 Difference between observed surface heat flux in the south eastern part of the Canadian Shield and the values estimated from CRUST1.0 with the layered crustal composition model of Huang et al. (2013).

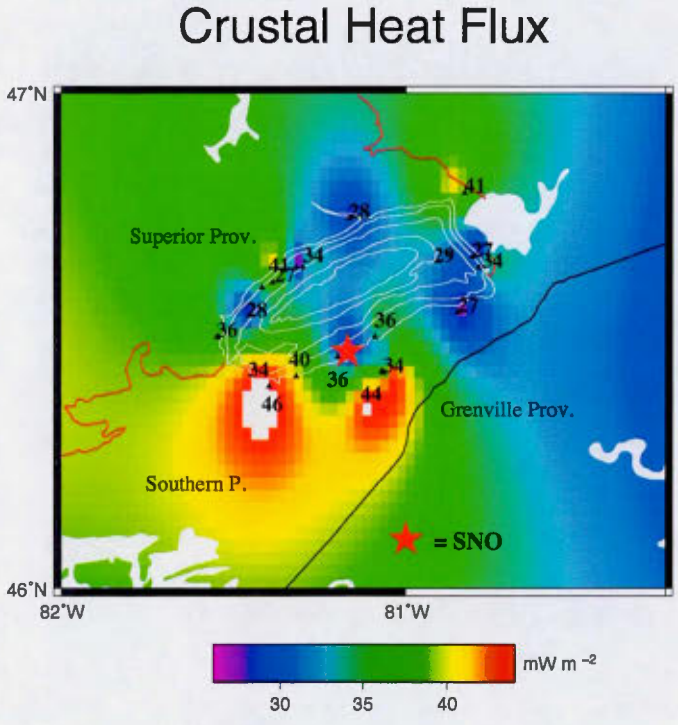

Figure 2.6 Crustal heat production map for the Sudbury region. Note that the lowest values on the map are higher than the mean heat production in the Superior and Grenville provinces. The black line shows the Grenville Front. White lines outline the boundaries of the different formations in the Sudbury Basin. The red line marks the boundary between the Southern and the Superior Provinces. The red star shows the location of SNO.

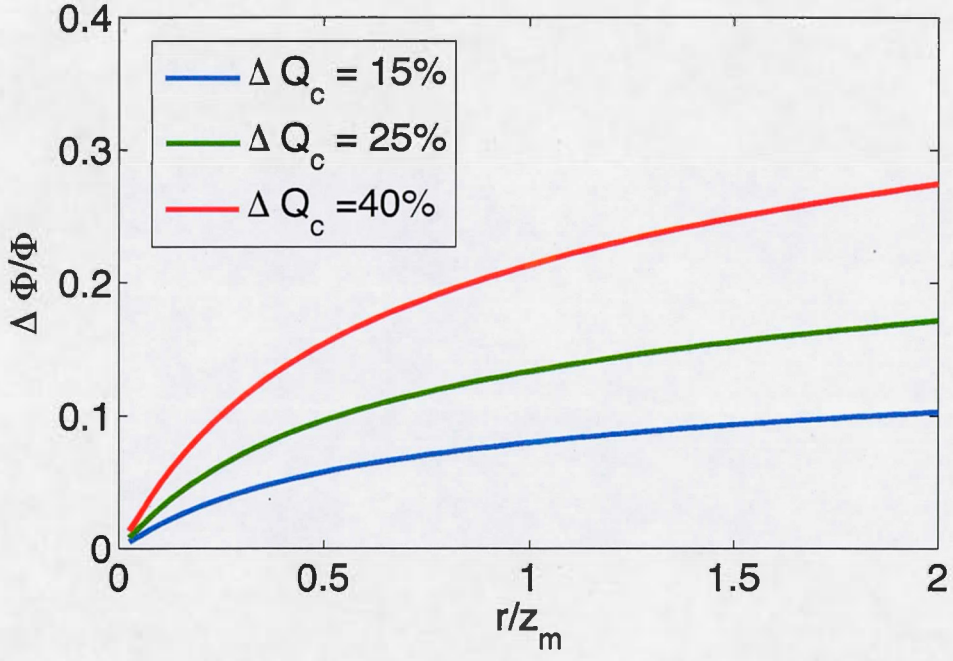

Figure 2.7 Relative increase in neutrino flux at the center of a region where crustal heat production is higher than background as a function of the radius of the anomaly (relative to crustal thickness z_m). ΔQ_c is the relative increase in surface heat flux. The thickness of the enriched layer is 1/4 the crustal thickness.

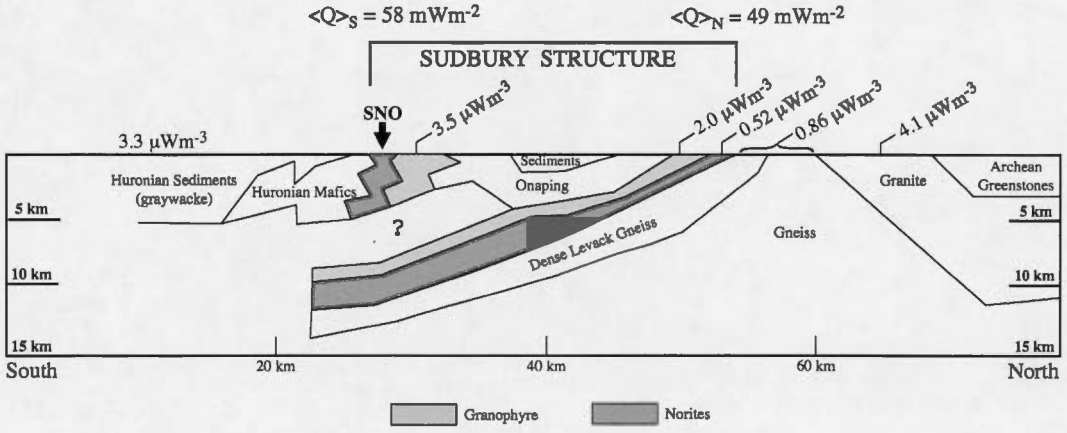

Figure 2.8 North-South section of the Sudbury Structure inferred from seismic, gravity, and magnetic data. SNO is located near the south rim of the structure where heat flux and crustal heat production are highest.

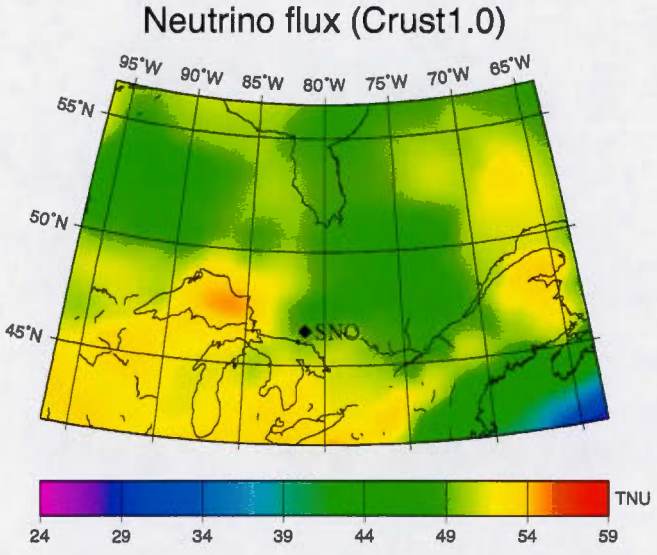

Figure 2.9 Crustal geoneutrino flux in eastern Canada estimated from CRUST1.0 crustal structure model with concentrations of heat producing elements proposed by Huang et al. (2013). The geoneutrino flux is given in Terrestrial Neutrino Unit (TNU) without oscillations and for 100% efficiency. A flux of one TNU corresponds to one event per year in a 10^{32} protons detector. The black diamond shows the location of the SNO.

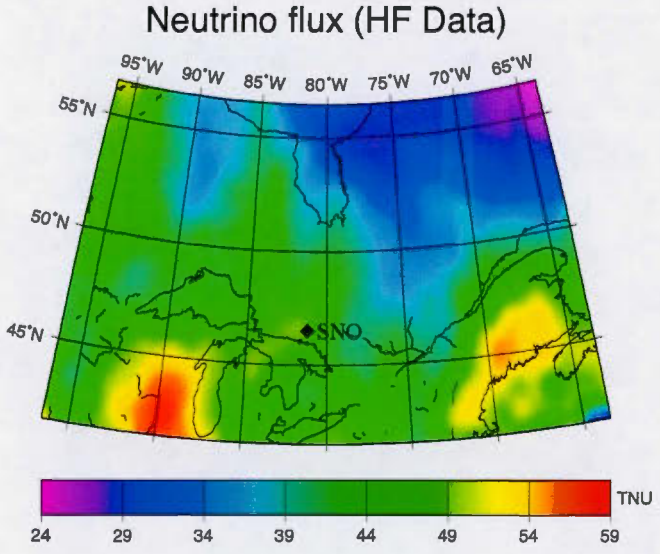

Figure 2.10 Crustal geoneutrino flux in eastern Canada estimated from heat flow data The total crustal radioactivity is the difference between mean surface heat flux and mantle heat flux ($\approx$ 15mW m^{-2}) in stable continental regions. For tectonically active regions, crustal radioactivity is estimated from crustal thickness. The flux is in TNU without oscillations and for 100% efficiency. The black diamond shows the location of the SNO.

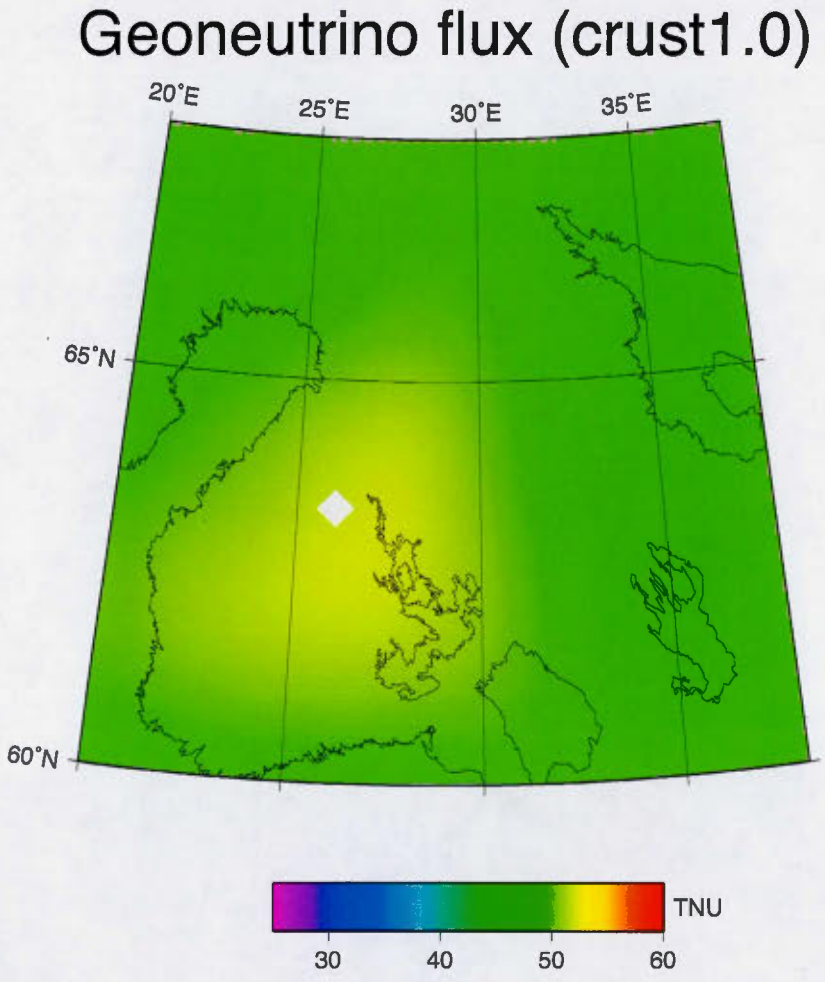

Figure 2.11Crustal geoneutrino flux map for central Finland estimated from CRUST1.0. Flux in TNU without oscillations for 100% efficiency. The white diamond shows the location of the Pyhäsalmi mine, one of the proposed sites for Lena.

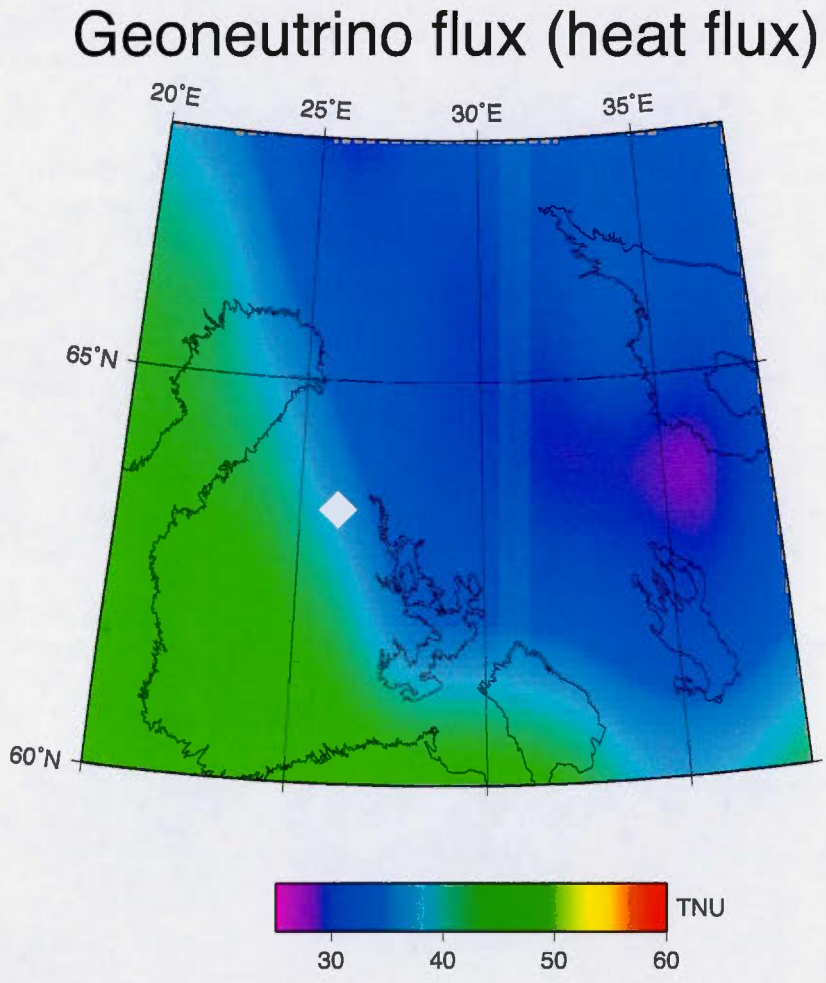

Figure 2.12 Crustal geoneutrino flux map for central Finland estimated from heat flow data. Flux in TNU without oscillations for 100% efficiency. The white diamond shows the location of the Pyhäsalmi mine, one of the proposed sites for Lena.

3

The Effect of Internal Heating of the Continental Lithosphere

In order to understand at how continental crust was formed, we investigate the thermal effects of belts accreting at the margins of continents. During continental accretion events, belts of crustal material assemble together to form larger crustal blocks. We were interested in the effect of heat producing elements on the temperature profiles in the lithosphere and how it affected crustal growth during the Archean.

The temperature is a key factor that controls partial melting and metamorphism in the crust and lithosphere. Looking at the temperature profiles and the temperature at the Moho informs us on the presence of the thermal alterations in the rocks. The most important ele-

ment affecting temperature in the lithosphere is the vertical distribution of heat production. In this section, we are investigating the effect of the distribution of heat producing elements on temperature profiles and Moho temperature.

To calculate the temperature profile we used a simple model of the lithosphere where the heat producing elements are distributed in the crust while the lithospheric mantle produces no heat.

The vertical differentiation of radioactive elements is measured by the differential index(DI). We consider the crust as an infinite horizontal layer for calculating the effect of DI and crustal thickening. We also use crustal belts of finite width to mode the lateral accretion and the effect of the depth of an enriched layer.

3.1 Effect of the Differentiation Index

The differentiation index DI ratio discussed in chapter 1 section 1.6.3.2 and in chapter 2 section 2.6.3 is the ratio of the surface over average crustal heat production. A DI greater than one means that the surface heat production is higher than the crustal average which implies a faster heat evacuation. We calculated the Moho temperature for different DIs and average heat productions. The effect of the DI and average heat production on Moho temperatures can be observed in figure 3.2.

We can see that the temperatures reached at the Moho decreases with increacing DIs. In other words, the more differentiated crust, the cooler. Higher average heat production increases temperature throughout the lithosphere. The effect of both the DI and average heat production increase with crustal thickness. The increase is smaller for the DI than the average heat production.

Considering an crust of two layers with an enriched upper layer of 12 km, we looked at the lower crustal heat production A_{low} for a known surface heat production.

$$A_{low} = A\left(\frac{z_m - DI \times 12km}{z_m - 12km}\right) \tag{3.1}$$

Where A is the average heat production, z_m is the Moho depth and DI is the differentiation ratio. We calculated A_{low} for a range of differentiation indexes and average heat productions in figure 3.3. We see that the DI has a large effect on the lower crustal heat production for thin crust. Heat production is less important for large DI and for thin crust. For a crust thicker than 45 km the effects of the DI and the average heat production are equally important. For thin crust, the DI is more important than the average heat production.

3.2 Continental Growth

We also wanted to see how the temperature profile would vary considering changes in crustal geometry that occur during continental growth.

With the models illustrated in figure 3.5, we calculated a the effect of the width of an enriched belt and crustal thickening on the temperature profile in the lithosphere.

3.2.1 Lateral Growth of Continental Crust

Assuming a two-dimensional (2D) model extending at infinity in the direction perpendicular to the models cross section, we calculated the temperature field with equation A.1.

The cross section of the temperature field of a belt enriched in heat producing elements is shown in figure 3.4a for a belt with a half width of 100km. This is compared to the temperatures obtained with a belt twice as wide 3.4b. We show only the temperature contributed by heat production in the crust. In other word we are not adding the contribution of the mantle heat flux.

We see that the heat is conducted towards the surface but the lithosphere beneath the

crust is also heated. For a wider belt, the maximum temperature reached is significantly higher and the heating is deeper. In the uppermost layer of the crust, there is no significant difference other than the increase in temperature gradient. All of the above observations can be made by looking at the center of the crustal belt.

We have compared vertical temperature profiles at the centers of belts of an range of half widths between 10 and 200 km in figure 3.6. We see that the depth of the maximal temperature reached increases with width until 100km of half width and remain nearly constant for wider belts while the maximum temperature remains above the Moho. Thus the maximum effect of radiogenic heating occurs within the crust.

The complete temperature profile is obtained by adding the mantle heat flux component in figure 3.7. We see that for a belt larger than 300km the temperatures at the Moho reach exceed 800°C which is above the melting point of most crustal rocks.

The radiogenic heating heating of the crust causes differentiation which is a most effective cooling mechanism.

Radioactive elements are poorly fitted in the crustal crystalline mesh. Thus, melts, partial melts and hight temperature metamorphism in the crust result in a upward redistribution of heat producing elements. As seen in the previous section, the increased differentiation reduces the temperature profile.

3.2.2 Crustal Thickening

For a surface temperature of 0°C the vertical temperature profile in an infinite horizontal heat producing layer (the crust) is given by :

$$T(z) = \frac{q_s z}{\lambda} - \frac{A z^2}{2\lambda}, \tag{3.2}$$

where q_s is the surface heat flux, A is the heat production and λ is thermal conductivity. The temperature in the underlaying mantle is given by :

$$T(z) = T_m + \frac{q_m(z - z_m)}{\lambda}, \tag{3.3}$$

where T_m is the Moho temperature, q_m is the mantle heat flux and z_m in the Moho depth. The steady state temperature profile for a 40 km crust is shown in green in figure 3.8. We then strechted vertically the lithosphere to double its thickness maintaining the same Moho temperature to obtain the blue profile which is not in equilibrium. The temperature profile for the 80 km crust in steady state is the red curve in the graph. We note that the two steady state lines have the same mantle gradient. The two 80km plot line change their regime at the same depth.

For an average heat production in the Archean of $A = 1.6\mu\text{W m}^{-3}$ we obtain the temperature profiles of crusts of 30 to 80 km thick in thermal equilibrium (figure 3.9). The 800°C isotherm goes above the Moho when crustal thickness exceeds 37.5 km. In other words, in the Archean, a non differentiated crust of 40 km, would melt at its base. The melting redistributes heat producing elements, increasing the DI thus reducing the lithospheric temperatures.

Similarly, for the present average heat production of $A = 0.8\mu\text{W m}^{-3}$, an undifferentiated crust cannot exceed 50 km without having partial melts.

All in all, continental growth, whether it is by accretion or thickening, will increase crustal temperatures, cause melting and an upward redistribution of heat producing elements, thus a higher DI and a cooler hence more rigid lithosphere. Any growth induces differentiation as a cooling process and any stable crust must be cold enough to support itself. In other words, stable continental crust must be differentiated or have low heat production. Hence heat production in the crust can be imposes an upper limit on the thickness of a stable crust.

3.3 Depth of enriched layer

In a differentiated crust, the enriched layer is generally a $\approx$ 10 km thick upper crust and is situated near the surface. In various tectonic settings especially in the case of continental collisions, the enriched layer can be at greater depth.

We put a 10km thick heat producing layer at various depths within the crust to investigate how it impacts the temperature profiles at the center of a 200 km wide crustal lithosphere. In figure 3.11 the temperature is calculated without the mantle heat flux contribution. Thus as seen in the previous section the maximal temperature should be reached within the heat producing layer. With increasing depth of the layer, heat conduction towards the surface will occur over larger distance causing the temperatures to be higher for deeper enriched layers.

We see that the deeper heat producing layers increase the temperature more the the superficial ones. Hence, events causing a heat producing layer to be at great depth will cause greater temperature growth resulting as seen before in vertical redistribution of heat producing elements towards the surface.

3.4 Conclusion

Inside the lithosphere, temperatures get higher with increasing heat production in the crust and get lower with increasing crustal differentiation index. Crustal heat production raises lithospheric temperatures during continental growth. Heat producing elements at depth raise the temperature profiles more than superficial radiogenic materials. Every phenomenon leading to temperature increase leads to upward redistribution of heat producing elements and cooling of the lithosphere. These conclusions are discussed at length in the following chapter.

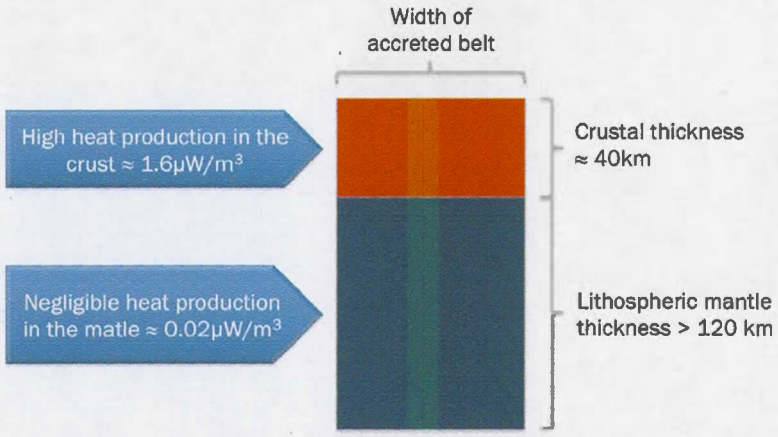

Figure 3.1 An illustration of the structure of the model used to calculate the temperature profiles.

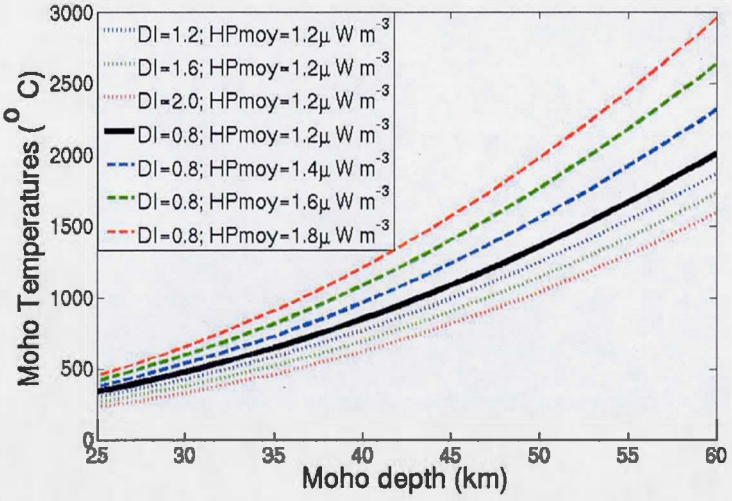

Figure 3.2 Moho temperatures as a function of crustal thickness for different DI and heat production.

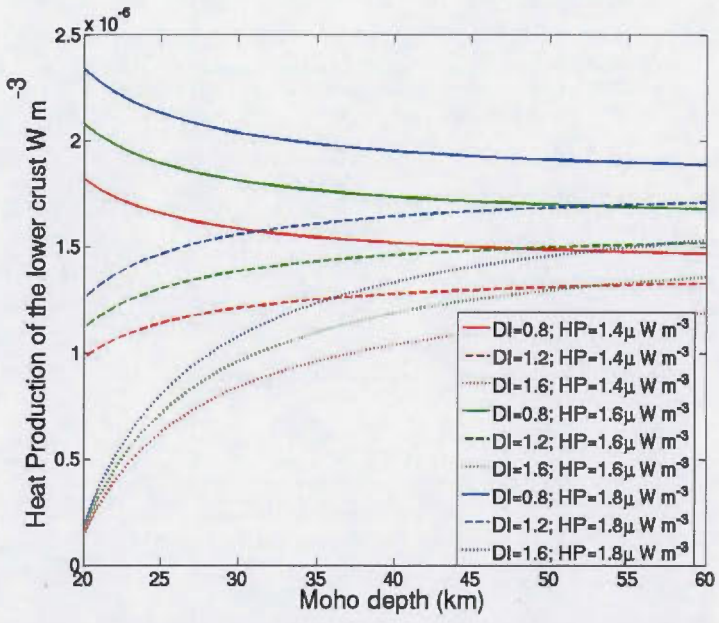

Figure 3.3 Heat production of the lower crust as a function of crustal thickness for varying DI and surface heat production.

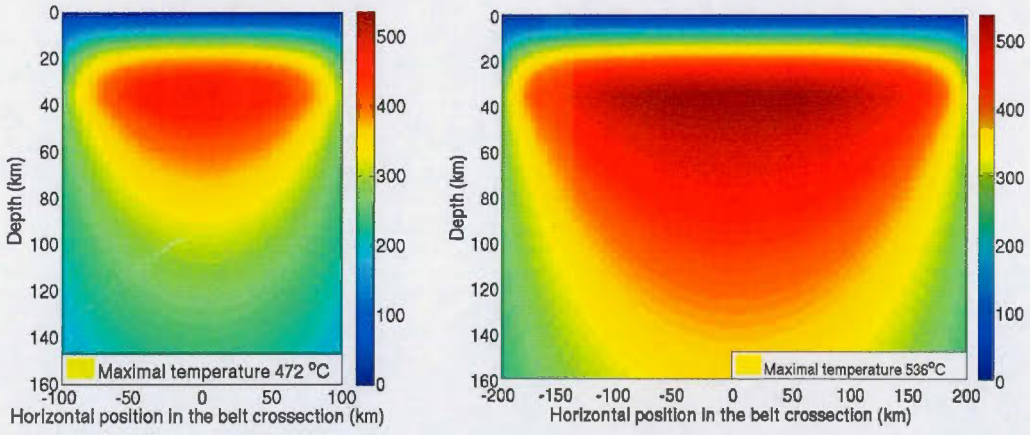

(a) (b)

Figure 3.4 Temperature field contributed by crustal heat producing elements : cross sections for a 2D crustal belt of infinite length, 40 km thick and 200 km wide in (a) and 400km wide in (b).

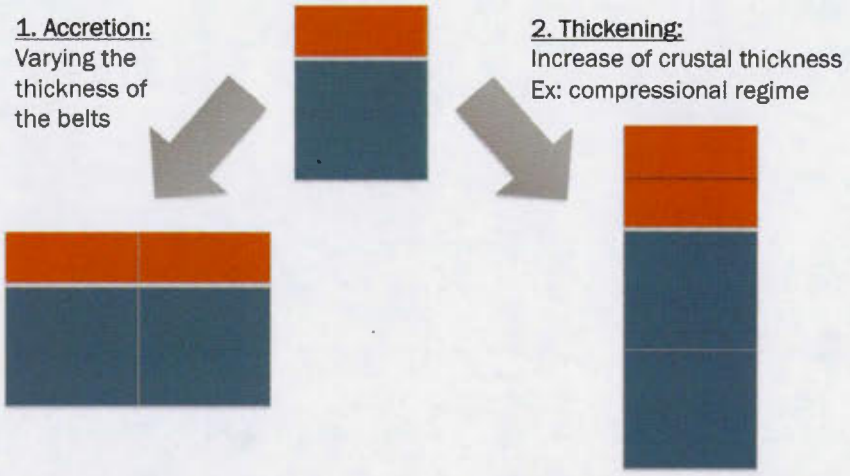

Figure 3.5 An illustration of the crustal structure variation that have been considered.

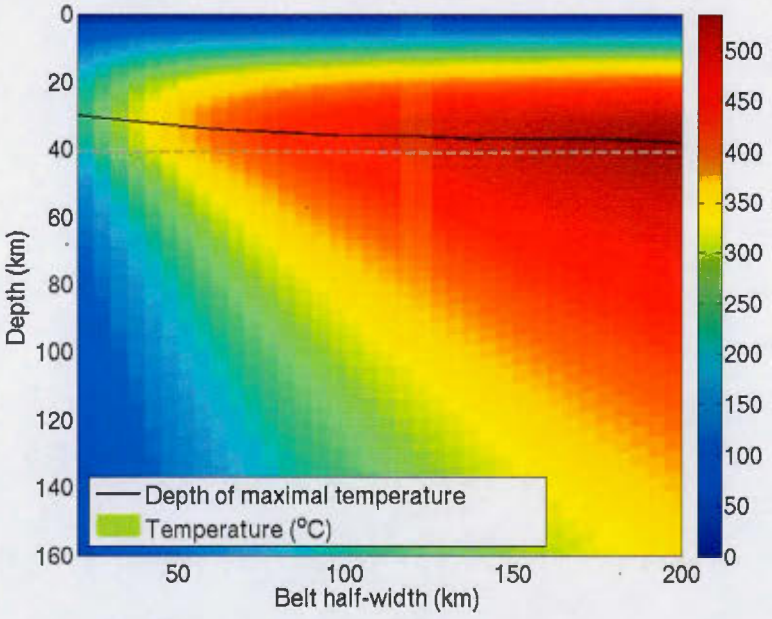

Figure 3.6 Temperature contributed by heat production profiles at the centers of belts as a function of their half width. The Moho is represented by the dotted grey line. The depth of the maximal temperature is represented by the black line.

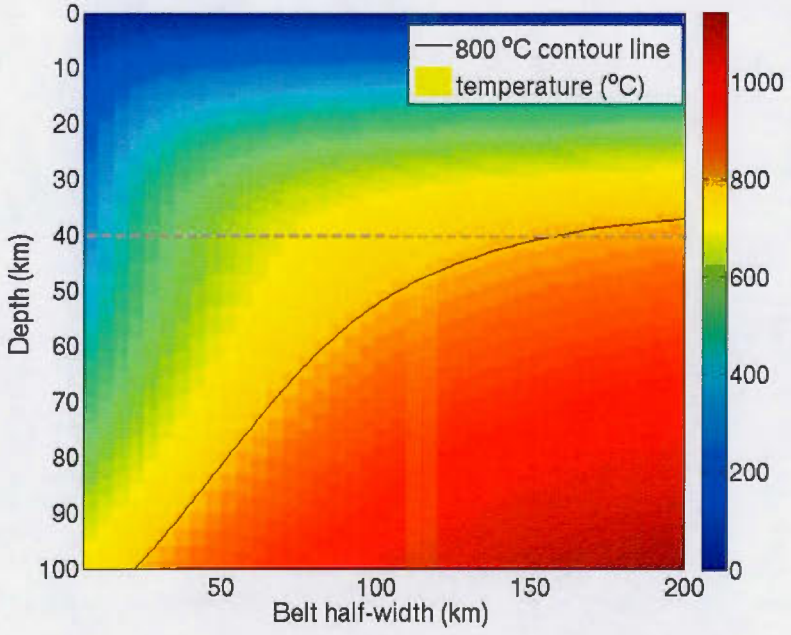

Figure 3.7 Vertical temperature profiles at the centers of belts as a function of their half width. The Moho is represented by the dotted grey line. The black line is the 800°C isotherm.

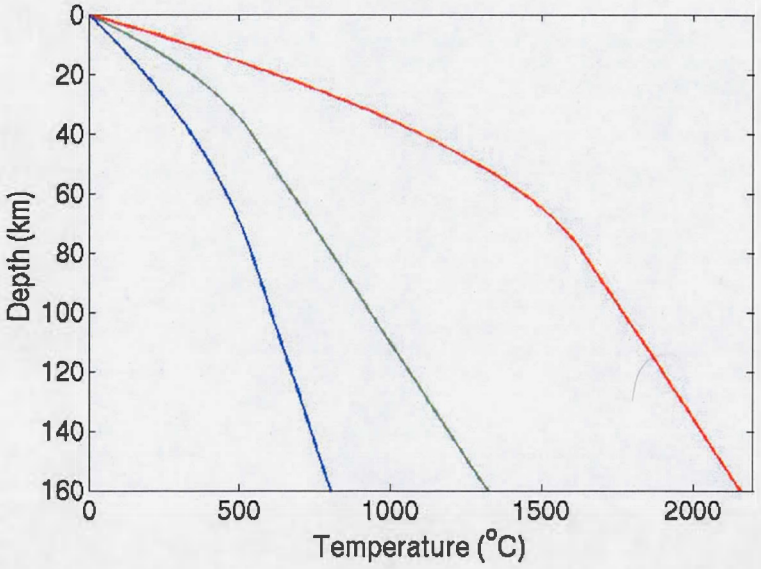

Figure 3.8 Temperature profiles for doubling the thickness. Green : 40km steady state crustal initial condition. Blue : instantaneous thickening of the lithosphere not in equilibrium. Red : 80km crust after it returns to steady state

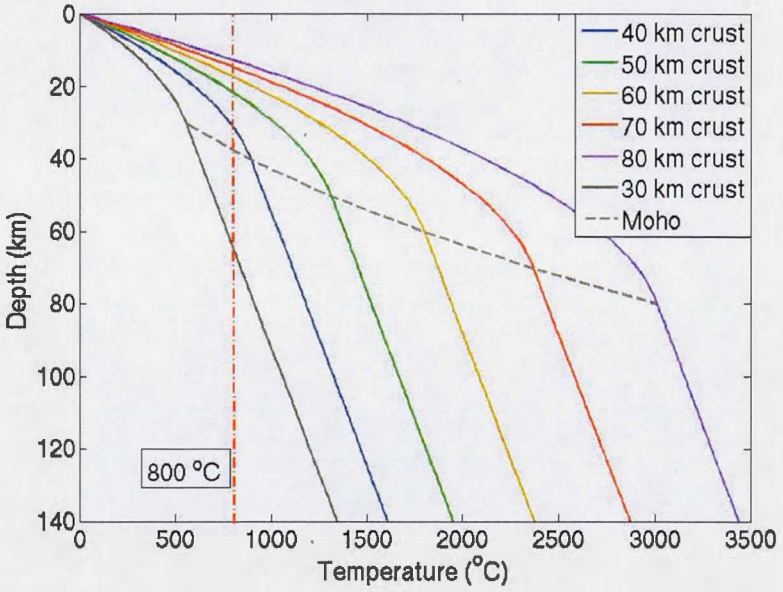

Figure 3.9 Temperature profiles as a function of crustal thickness with Archean average heat production. The Moho is represented by the dashed grey line. The red dashed line follows the 800°C isotherm.

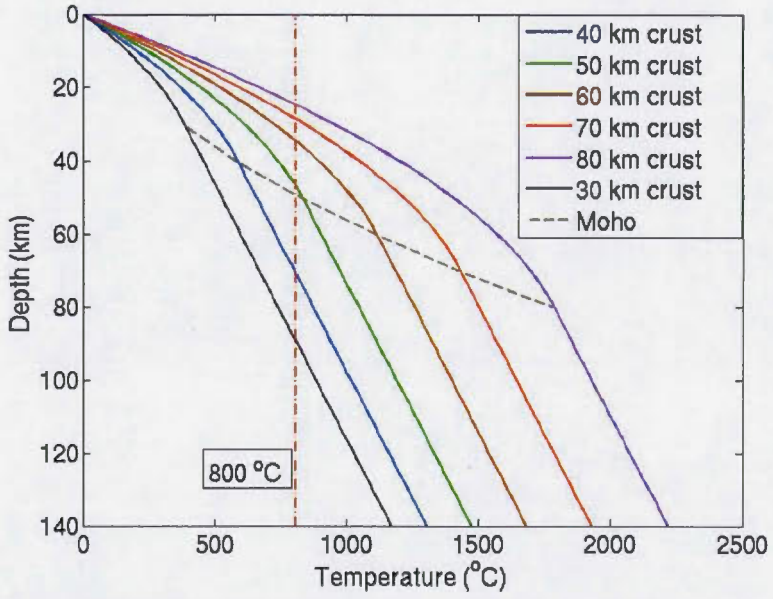

Figure 3.10 Temperature profiles as a function of crustal thickness with present day average heat production. The Moho is represented by the dashed grey line. The red dashed line follows the 800°C isotherm.

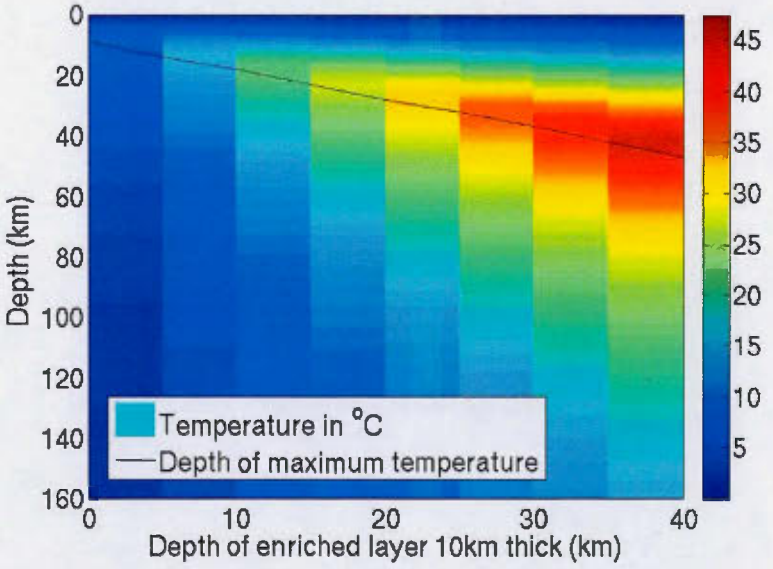

Figure 3.11 Temperature profiles as a function of depth of the enriched crustal layer.

4

Radiogenic Heat Production in the Continental Crust

Claude Jaupart *Institut de Physique du Globe de Paris, France*

Jean-Claude Mareschal *GEOTOP, University of Quebec, Montreal, Canada*

Lidia Iarotsky *GEOTOP, University of Quebec, Montreal, Canada*

Jaupart C., Mareschal, J.C., Iarotsky L., 2016. Radiogenic Heat Production in the Continental Crust, Lithos 262, 398-427, doi :10.1016/j.lithos.2016.07.017

Abstract

The thermal structure and evolution of continents depend strongly on the amount and distribution of radioactive heat sources in the crust. Determining the contribution of crustal rocks beneath a superficial layer is a major challenge because heat production depends weakly on major element composition and physical properties such as seismic wavespeed and density. Enriched granitic intrusives that lie at the current erosion level have a large impact on the surface heat flux but little influence on temperatures in the deep crust. Many lower crustal rocks that are poor in heat producing elements are restites from ancient orogenic events, implying that enrichment of the upper crust was achieved at the expense of deeper crustal levels. For the same total amount of heat sources, formation of an enriched upper layer at the expense of deeper crust acts to reduce temperatures in the lower crust, thereby allowing stabilization of the crust. The present-day structure of the crust is thus a consequence of orogeny and should not be adopted for thermal models of the orogenic event itself.

Analysis of global and regional data sets reveals the absence of a positive correlation between surface heat flow and crustal thickness, showing that the average crustal heat production is not constant. Differences of heat flow between geological provinces are due in large part to changes of crustal structure and bulk composition. Collating values of the bulk crustal heat production in a few age intervals reveals a clear trend of decrease with increasing age. This trend can be accounted for by radioactive decay, indicating that thermal conditions at the time of crustal stabilization have not changed significantly. For the average crustal thickness of 40 km, Moho temperatures are near solidus values at the time of stabilization, suggesting an intrinsic thermal control on crustal thickness and heat production distribution. Crustal thickening by more than about 10 km above this mean value induces changes of gravitational potential energy that exceed the strength of the lithosphere.

For several provinces where strong constraints on heat production are available, it is shown that, prior to intracrustal fractionation, only modest amounts of thickening were

needed to generate the conditions of ultra-high temperature metamorphism. The tell-tale signature of crustal heat production is anatectic and metamorphic events that lag the cessation of orogenic activity by several tens of million years.

The radioactive decay of crustal heat sources is responsible for the secular cooling of lithospheric roots at a typical rate of about 100K Gy^{-1}, implying complex thermal interactions with a convecting mantle that is not cooling at the same rate.

This review summarizes information extracted from large data sets on heat flow and heat production and provides estimates of crustal stratification and heat production in several geological provinces.

Keywords

Cratons || Lithosphere || Heat flow || Crustal heat production || Crustal evolution ||

High temperature metamorphism || Post orogenic metamorphism

4.1 Introduction

In the last few decades, physical models of geological phenomena have become increasingly detailed and have been used to account for the timing and characteristics of thermal events as well as for the rates of tectonic deformation. Model outputs critically depend on thermal structure and evolution. A comprehensive overview of such models past and present is not available but it is fair to say that thermal properties and variables have received much less attention than geodynamic processes such as mantle plumes and lithospheric instabilities for example. Thus, there has been a tendency to attribute the failure of a model to an erroneous geodynamic setting rather than to incorrect choices of physical parameters. In this context, it is worth emphasizing the fundamental difference between properties such as thermal conductivity and heat capacity on the one hand and radiogenic heat production on the other hand. The former are intrinsic mineral properties that are independent of the

geological setting. They vary within restricted ranges and can be specified with little error without detailed knowledge of local conditions. The latter, in contrast, depends weakly on rock type and major element composition and must be determined on a case by case basis (Fountain, 1986; Kukkonen and Peltoniemi, 1998; Slagstad, 2008).

There can be no doubt that heat released by radioactive decay in crustal rocks accounts for a large fraction of the surface heat flux and strongly affects the thermal regimes of both crust and lithosphere (England and Thompson, 1984; Jaupart et al., 1998; Sandiford et al., 2002; Mareschal and Jaupart, 2013). In spite of this, heat production data are rarely considered as an important part of geophysical studies and are not systematically collected with heat flow measurements. For example, a global compilation of heat flow data contains more than 17,000 conventional heat flow measurements on land but only 1,785 of these are associated with heat production values. Such a dearth of heat production measurements has been circumvented in different ways, as will be shown in this paper, but this has prevented robust conclusions on the thermal conditions of many geological events. For example, there is still no consensus on what causes the ultrahigh temperature metamorphism (900-1000°C) that has affected many geological provinces (Heaman et al., 2011). A dominant role for crustal heat sources has been advocated in a few cases (Chamberlain and Sonder, 1990; Kramers et al., 2001; McLaren et al., 2006; Jaupart and Mareschal, 2015), but this idea has not enjoyed wide acceptance.

Determining the rate of crustal heat production in a geological province has proven to be a major scientific challenge because continental crust is the end result of a complex sequence of processes. Crustal material is extracted from the mantle through melting in a variety of settings and gets accreted to the margins of older nuclei in piecemeal fashion. Once it has been incorporated in a continent, a juvenile terrane may be subjected to later magmatic, metamorphic and tectonic events that modify it comprehensively. In addition, parts of it get redistributed by erosion and sediment deposition. As a consequence, the composition and vertical structure of continental crust do not conform to a single universal model and exhibit considerable variety amongst geological provinces.

In this paper, we provide a review of crustal heat production and its impact on the thermal structure and evolution of continental crust. We limit ourselves to a few issues. Can crustal heat production account for some of the thermal events that affect continental crust, such as high-T metamorphism for example ? What information is required for a reliable thermal model and what can be done if this information is not directly available ? What are the scales and magnitudes of lateral variations of heat production in a geological province ? For reference, we begin by reviewing geochemical models focussing on the vertical stratification of the crust and heat production in the lower crust. We then discuss the required inputs for thermal models of the crust and lithosphere, focussing on how they can be retrieved from an analysis of heat flow data. We show that, with adequate heat flux and heat production data coverage, it may be possible to identify different types of crust and evaluate their stratification degrees. This allows calculations of thermal structure and evolution that are reliable enough for most practical purposes. The data emphasize that heat flow and crustal heat production both vary laterally by large amounts, even within a single geological province. These variations may occur on a large scale, with enriched belts at the boundaries of older continental blocks, with important implications for the mechanical behaviour of continents. In a last section, we summarize a few important facts about the transient thermal evolution of continents and describe a few tell-tale effects of crustal heat production. This paper brings together a large amount of data from representative geological provinces throughout the world.

4.2 Geochemical Models of the Continental Crust

Continental crustal material is extracted from the mantle in subduction zones and hot spot environments. Extraction is followed by a magmatic phase which includes fractional crystallization and the separation of felsic melts from mafic residues. It has long been recognized that the bulk continental crust differs significantly from its parent melts. Almost all mantle-derived magmas are basaltic, whereas the average continental crust is closer to an andesite (Rudnick and Gao, 2014; Kelemen et al., 2014). Several mechanisms have

been invoked, including delamination of dense mafic cumulates and relamination of felsic gneisses to the base of the crust (Hacker et al., 2015). Which mechanism dominates has major consequences that go far beyond petrological and geochemical interests. Should the relamination model be valid, a significant fraction of the lower crust would be made of felsic rocks with higher heat production than mafic ones.

A big stumbling block is that radiogenic heat production cannot be related in any meaningful way to major element composition on the one hand and bulk physical properties such as density and seismic velocities on the other hand (Figures 4.1 - 4.2). Thus, one cannot readily convert geophysical or petrological information into constraints on crustal heat sources. This is of particular concern for the lower crust because, as we shall see, it has a major impact on the thermal structure of continents.

One could hope to determine the crustal structure directly by studying exposed vertical cross-sections, but they are rare and seldom complete. Exposures of rocks that have equilibrated over the whole range of crustal pressures and that reach into mantle peridotites have been studied in two areas, Talkeetna, Alaska, and Kohistan, Pakistan (Hacker et al., 2008; Jagoutz, 2010; Jagoutz and Schmidt, 2012). Both were oceanic volcanic arcs but have bulk major element contents that are close to those of the continental crust. Unfortunately, the Talkeetna exposures lack substantial outcrops of mid-crustal plutonic rocks. One other crustal cross-section was reconstructed in the North American Cordillera using thick batholithic sequences that span upper and middle crustal pressure ranges and xenoliths from the lower crust (Lee et al., 2007). Xenolith populations, however, may not be fully representative of average continental crust because their carrier basaltic magmas cannot go through thick felsic environments that are less dense than them. There may thus be a sampling bias in favor of mafic rocks. With due caution for this, the North American Cordillera provides us with a section through a continental volcanic arc, which complements the oceanic ones from Alaska and Pakistan.

Table 4.1 lists recent models for the continental crust, including global ones based on

large geochemical data sets and the two complete vertical cross-sections that have been described above. In order to derive a crustal model from geochemical data, one must separate the crust into components (layers in practice) with distinctive physical properties and chemical compositions. Following global seismic syntheses, the crystalline part of the crust is split into three layers (Mooney et al., 1998; Bassin et al., 2000). Huang et al. (2013) included continental shelves and rifts to define a global average crust with 34 km thickness. Rudnick and Gao (2014) and Hacker et al. (2015) took shields and platforms only, with total crustal thicknesses of 40 and 39 km, respectively. The composition of the upper layer was derived from surface sample compilations and is nearly the same in the three global models (Table 4.1). The other two layers were assigned compositions on the basis of their densities and seismic wavespeeds. Hacker et al. (2015) allowed for different end-members, leading to four alternative models (Table 4.1). For the crustal cross-sections, layer thicknesses were derived from metamorphic barometric data and field measurements. The latter may not be fully representative due to syn-emplacement deformation and thrusting, which led Jagoutz and Schmidt (2012) to propose three different alternatives.

There is little disagreement between the crustal models of Table 4.1. Heat production values for the Kohistan oceanic volcanic arc are significantly smaller than those of all the other entries. The bulk heat production of the American Cordillera continental arc falls within the range of the "global" geochemical models. For our present purposes, it is significant that these models are consistent with heat flow data constraints (Table 4.1).

The global crustal models rely on both geochemical and geophysical data. For expediency reasons, geophysical constraints have been collapsed into a few type-structures involving a small number of crustal layers (Mooney et al., 1998; Bassin et al., 2000), which gloss over the complex architecture of continents. For example, it is not clear how one can go from the detailed seismic models of the Western Superior Province (Musacchio et al., 2004), which emphasize crustal-scale low-angle thrusts and across-strike fabric variations, to a single layered structure. Some "averaging" process has been applied to the data at a scale which is not well-defined and which may not be consistent with the requirements of

thermal models. The issue of the proper scale forms one of the major themes of this paper.

The crustal models of Table 4.1 were designed to address geochemical and petrological problems and provide indispensable references. For heat flow studies, however, they suffer from several important shortcomings. The most critical one is certainly that they are generic models that cannot be applied to any particular province. They do not inform about the large horizontal variations of crustal structure and composition that exist within a single province. They correspond to a worldwide average crustal thickness and it is not clear how they can be extended to crusts that are thicker or thinner than the average. In the Archean Superior Province, for example, crustal thickness varies between of 35 and 55 km (Perry et al., 2002). Yet another shortcoming is that the spread of heat production values that is allowed is too large for comfort. Estimates of the bulk crustal heat production vary within a 0.75-0.93 μWm^{-3} range and get amplified when they are extrapolated back in time. In studies of the Archean, for example, one must correct for radioactive decay over more than 2.5 Gy, which increases heat production values by a factor of at least two. The wider spread of heat production values that is induced allows for a wide temperature range of about 200°C in the deep crust during the Archean.

4.3 Thermal Models of the Continental Crust : Inputs and Uncertainties

In this section, we evaluate the importance of crustal heat production for thermal models of continents and discuss the thermal consequences of lateral and vertical variations of heat production. For this purpose, we use steady-state models because transient phenomena cannot be studied in a generic manner and must be developed on a case-by-case basis. Further, we take thermal conductivity to be constant. As shown in appendix 4, using an average value of thermal conductivity ($\approx 2.1 W\, m^{-1}\, K^{-1}$), provided that it is chosen properly, results in negligible errors on Moho temperature. These two assumptions, which will be relaxed in other sections, allow a clear separation of the various effects that come into play.

Temperatures in the crust are solutions of the heat equation :

$$\lambda \nabla^2 T + A = 0 \tag{4.1}$$

where λ is the thermal conductivity and A is the heat production rate. Two boundary conditions are needed. One states that the surface temperature T_0 is constant (= 0) and the other one deals with the heat flux at the surface, q_0, or at the Moho, q_m. The former is taken from field measurements and the latter may be inferred from the systematics of heat flow and heat production data as well as from several independent constraints, as discussed in Appendix 4. One must also specify the vertical distribution of heat production in the crust.

It is useful to decompose the temperature field into a horizontal average and a fluctuation, such that $T = \overline{T} + \delta T$. The heat equation may then be split into two equations, one for each component :

$$\begin{aligned} \lambda \frac{d^2 \overline{T}}{dz^2} + \overline{A}(z) &= 0 \\ \lambda \nabla^2 \delta T + \delta A(x,y,z) &= 0 \end{aligned} \tag{4.2}$$

where $\overline{A}$ is the horizontally-averaged heat production, which may vary only as a function of depth z, and δA describes the horizontal variations of heat production around the mean.

4.3.1 The Total Amount of Heat Produced in the Crust

Here, we deal with average values in a province, such that the horizontally-averaged heat flux is :

$$\overline{q_0} = q_m + \int_0^{h_m} \overline{A} dz = q_m + q_c \tag{4.3}$$

where q_m is the Moho heat flux, h_m is the Moho depth, and q_c the contribution of crustal heat sources to the heat flux, which shall be called the crustal heat flow component.

One should note that, in the above equation, the Moho heat flux has not been written as a horizontal average. Ignoring radioactive sources within the lithospheric mantle, whose contributions can only be small (Jaupart and Mareschal, 1999; Michaut et al., 2007), the Moho heat flux is equal to the rate of heat supply from the asthenosphere, which will be called the mantle heat flux. The base of the lithosphere lies at depths of 150 km or more beneath stable geological provinces, implying that lateral variations of the mantle heat flux at scales of 500 km or less are effectively smoothed out by horizontal heat transport (?). This cut-off scale can be as large as 800 km for the Archean lithosphere that is 250 km-thick. Thus, in a geological province, the Moho heat flux can be taken as uniform for all practical purposes, implying that lateral variations of the surface heat flux can only be due to crustal heat sources. This separation of scales can be turned to one's advantage when one is interpreting heat flow data. We review in Appendix 4 various methods that have been used to calculate the Moho heat flux. They all converge to a narrow range of 12 - 18 mW m^{-2} , which will be used throughout the following. This is less than estimates that have been used in many past studies, with important implications for the thermal regime of the crust.

For homogeneous crust, $q_c = A_c h_m$ and the temperature at Moho T_m is :

$$T_m = T_0 + \frac{q_c}{2\lambda} h_m + \frac{q_m}{\lambda} h_m \tag{4.4}$$

where the first term represents the contribution of crustal heat production to Moho temperature and the second is the contribution of the mantle heat flux. For Archean cratons, q_0 = 42 mW m^{-2} and q_m = 15 mW m^{-2} (Jaupart and Mareschal, 1999), so that $q_c = 27$ mW m^{-2} . Thus, the crustal and mantle contributions to the Moho temperature are about equal today. Accounting for radioactive decay, q_c in the Archean had to be > 54 mW m^{-2} ,

at least twice as large as present. Unless the Moho heat flux was higher than today, this implies that, in the Archean, crustal temperatures were very sensitive to heat production and also that they were much higher than today.

The assumption of a homogeneous crust is not tenable in many provinces because the surface heat production is much larger than the crustal average. This is usually associated with the presence of evolved granitic rocks with high concentrations of uranium and thorium. For the same total heat production, a crust that is stratified vertically in this manner has much lower temperatures than a homogeneous one. Information on the vertical distribution of heat production is therefore required for a reliable thermal model. One should be aware, however, that this vertical distribution got established at some time in the past and hence is not appropriate for earlier events. In many provinces, for example, the enriched granitic plutons that now lie in the upper crust were intruded in the midst or after the end of orogenic activity, implying that the present-day distribution of heat production is not relevant to the orogenic event itself.

4.3.2 Sensitivity of the Moho Temperature to the Depth of Heat Sources

Here, we show that an enriched upper crust has little impact on temperatures in the lower crust. To demonstrate this, we split heat production into three components. One is a homogeneous background with heat production at its lowest value A_o, which corresponds to that of lower crustal rocks. The two other components account for the upper and middle crust, with heat production values $A_1 = A_o + \Delta A_1$ and $A_2 = A_o + \Delta A_2$, respectively. The contribution of crustal heat production to the Moho temperature can then be calculated as the sum of three components, one for $A = A_o$ over the whole crustal thickness h_m, and two others for $A = \Delta A_1$ over thickness h_1 and $A = \Delta A_2$ for the middle crust over thickness h_2. For our present purposes, we need only focus on the first two, whose contributions to the

Moho temperature are :

$$\Delta T_o = \frac{A_o h_m^2}{2\lambda}$$
$$\Delta T_1 = \frac{\Delta A_1 h_1^2}{2\lambda} \tag{4.5}$$

which are such that :

$$\frac{\Delta T_o}{\Delta T_1} = \frac{A_o}{\Delta A_1}\left(\frac{h_m}{h_1}\right)^2 \tag{4.6}$$

Typical values for h_m and h_1 are 40 km and 10 km respectively, such that $\Delta T_o/\Delta T_1 \approx 16 \times A_o/\Delta A_1$. It therefore takes very high values of heat production in the upper crust to increase significantly lower crustal temperatures. Even if we use the extreme values from Table 4.1, $A_o = 0.2$ and $A_1 = 1.6\ \mu\text{W m}^{-3}$, we find that $\Delta T_o/\Delta T_1 \approx 2$.

4.3.3 Sensitivity of Heat Flux and Temperature Anomalies to the Depth of the Sources

Models of the temperature and heat flux fields require the specification of the heat production distribution, which is not known. Simple calculations demonstrate that horizontal heat conduction smoothes out lateral changes of heat production and operates as a low-pass filter whose cut-off wavelength increases with source depth (Jaupart, 1983; Vasseur and Singh, 1986; Nielsen, 1987). In this section, we compare the sensitivities of the surface heat flux and the Moho temperature to lateral variations of heat production. We assume that the horizontal distribution of heat production remains the same over some thickness h and that it can be described by elementary periodic functions $f(x,y)$ such that :

$$\nabla_H^2 f(x,y) = \frac{\partial^2 f}{\partial x^2} + \frac{\partial^2 f}{\partial y^2} = -k^2 f \tag{4.7}$$

where k is the equivalent of a wavenumber. For simplicity, we refer to a single scale or wavelength Δ such that :

$$k = \frac{2\pi}{\Delta} \tag{4.8}$$

For the sake of example, we set $h = 10$ km in crust of 40 km thickness. Using the results derived in Appendix 4, we compare the variations of surface heat flux and Moho temperature that are induced by such a layer in the upper and lower crust.

For an upper crustal layer, the Moho temperature is much less sensitive to lateral heat production variations than the surface heat flux and, in practice, is not affected by variations at scales that are less than about 100 km (Figure 4.3a). Thus, for example, an isolated radioactive granitic pluton of typical dimensions ($\approx$ 10 km) generates a positive heat flux anomaly at Earth's surface but does not induce any significant temperature rise at the base of the crust.

Results are completely different for heat production in the lower crust, as shown by Figure 4.3b. In that case, the Moho temperature and the surface heat flux are both equally sensitive to lateral heat production fluctuations. This has two important consequences. One is that variations of heat production in the lower crust at scales that are less than 100 km, if they exist, are not detectable by surface heat flux measurements. Thus, the surface heat flux records a large-scale average of heat production in the lower crust. The other consequence is that, as regards the contribution of lower crustal heat sources, the Moho temperature and the surface heat flux vary on almost identical scales. Stated differently, the Moho temperature is nearly as sensitive as the surface heat flux to lateral variations of heat production in the lower crust.

4.4 Horizontal Variations of Crustal Heat Production

4.4.1 Global Data Sets

For a statistically homogeneous crust, the total crustal heat production, and thus the surface heat flux, should increase with crustal thickness. One should therefore expect a positive correlation between heat flow and Moho depth, which may be tested by comparing maps of Moho depth and continental heat flow (Figures 4.4 and 4.5). For our present purposes, we exclude the tectonically active regions, where heat flow records transient thermal perturbations and is often higher than 80mW m^{-2} , and observe that there is no correlation between heat flow and crustal thickness at the global scale (Figure 4.6a).

The above analysis is based on imperfect data sets. Moho depths are extracted from the CRUST1.0 model (Laske et al., 2013), which assumes that the crust is stratified in 7 different layers, and gives their average thicknesses within $1^o \times 1^o$cells, even where no geophysical data are available. In these areas, a crustal column is assigned according to age and tectonic type. The heat flow map, on the other hand, is interpolated between unevenly distributed heat flow measurements on continents (Jaupart and Mareschal, 2011; **?**). For verification purposes, we have also compiled measurements of both heat flow and crustal thickness at a large number of cells in eastern Canada and confirm the lack of a correlation between heat flow and crustal thickness (Figure 4.6b). This implies that the average crustal heat production tends to decrease with increasing crustal thickness, such that $\delta\overline{A}/\overline{A} \approx -\delta h_m/h_m$. One cannot use this to try and estimate heat production from crustal thickness, however it is an indication that thick crust can only be stable if its bulk heat production is less than average. We return to this point later.

For further interpretation, it would be useful to separate between the contributions of the upper and lower crusts. We find that the power spectrum of the heat flow field is more rugged that that of the crustal thickness due to the strong contribution of the enriched

upper crust. A more detailed analysis is not warranted because of the sparsity and uneven distribution of the data.

4.4.2 The Scales of Heat Production Variations

The horizontal scales of heat production variations in the continental crust are not known a priori and must be determined from field measurements. Depending on scale, different mechanisms and processes are involved and must be considered separately. Scales of less than about one kilometer involve igneous, metamorphic and late alteration processes. For example, one observes that heat production changes across individual horizons in the interior of many plutons, such as the White Mountain batholith, New Hampshire, or the Bohus granite, Sweden (Rogers et al., 1965; Landstrom et al., 1980). At scales of up to a few tens of kilometers, one deals with the dimensions and distances between igneous bodies and metasedimentary formations, with enriched intrusives that may be responsible for very large local heat production anomalies (Table 4.2). Both types of heat production variations can be assessed easily and do not affect the regional thermal regime, as shown above. Larger scales in a 50-500 km range represent the most difficult challenge. Such scales correspond to the geological fabric of a province over dimensions that are larger than those of individual igneous bodies and are the relevant ones for thermal models of geological interest (Jaupart, 1983; Vasseur and Singh, 1986).

Determining the scales of heat production variations at the surface would require a labour-intensive program of systematic sampling which, to the best of our knowledge, has only been attempted by Eade and Fahrig (1971). These authors collected rocks at the nodes of a periodic grid in the Canadian Shield, but the large number of samples proved to be intractable and powder mixtures were used for chemical analyses. To get around this difficulty, some authors have turned to airborne gamma ray surveys (Bodorkos et al., 2004; Andreoli et al., 2006; Phaneuf and Mareschal, 2014). Using comparisons with a large number of conventional measurements on rock samples in the Sudbury area, Ontario, Phaneuf

and Mareschal (2014) have found that the airborne data accurately record differences in heat production from one area to the next, but also that they systematically underestimate the true heat production by a factor of > 3. The difference can be attributed to alteration and weathering processes that deplete a thin and shallow veneer in Uranium.

Securing a comprehensive set of evenly distributed heat production measurements in surface rocks seems to be a remote possibility and, even if it was achieved, would not provide information on the lower crust. At present, the only alternative is to use heat flow data. Data are too sparse and unevenly distributed to properly estimate the power spectrum of surface heat flow, but there are enough measurements to assess the scales of heat flow variations in the Precambrian of North America. To this aim, **?** paved the Shield with squares of given dimensions and calculated the average heat flow for each square. They then determined how the mean and standard deviation of these averages vary with the square size, *i.e.* with scale. The mean is almost unaffected by the square size, which shows that the heat flow field is adequately sampled. There is almost no difference between the standard deviation of the individual heat flow values and that of the 50×50km averages (8.9 vs 8.8mW m^{-2}). The standard deviation decreases slightly to 7.3 mW m^{-2} for $250\times$ 250km squares and markedly to 4.3 mW m^{-2} for 500×500km ones. This analysis shows that most heat flow variations occur over wavelengths that are $\leq$ 250km. As explained above, variations at these scales cannot be due to the mantle heat flux because it originates from the base of the lithosphere. These variations, therefore, can only be generated by crustal heat sources.

4.4.3 Relationship Between Heat Flow and Heat Production

Figure (4.7a) shows that there is no meaningful relationship between the local values of heat flow and heat production at the surface in a province. It takes isolated and enriched granitic intrusives, which generate large heat flow anomalies on top of a smoother background, for such a relationship to hold. An affine dependence between heat flow and heat

production was found for exceptional sites of this kind by Birch et al. (1968). This remarkable relationship has blinded us to the necessity of determining the background heat flow field away from enriched plutons.

In shield areas, surface heat production contrasts tend to be small and heat flux variations are mostly due to changes of basement composition that reflect the geological fabric of a province. This fabric results from the accretion, thrusting and folding of individual belts and older continental fragments. The erosion surface is rarely parallel to the boundaries between individual terranes and cuts across rocks from a range of crustal environments and emplacement depths. One can hope that, over a sufficiently large distance, surface exposures allow a representative sampling of the different rocks that make up the upper crust. If this was true, the average surface heat production would account for a significant volume of upper crustal rocks and would be positively correlated with the heat flux averaged over the same area.

These ideas have been tested in North America by Lévy et al. (2010). They have considered how the relationship between heat flux and heat production depends on horizontal scale. Local values of these two variables are not related to one another, as explained above, and they calculated their average values over two different scales, in geographical windows with dimensions of about 250 km in the interior of several geological provinces of North America and then in the whole provinces, corresponding to a scale of about 500 km. The 250x250 km windows are large enough to include enough measurements for the smoothing of small-scale variations and are distributed amongst provinces with contrasting magmatic and tectonic histories. With these windows, a relationship between heat flux and heat production begins to emerge (Figure 4.7b). At a larger scale, average values of heat flow and heat production for the five main provinces of North America exhibit a remarkable linear relationship, with a heat flux intercept of $\sim 33\,\mathrm{mW\ m^{-2}}$ for zero surface heat production (Figure 4.7c). The 250x250 km averages lie close to the province-wide relationship but exhibit greater scatter. Comparing results for the different scales illustrates clearly the difference between heat flow and heat production. In the Grenville province, for example,

the 250x250 km and province-wide averages are (39 mW m^{-2} , 0.47 μW m^{-3}) and (41 mW m^{-2} , 0.80 μW m^{-3}), respectively. The heat flux is barely affected by the change of scale, whereas the heat production almost doubles.

The remarkable relationship between the province-wide values of heat flow and heat production (Figure 4.7c) is difficult to reconcile with significant variations of the Moho heat flux beneath North America. This relationship requires that, if such variations do exist, they get cancelled by opposite variations of lower crustal heat production. It is impossible to find a physical explanation for such a strong link between two completely independent variables and the most sensible hypothesis is that the Moho heat flux is approximately the same beneath the five provinces. Variations of the Moho heat flux may not be exactly zero but must be smaller than departures from the best-fitting relationship, or about 2 mW m^{-2} , which is close to the intrinsic uncertainty of heat flow measurements (?).

It would be desirable to carry out the same type of analysis in other continents but no data set of comparable size seems to be available, due mostly to incomplete heat production coverage. We now discuss two continental regions where heat flow and heat production measurements allow useful insights.

4.4.4 United Kingdom

The crystalline basement of the United Kingdom is made of three large granitic batholiths that surround the late Proterozoic and Phanerozoic gneisses and metasedimentary rocks of central England and Wales. The batholithic regions extend over lateral distances of at least 100 km in all directions, such that they represent significant portions of continental crust. The three batholiths and the gneisses of central England and Wales show up as well-separated fields in a heat flow versus heat production diagram (Figure 4.8). Taken as a whole, the UK data set suggests a very rough trend of increasing heat flow with increasing heat production but does not indicate any meaningful relationship between the two variables, with heat flow that may vary by more than a factor of 2 at a constant value of heat

production. Compared to the small heat flux values of central England and Wales, the elevated batholithic ones can be accounted for by heat production contrasts over thicknesses that differ markedly between the three batholiths.

4.4.5 Norwegian Shield

The heat flow field of Fennoscandia is now well documented (Figure 4.9) and shows a marked contrast between the western regions and the generally older shield that lies to the east. Heat production measurements have been made in large quantities in Norway over different types of crust, including part of an Archean province, several Proterozoic belts and the recent Oslo rift. Heat flow and heat production values at individual sites are not correlated with one another : heat production may vary by as much as a factor of 3 for sites with the same surface heat flow (Slagstad et al., 2009). Recognizing that heat flow records heat production over a larger volume than the immediate neighbourhhod of a drillhole, Slagstad et al. (2009) have also determined the average heat production of rocks within a 10 km radius and found no correlation with heat flow. This shows that the crust is highly heterogeneous on a 10 km scale in both the horizontal and vertical directions, at least from the standpoint of heat production. Averaging measurements within each geological sub-province, however, one finds a stronger relationship between heat flow and heat production (Figure 4.10). As in the United Kingdom, the data do not conform to an affine relationship, indicating that the sub-provinces have different upper crustal structures. Large changes of heat flow occur over small lateral distances, which confirms that they are mostly due to variations of heat production in the upper crust.

4.5 Large-scale Controls on the Bulk Crustal Heat Production

The above overview has established a few important points. Geological provinces and sub-provinces can be identified and separated from one another according to their respective average values of heat flow and heat production. With only one of these two values,

such separation would not be possible. Heat flow differences are largely due to changes of the composition and vertical stratification of the crust, with variations of the Moho heat flux that are near the resolution threshold of heat flow data.

4.5.1 Significance of Average Crustal Characteristics

The need to work with averaged values of heat flux and heat production puts us at a disadvantage. At the large scale that is required, the averaging procedure lumps together a variety of terranes and tectonic features, so that the end result may not reflect the geological processes that have shaped a province. To check that the average values of heat flow and heat production are truly representative of the crust of a province, one can divide the province in different sub-provinces and compare their thermal characteristics. This also allows a test of the repeatability of crust forming mechanisms. There are enough measurements for such an analysis in the Superior province and the Appalachians (Table 4.3). In the former province, data are available for three different volcanic belts whose accretion to an older core marked the end of the craton assembly process at 2.7 Gy. Their average values of heat flow and heat production are remarkably close to one another, testifying to a tight control on the composition of juvenile crust at that time. The Appalachians province, which stretches over a large distance along the eastern edge of North America, can be split arbitrarily into its US and Canadian parts. Heat flow and heat production data for these two parts are statistically identical (Table 4.3), which shows that the characteristics of the Appalachian crust do not vary significantly along strike.

4.5.2 Large-scale Pattern

Nyblade and Pollack (1993) had noted a rather systematic pattern of low heat flow in Archean cratons and higher heat flow in adjacent Proterozoic terranes, which they attributed to change in mantle heat flux. In light of the new data that have been collected, this observation and their conclusions should be qualified. In the Superior Province, the

core of the craton is characterized by low heat flow and is surrounded by younger accreted belts with higher heat flow (?), but these belts are also Archean, so that the difference has nothing to do with age. One can attribute such heat flux contrasts to three causes : (1) a long-term transient reflecting the slow thermal relaxation that follows continent formation, (2) differences of crustal heat production and (3) differences of heat supply to the base of the lithosphere (the mantle heat flux). The transient effect has been convincingly rejected by Nyblade and Pollack (1993) using both observations and obvious theoretical arguments which need not be repeated here. In all cases that are known to us, it may be shown that the heat flux contrast between craton core and surrounding belts is in large part due to a change of crustal heat production. One observation is simply that the heat flux contrast is associated with one of heat production. In addition, the change of surface heat flux occurs abruptly at the edge of the craton over a distance that is less than the crustal thickness, showing that it has a shallow origin. This is observed at the boundary between the Archean Kaapvaal craton and the Proterozoic Namaqua-Natal belt in Lesotho, for example (Jones, 1992). Where the contrast in crustal heat production is not present, such as between the Archean Superior province and the Trans-Hudson orogen or the Grenville province, there is no difference in heat flux (Jaupart and Mareschal, 1999).

Variations of heat flux at the base of the lithosphere, if they exist, can only affect the surface heat flux over very large horizontal scales ($>\approx 500$ km), as shown above. Because of this, they are difficult to detect with measurements of the surface heat flux. In fact, they are not required by the data and it may be worth pointing out that, within a continent, variations of lithosphere thickness do not necessarily require variations of the mantle heat flux. By analogy with the oceans, there has been a tendency to link surface heat flux to lithosphere thickness, such that an elevated heat flow implies a thinner lithosphere. With the large values of heat production that characterize continental crust, this interpretative framework is not valid. Horizontal changes of crustal heat production are large enough to induce significant variations of Moho temperature and lithosphere thickness by themselves. Large lateral variations of the mantle heat flux are indeed ruled out by the parallel (P,T)

arrays of lithospheric xenolith suites from different parts of Canada and South Africa (**?**).

4.5.3 Variations of Crustal Heat Production with Age

Using global heat flow data sets, several authors have proposed that continental heat flow decreases with age, which can be attributed to the thermal relaxation of an early lithospheric thermal event or to a decrease of crustal heat production. This ambiguity cannot be resolved without a joint analysis of heat flow and heat production data. The apparent variation of heat flow with age is essentially due to the large difference that exists between tectonically active regions and Archean provinces. Morgan (1985) pointed out that, if one excludes these two extremes, the differences in heat flow between age groups are not statistically significant. He further noted that the low heat flow of Archean provinces is associated with low values of heat production. Using a large data base of heat flow and heat production data, Jaupart and Mareschal (2014) found that there is indeed a trend in the distribution of crustal heat production with age (Table 4.4, Figure 4.11). One must beware, however, that there is a very wide range of crustal heat production within each age group. Extremely high values of heat production ($>5\mu$W m^{-3}) have been measured on granitic plutons and gneisses of all ages and provenances, including Archean ones (Table 4.2). When corrected for the rundown of the radioactive elements, heat production values in some Archean granites and gneisses are comparable to, and in some cases greater than, that of the young and markedly enriched Appalachian White Mountain pluton. Very high values of heat production have also been found in several Proterozoic provinces, including the entire Gawler craton, central Australia (McLaren et al., 2003; Neumann et al., 2000), or the Wopmay orogen in northwestern Canada.

Accounting for the rundown of heat producing elements due to radioactive decay, we find little change in the value of heat production at the time of crustal stabilization (Figure 4.11), suggesting that the thermal conditions for stabilization have not varied significantly. Table 4.5 lists data for four well-documented provinces spanning a large age range.

These four provinces have been affected by high-temperature metamorphism, indicating that crustal temperatures have not changed markedly through geological time. At present, the crustal heat flow component is smaller in the Archean province than in the younger ones but, once it is corrected for age, it is as large as in these provinces.

4.6 Vertical Distribution of Heat Producing Elements

It was understood very early that heat production must decrease with depth in the Earth's crust because otherwise, with the heat production rates of surface rocks, the crustal heat flow component would exceed the surface heat flux (Jeffreys, 1936; Birch et al., 1968). The geochemical models of Table 4.1 illustrate this but allow a large range of values for the lower crust. This is due in part to the non-uniqueness of the relationship between seismic velocities and composition and in part to the different crust-building processes that may be active in island arcs. Hacker et al. (2011) have argued that felsic gneisses may be "relaminated" to the base of the crust, leading to lower crust that is less depleted than commonly thought. Given the number of accretion mechanisms and tectonic events that shape the continental crust, one can hardly advocate a single universal model for the vertical distribution of heat production. One must again devise methods that may be implemented locally and there is at present no alternative to the use of heat flow data. A major difficulty is that upper crustal heat sources are responsible for a significant part of the surface heat flux but have a small impact on deep crustal temperatures, as explained above. Thus, it is essential to determine that part of the surface heat flux that is not generated in the upper crust, which will be noted q_r. In steady-state, this heat flux component is the sum of the Moho heat flux and heat released in the mid and lower crusts.

4.6.1 Determining the Upper Crustal Heat Flow Component

In order to determine the heat flux at the base of the enriched upper crust, which has been called the "reduced" heat flux, an obvious method is to find areas where the upper

crust has zero or very small heat production. This is rarely possible and an alternative method is to seek a relationship between heat flux and heat production that can be extrapolated to zero heat production. In a few cases, the data conform to an affine function of the form :

$$q_o = q_r + DA_S \tag{4.9}$$

where q_o and A_S are the surface values of heat flow and heat production at individual sites. This simple relationship allowed excellent fits to measurements that were available to Roy et al. (1968) in a few North American provinces. In the simplest interpretation, the intercept q_r is the heat flux at the base of an upper crustal layer of thickness D. It is now recognized that this relationship is not valid in many geological provinces, as discussed above and demonstrated by Figures 4.7a and 4.8. It is still used by many authors for a least-squares fit through heat flux and heat production data.

In the early days of heat flow studies, there were very few "heat flow provinces" where enough data were available for an analysis of heat flux and heat production. For those provinces, measurements were biased in favour of enriched intrusives and turned out to be approximately consistent with an affine relationship. Pollack and Chapman (1977) derived values of the average surface heat flux and reduced heat flux and found that $q_r \approx 0.6\overline{q_o}$. They noted that the slopes of the heat flow heat production lines are all of the order 10km and proposed that it represents the near constant thickness of the enriched upper crustal layer. Assuming that the heat production is 0.25 μW m^{-3} throughout the middle and lower crust, they came up with estimates of the mantle heat flux even in areas with no heat production data, and to propose characteristic continental geotherms that depend only on the surface heat flux. With this approach, values of the surface and mantle heat flux must vary in tandem. Temperature variations at the base of the crust are larger than in models where differences in heat flux come mostly from changes of crustal heat production.

In a more recent world-wide compilation, Artemieva and Mooney (2001) have used

the affine relationship to derive values of q_r and D in a large number of provinces. In many cases, the data are clearly not consistent with such a relationship and the method was adopted for want of an alternative one. Artemieva and Mooney (2001) assumed that heat production decreases exponentially with depth, as $\exp(-z/D)$, and that, below a depth that was set equal to D, heat production remains constant in the mid and lower crustal layers (with values of 0.4 and 0.1μW m^{-3} respectively). Values of D, where they can be estimated, seem to lie in a restricted range around a mean value of 10 km. In this framework, the heat production of the mid and lower crust is almost constant if one excludes variations in crustal thickness, so that variations in the Moho temperature are due mostly to changes of mantle heat flux.

Acknowledging the limitations of a best-fit procedure through highly scattered heat flux and heat production data, Hasterok and Chapman (2011) have proposed a new approach. They postulated that q_r is proportional to the surface heat flux, such that $q_r = \beta \overline{q_o}$, where β is a constant to be found. For a prescribed value of 0.4 μW m^{-3} for heat production in the mid and lower crusts, they calculated lithospheric geotherms for different values of the surface heat flux and a fixed β. Additional constraints were required to determine the value for β. Hasterok and Chapman (2011) calculated elevation in the isostatic limit for several geological provinces and obtained the best agreement with the observations for $\beta = 0.74$. With such a large value, variations of the surface heat flux get transferred to the reduced heat flux with little change and, with the low value of crustal heat production that is postulated, to the Moho heat flux also. This allows for large variations of the mantle heat flux, which induce the deep seated differences in lithospheric temperature and density that are required for thermal isostasy. Calculations rest on the assumption of thermal steady state, however, which is not verified for the active tectonic regions with the highest heat flow (> 75 mW m^{-2}) and "compositionally adjusted" elevation values. Hyndman (2010) showed that the elevation and crustal thickness data follow two distinct trends, one for stable and one for active regions. With the method of Hasterok and Chapman (2011), geotherms are slightly higher and the range of mantle heat flux values is wider than those obtained by

Artemieva and Mooney (2001).

4.6.2 Sampling the Mid and Lower Crust

The above methods require values for heat production beneath the upper crust, which cannot be measured directly. One has to turn to rocks that have been exposed to deep crustal conditions and that are available either as xenoliths in kimberlites (Rudnick and Taylor, 1987) of have been brought to the surface along thrust faults (Fountain and Salisbury, 1981) or, exceptionally, by rebound of the crust following a large meteorite impact (Nicolaysen et al., 1981). Hasterok and Chapman (2011) have compiled data from 31 granulite facies terranes throughout the world and found a very wide spread of heat production with a mean of 0.68 ± 0.62 μW m^{-3} (mean and standard deviation). Granulite facies metamorphism, however, can occur over a rather large pressure range and is not necessarily representative of lower crustal conditions. Table 4.6 lists measurements for 18 terranes sorted by age and metamorphic pressure conditions. A rigorous statistical analysis is not warranted for such a limited data set but one can note a definite trend of decreasing heat production with increasing metamorphic pressure. There seems to be no significant variation as a function of age. The lowest values are found in Archean terranes but they fall within the range of values for younger provinces once they are corrected for radioactive decay.

This brief overview shows that heat production in the mid to lower crusts is not negligible and can be much larger than the global estimates of Table 4.1. It varies by large amounts between provinces and may be responsible for significant heat flow variations.

4.6.3 Assessing the Extent of Crustal Stratification

We have described several attempts to deduce the crustal heat flow component and, by way of consequence, the mantle heat flux from heat flux and heat production data. An alternative approach relies on estimates of the mantle heat flux, which has the advantage

of imposing no *a priori* constraints on crustal stratification. On the contrary, this method aims at estimating the degree of crustal stratification (Perry et al., 2006).

If the mantle heat flux q_m and the crustal thickness h_m can be determined independently, one can estimate the bulk average heat production of the crust, noted $\overline{A}_c$, as follows :

$$\overline{A}_c = \frac{\overline{q_o} - q_m}{h_m} \tag{4.10}$$

From knowledge of the average value of heat production in surface rocks, A_S, one can calculate a "differentiation index" (Perry et al., 2006) :

$$DI = \frac{A_S}{\overline{A}} = \frac{A_S \times h_m}{\overline{q_o} - q_m} \tag{4.11}$$

DI is equal to 1 if the crust is not stratified and is larger than 1 in many geological provinces because the upper crust is enriched compared to the bulk. This does not specify the thickness h of the superficial layer, which must be less than the crustal thickness h_m. If $DI > 1$, an upper bound for h is obtained by assuming that the lower crustal heat production is negligible (Sandiford and McLaren, 2002), such that $h = h_m/DI$. Estimates for h can be obtained by fixing heat production in the deeper crust, or can be deduced from a regional heat flow heat production relationship. It is difficult to assess the uncertainty on these estimates but it may be shown that, for a given *DI* value, crustal temperatures are not very sensitive to the exact form of the vertical heat production distribution.

The large-scale bulk thermal characteristics of the crust in a number of geological provinces are listed in Table 4.7. *DI* values are spread over a large range, indicating a wide variety of crustal structures. The differentiation index is about 1 in several cases. In the Grenville, North America, province, this is due to the small average value of surface heat production, which is itself a consequence of the many depleted anorthosite bodies that are

present in the upper crust. In some greenstone belts, such as the Abitibi or the Flin Flon Snow Lake belt, Canada, $DI < 1$ because the uppermost crust is made up of mafic volcanics that have been transported over a more radioactive basement. In the case of the Trans Hudson orogen, this basement has been recognized as the Archean Sask craton (Hajnal et al., 2005).

If an upper crustal layer is enriched by a factor DI with respect to the mean crust, the crustal component to the Moho temperature is obtained as :

$$\Delta T_m = T_o + (q_0 - q_m)\frac{h_m}{2\lambda}\left[1 + \frac{h}{h_m}(1 - DI)\right] \tag{4.12}$$

where h is the thickness of the enriched layer. One can see that the Moho temperature decreases with increasing DI value, *i.e.* with increasing enrichment of the upper crustal layer.

4.7 Thermal Control on Crustal Thickness

The thickness of continental crust varies but in a relatively narrow range (Figure 4.12). This range would be narrower if tectonically active regions were excluded. It is also notable that there are very few regions with crust that is thicker than 60 km.

4.7.1 Melting Conditions

For given values of the differentiation index, the surface and the mantle heat flux, one can calculate the Moho temperature. Figure 4.13 gives results for the present average heat production of Archean crust of 0.7 μW m^{-3} , corresponding to 1.5 μW m^{-3} at the time of crustal stabilization, which we take to be 2.7 Ga. At that time, the crustal temperature component ΔT_m was twice present, i.e. $\approx$ 600K. Accounting for the Moho heat flux, that

we assume to be at least as large as today ($\approx$ 15 mW m^{-2}), adds another 300K to Moho temperature. In steady state conditions, the base of a 40km thick undifferentiated crust, was at $\approx 830^{o}$C, near melting. This has been known for a long time, and motivated Morgan (1985) to propose that only Archean crust depleted in heat producing elements could have remained stable and survived. One alternative solution to stabilize the crust, however, is to redistribute the heat sources in an enriched upper crust, which lowers temperature. As shown in Figure 4.13, the differentiation of heat producing elements has a major impact on Moho temperature.

Independently of the degree of intra-crustal differentiation, the Moho temperature remains elevated when the crust thickens. For 50km thick crust, this temperature exceeds the non plausible value of 1500 ^{o}C for homogeneous crust and remains >900^{o}C for highly differentiated crust (Figure 4.13). It is therefore clear that crustal heat production puts an upper limit on crustal thickness in Archean time. These arguments rest on the assumption of thermal steady state which is, obviously, not valid at the time of crustal stabilization. Transient calculations require assumptions on the mechanism of crust formation as well as on the rates of tectonic deformation/accretion which are outside the scope of this paper (Gaudemer et al., 1988; Mareschal and Jaupart, 2006; Michaut et al., 2009).

4.7.2 Strength of Crust and Lithosphere

We now discuss the impact of crustal thickening on the mechanical stability of the lithosphere. Crustal thickening has two consequences which reinforce one another. It enhances the gravitational potential energy of the crust and thus generates tensile stresses. At the same time, it acts to raise temperatures in both the crust and the underlying continental root, which reduces the integrated strength of the lithosphere and diminishes its capacity to withstand the tensile stress regime. In a first approximation, one may estimate the change of gravitational potential energy by assuming that the relationship between elevation and crustal thickness follows by Airy's isostasy. Considering only an average crustal density ρ_c

and an average mantle density ρ_m, we have :

$$\delta h = \frac{\rho_m - \rho_c}{\rho_c}\delta h_m$$
$$\delta U = g(\rho_m - \rho_c)\delta h_m \times (h_m + \frac{1}{2}\delta h_m) \tag{4.13}$$

where δh is the elevation change due to a δh_m change in crustal thickness; h_m is an arbitrary reference crustal thickness, g is the acceleration of gravity. For $h_m = 40$km, $\rho_c = 2,850\text{kg m}^{-3}$ and $\rho_m = 3,250\text{kg m}^{-3}$, we have $\delta U/\delta h_m \approx 0.16\text{TNm}^{-1}/\text{km}$. This force can be compared with the total strength of the lithosphere, which depends on the thermal structure.

Following the standard approach summarized in appendix 4, we have calculated how the strength of the lithosphere varies with crustal thickness and differentiation for two different values of the average crustal heat production (1.1 and 1.5 $\mu\text{W m}^{-3}$). For the value of $1.5\mu\text{W m}^{-3}$, which represents the mean heat production of newborn Archean crust at 2.7 Ga (?), we find that undifferentiated crust cannot withstand more than 5 km of crustal thickening without collapsing (Figure 4.14a). The upward segregation of heat sources in an upper crustal layer increases the lithospheric strength by a large factor and crust thickened by up to 15 km may remain stable. Crust with an average heat production of $1.1\mu\text{W m}^{-3}$, which is that of the Appalachian mountains today, is considerably stronger than with $1.5\mu\text{W m}^{-3}$, but the strength decreases rapidly when the crust is thickened. The tensile stress due to gravitational potential energy exceed the strength of differentiated crust when it is thicker than 60km (Figure 4.14b).

These calculations do not account for thermal expansion in both crust and lithospheric mantle. Including such effects would lead to higher differences of elevation and potential energy, which would reinforce our conclusions.

4.8 The Role of Crustal Heat Production in High-T Metamorphism and Crustal Anatexis

The cause of high-T metamorphism, which is characterized by temperatures exceeding 800°C at pressures in a 0.7-1.0 MPa range, has not been ascertained yet despite decades of research (Heaman et al., 2011). Many authors have called on the emplacement of large quantities of mafic magma in the crust, but this does not seem consistent with the time-lag of several tens of million years that separates metamorphic events from voluminous magmatism (Krogh, 1993; Heaman et al., 2011). Others have argued in favour of anomalously high rates of crustal heat production (Chamberlain and Sonder, 1990; Kramers et al., 2001; Andreoli et al., 2006; McLaren et al., 2006; Jaupart and Mareschal, 2015). We address this question in two different ways. In this section, we evaluate the amount of crustal heat production in several high-T provinces and show that they are high compared to global averages. We also discuss how one should use present-day data in thermal models for past events. In the next section, we show that the thermal evolution of crust with high heat production is characterized by a late heating event that lags the cessation of orogenic activity by a few tens of million years.

4.8.1 Some General Characteristics

Crustal heat production varies from province to province, implying that its relevance to high-T metamorphism cannot be assessed with generic models. Table 4.5 lists data for four geological provinces which span a large part of Earth's history, showing that high crustal temperatures are not specific to any particular geological era. After corrections for radioactive decay since the times of the orogenic events, values for the crustal heat flow component q_c are in the $43-85$ mW m^{-2} range, clearly higher that those of the "average" crusts of Table 4.1, which are in a $28-36$ mW m^{-2} range.

In recent calculations of the thermal evolution of continental crust during a cycle of tectonic thickening and erosion, Clark et al. (2011) have imposed zero heat production in

the lower crust. With such an extreme distribution, they have effectively minimized the impact of crustal heat sources. A highly stratified crust with enriched granites at the top is a consequence of orogenesis and should not be taken as a realistic initial condition unless there is strong evidence to the contrary. Delving into the details of the time-dependent calculations by Clark et al. (2011) would be outside the scope of this paper and we only evaluate the consequences of their starting heat production model. Redistributing over the whole crustal thickness h_m heat sources that are concentrated in an upper layer of thickness h with heat production A_s leads to a uniform crustal heat production $A_c = A_s h/h_m$. For these two cases, contributions of heat production to the Moho temperature are $A_s h^2/(2\lambda)$ and $A_c h_m^2/(2\lambda)$, respectively. The latter is larger than the former by a factor equal to h_m/h, or typically about 4. Smaller enhancement factors would be obtained for distributions that are intermediate between these two extremes (*i.e.* involving for example a mid-crustal layer).

4.8.2 Crustal Thickening

In compressional regime, the crust can be thickened by uniform shortening or by over-thrusting. Both mechanisms increase the total crustal heat production in proportion to the amount of thickening. The thermal consequences can be laid out very simply for a homogeneous crust. Defining the thickening $\phi = \delta h_m/h_m$ and assuming that the Moho heat flux is unchanged, the crust and mantle contribution to Moho temperature vary as follow :

$$\begin{aligned} \Delta T_m &= \frac{q_m(h_m+\delta h_m)}{\lambda} = \frac{q_m h_m}{\lambda} \times (1+\phi) \\ \Delta T_c &= \frac{A(h_m+\delta h_m)^2}{2\lambda} = \frac{A h_m^2}{2\lambda} \times (1+\phi)^2 \end{aligned} \tag{4.14}$$

Doubling the crustal thickness multiplies the mantle component of Moho temperature by a factor 2 and the crustal component by 4. Referring to section 4, the mantle and crustal contributions to Moho temperature are about 300K each. Thickening the crust by a factor 2 results in a very implausible 1200K increase in steady state Moho temperature, unless

the heat producing elements are redistributed before steady state is reached. This redistribution can be achieved in two different ways : partial melting and vertical differentiation of the heat producing elements and/or lateral extrusion. McKenzie and Priestley (2016) have investigated a crustal thickening model where the radioactive elements are brought near the surface as soon as partial melting occurs. In numerical models of the evolution of the Himalayas, Beaumont et al. (2004) have shown how heating and weakening of the lower crust allows extrusion and exhumation. Regardless of the mechanism, the point is that self-heating of the crust plays a key role in the evolution of compressional orogens.

4.8.3 The Appalachian Province and the Acadian Orogeny

Ague et al. (2012) have recently found evidence for ultra-high ($\approx 1000^{o}$C) metamorphism during the Devonian Acadian orogeny. Referring to calculations by Chamberlain and Sonder (1990), they have argued that the thermal relaxation of overthickened crust during exhumation is unable to produce the required thermal conditions. We now show why these calculations underestimate the thermal conditions of the Acadian orogeny. Heat production data for the main rock types of the province are given in Table 4.8. We have verified that the present-day exposures are representative of large crustal volumes by turning to shales from the adjacent Atlantic continental margin, which were derived from Appalachian upper crustal material. These shales have almost the same heat production as the currently exposed rocks (Table 4.8).

In their model, Chamberlain and Sonder (1990) took $q_c = 35$ mW m^{-2} , less than our best value of 39 mW m^{-2} (Table 4.5). They also considered that heat production decreases exponentially with depth according to $A(z) = A_s \exp(-z/D)$ where z is depth and $D = 10$ km, leading to very low values in the lower crust (less than 0.17 μW m^{-3} for $z > 30$ km). All these assumptions err in the direction of lower temperatures. When dealing with the Acadian orogeny, the very concept of a highly stratified crust with small heat production in the lower crust is highly questionable. The Appalachians crust is certainly

stratified today, as shown by heat flow data, but its stratification is partly due to crustal melting and melt transport to the upper crust, in other words it is a consequence of the orogenic event itself. The large syntectonic intrusives of the New Hampshire plutonic suite and the highly radioactive post-tectonic Concord granites that are scattered throughout New England testify to both enrichment of the upper crust and depletion of the lower crust (Table 4.8). The Appalachian crust was modified further by the event that led to the formation of the very enriched anorogenic plutons of the White Mountain Magma Series. The large amounts of uranium and thorium of these plutons are difficult to attribute to their parent mantle melts, all the more as they came from depleted mantle (Foland and Allen, 1991). Isotopic studies show that the White Mountains magmas have incorporated large amounts of pre-existing crust (Foland and Allen, 1991), thereby scavenging heat sources from the basement. Returning materials from the exposed intrusives to their original crustal positions acts to enhance heat production deep down in the crust.

For the sake of discussion, we have calculated steady-state geotherms for several distributions of heat production. The Appalachian crust of today is 40 km thick and the mantle heat flux is probably as high as 18 mW m^{-2} (Lévy et al., 2010). Heat production in its approximately 10 km thick upper crust is 2.6 μW m^{-3} and the crustal heat flow component is 39 mW m^{-2} . We apply a small correction for the age of the Acadian orogeny (a 10% increase). For mid and lower crusts that are both 15 km thick, we have first taken heat production rates to be 0.7 and 0.3 μW m^{-3} , respectively, which are consistent with the global crustal models (Table 4.1). Using temperature-dependent conductivity (Appendix 4), the predicted Moho temperature is 548^{o}C. The crust of today is thinner than at the end of the orogeny and the sediments of the US continental margin show that the crust that was eroded away in the last 200 million years has the same composition as today's surface average (Table 4.8). We can estimate the amount of denudation from the crystallization conditions of the White Mountains intrusives, which indicate pressures in a 0.1-0.15 GPa range. Adding 5 km of upper crustal material leads to a paleo Moho temperature of 733^{o}C. Redistributing heat sources throughout the crust, the temperature at the base of a

homogeneous crust would be 939°C. These estimates bracket the Moho temperature in the Appalachians and it is clear that even modest amounts of thickening would lead to the ultra-high metamorphic temperature reported by Ague et al. (2012).

4.8.4 The Archean Lewisian Complex, Northern Scotland

The Scourie granulitic rocks of northern Scotland were amongst the first ones to be recognized as exposures of the lower crust and are worth discussing because of their notoriety. These rocks were heated to 875-975 °C at pressures of 0.85-1.15 GPa $\approx$ 2.8-2.7 Gy ago (Johnson and White, 2011). They are strongly depleted in uranium and thorium, which has led many authors to conclude that crustal heat sources did not play an important role (Rollinson, 2012).

The Scourie granulites are part of the Archean Lewisian complex which also includes the Torridon ampholite facies gneisses. The Scourie granulites and the Torridon amphibolites share the same geological history and belonged to the same crustal block (Rollinson, 2012). They have barely been affected by later deformation events and provide samples of middle and lower crustal levels. Parts of the Lewisian upper crust have been preserved in local sedimentary rocks, notably in the Stoer Group mudstones (Young, 1999; Kinnaird et al., 2007) and probably in the Loch Maree clastic metasediments although this is controversial (Floyd et al., 1989; Park et al., 2001).

Table 4.9 lists data for the main rock types of the Lewisian complex and associated metasediments. The Stoer mudstones and Loch Maree shales have almost identical uranium and thorium contents. Heat production decreases steadily as one goes through the supracrustals-amphibolites-granulites sequence. In order to discuss the Lewisian crust in the Archean, we have corrected the present-day U, Th and K concentrations for radioactive decay (Table 4.9). The Archean heat production values do qualify as high by the standards of the global geochemical models (Tables 4.1). In particular, with heat production that is higher than all the global geochemical estimates for the lower crust, the Scourie granulites

no longer appear as exceptionally depleted. These granulites are in fact restites from a partial melting event that is dated at about the time of high-T metamorphim (Rollinson, 2012). Their protolith lost most of its uranium and thorium to melts that rose to shallower crustal levels. It is therefore an enhanced lower crustal heat production that should be entered in a thermal model for the metamorphic event.

For the sake of example, we have built a tentative Lewisian crustal column using the Stoer composition for the upper crust, the Torridon amphibolites for the middle crust and the Scourie granulites for the lower crust. Using a standard crustal model with three layers of 13.7, 13 and 12.1 km thicknesses, respectively (see Table 4.1), a Moho heat flux $q_m = 15$ mW m^{-2} and the thermal conductivity equation given in Appendix 4, we find a Moho temperature of 714^{o}C at steady-state. This calculation is only valid for Lewisian crust that had returned to thermal equilibrium after an orogenic event and an episode intracrustal fractionation. For homogeneous crust with the same crustal heat flow component, the steady-state Moho temperature would be 988^{o}C. These steady-state calculations may not capture accurately the thermal conditions of the Lewisian orogenic event, which saw the thickening of the crust and the burial of the Scourie protolith (Rollinson, 2012). They do indicate, however, that heat production in the Lewisian crust was probably large enough to account for high-T metamorphism.

4.9 Thermal Transients

There are two types of thermal transients that are intrinsic to radiogenic heat production. One derives from the very process of radioactive decay, such heat production decreases with time as the unstable isotopes of uranium, thorium and potassium get progressively exhausted. The consequences for the thermal evolution of thick roots and for the interpretation of heat flow data have been studied in a series of papers (Jaupart and Mareschal, 1999; Michaut et al., 2007, 2009; **?**). The other type of thermal transient has been described recently and arises in the aftermath of an orogenic event (Jaupart and Mareschal,

2015).

4.9.1 Post-Orogenic Metamorphism and Anatexis

Many ancient metamorphic events were followed quasi-isobaric cooling over long time intervals of 300 My or more, indicating negligible rates of denudation (Mezger et al., 1990; Heaman et al., 2011). We may therefore ignore erosion, which simplifies matters considerably. Post-orogenic thermal evolution is best understood by breaking down the temperature field in two components, which is possible for a constant thermal conductivity (Jaupart and Mareschal, 2015) :

$$T(z,t) = T_i(z,t) + T_r(z,t) \tag{4.15}$$

Component T_i describes the diffusive relaxation of the initial thermal structure $T_o(z)$, such that the initial condition is $T_i(z,0) = T_o(z)$. Component T_r accounts for crustal heat production and starts at zero by construction. The breakdown of temperature in these two components is not arbitrary, but the time of the breakdown is. One can begin the calculation at any time and the initial thermal structure $T_o(z)$ is a snapshot in an evolution that started earlier and that involved crustal heat production.

The key aspect is that the two components evolve over two different time-scales, noted τ_i and τ_r respectively. τ_i depends on the vertical extent of the initial thermal anomaly and lumps together two transients : a fast one for an initial crustal anomaly such as a lower crustal "hot zone" and a slower one for perturbed lithosphere to return to equilibrium. τ_r is also set by the lithospheric response because the crustal sources must provide heat to both the crust and its underlying mantle root. Although both temperature components are affected by heat transport through the whole lithosphere, one has $\tau_r > \tau_i$ for the following reason. In both cases, the thermal evolution depends on heat loss through the surface, which acts in opposite senses for the two components. The surface heat loss accelerates cooling and hence the thermal relaxation of the initial anomaly, but it slows down the heating by

crustal heat sources. Starting from an initial "hot geotherm", as appropriate for the end of the orogenic event proper (*i.e.* the end of tectonic deformation and magmatic activity from external sources), one observes an initial cooling phase that gets interrupted by radiogenic heating. With sufficiently large values of heat production, one may return, or even exceed, the starting values of temperature in the crust, which accounts for post-orogenic metamorphism and plutonic activity. As shown by Jaupart and Mareschal (2015), the time-lag between the end of the orogeny and post-orogenic peak metamorphism is predicted to be several tens of million years, in agreement with the observations (Heaman et al., 2011).

One set of results from Jaupart and Mareschal (2015) is shown in Figure 4.15 for 150 km-thick lithosphere. Heating by crustal heat sources overwhelms the initial cooling after a time of about 10 My and temperatures in the lower crust rise to values larger than 850^{o}C after about 60 My. This time lag would be shorter for a smaller initial thermal perturbation and a higher heat production rate, and it would be longer for a smaller heat production rate. It is worth illustrating how the radioactive temperature component T_r evolves during the post-orogenic thermal ramp-up (Figure 4.16). In a first phase, temperatures rise steadily everywhere with a peak that is located just above the Moho because the heat sources are located in the crust and shed heat to the underlying lithospheric mantle. This phase segues into a second one characterized by the slow evolution of the lithospheric root towards thermal equilibrium with the crustal heat sources. Once this has been achieved, one enters a phase of secular cooling due to the rundown of radioactivity, which is described next.

4.9.2 Secular Changes of Lithospheric Temperatures

Following the thermal relaxation of the initial lithosphere formation event, two types of long-term transients may occur, due to changes of heat supply at the base of the lithosphere and to the rundown of radiogenic heat production. We restrict our attention to crustal heat sources and ignore lithospheric ones, whose effects have been described and analyzed in several papers (Jaupart and Mareschal, 1999; Michaut et al., 2007; Michaut and Jaupart,

2007). The thermal relaxation time of thick continental lithosphere, $\tau_{diff} = H^2/\kappa$, where H is thickness and κ thermal diffusivity, is very large. For $H = 200$ km and $\kappa = 8 \times 10^{-7}$ $m^2\ s^{-1}$, τ_{diff} = 1.6 Gy. Such a very long time is responsible for several peculiar thermal transients.

We first focus on heat production and its impact on the lithospheric geotherm, which we describe with the T_r temperature component. It takes a very long time for thick lithosphere to reach a regime of quasi-equilibrium with the crustal heat sources. For bulk Earth Th/U and K/U ratios, heat production follows closely an exponential decay with time constant $\tau_{radio} \approx 3.4$ Gy. This is not much larger than the diffusive relaxation time, implying that heat production decreases whilst lithospheric temperatures are catching up with the deep crust. Once secular quasi-equilibrium conditions have been attained, temperatures decrease everywhere (*i.e.* in both crust and lithospheric mantle) due to radioactive decay. Lithospheric temperatures therefore peak at a late time which increases with increasing lithosphere thickness (Figure 4.17).

The slow decrease of lithospheric temperatures proceeds at a rate which is set by the decay of the radiogenic isotopes. For a typical value of crustal heat production of 0.7 $\mu W\ m^{-3}$ today, corresponding to 1.5 $\mu W\ m^{-3}$ at the end of the Archean, this rate is about 100K/Gy. This is within the range of values for the secular cooling of the Earth's mantle (Jaupart et al., 2015), which raises interesting possibilities. The lithospheric root may cool down more rapidly than the underlying mantle, which may induce its thickening. It may also may cool down less rapidly than the underlying mantle. In this case, the lithospheric geotherm would turn at some depth, such that the deep lithosphere would in fact be supplying heat to the asthenosphere. This lower lithospheric region would be stably stratified thermally, but it would lie beneath a hotter and mechanically weak horizon, which would favour shearing and delamination. These possibilities have been studied in more detail by Michaut et al. (2009).

The geological implications of these transient behaviours are multifold. Changes in the

amount and/or vertical distribution of crustal heat sources that are induced by an orogenic event are rapidly translated into the thermal structure of the crust but can only affect the deep lithosphere after a long time lag. The crust and its thick lithospheric root may therefore remain thermally and mechanically decoupled for longer than the time between two orogenic events. In addition, the lower parts of lithospheric roots may be much more active than commonly thought.

4.10 Conclusion

The contribution of crustal heat sources to the surface heat flux remains insufficiently constrained. The range of global averages of heat production rates is wide (0.2μW m^{-3}) and translates into an uncertainty of $\pm$4mW m^{-2} for the crustal component and Moho heat flux. This is comparable to the uncertainty associated with heat flow and heat production studies. It should be emphasized, however, that the Moho heat flux can only vary on scales of 500 km or more, so that heat flow studies allow the resolution of local variations in the crustal heat flow component within a province. Long wavelength variations of heat production in the lower crust are difficult to detect but they would have a strong effect on Moho temperatures if they exist. For a given surface heat flux, as far as lower crustal temperatures are concerned, overestimating present Moho heat flux counterbalances to a large degree the underestimated lower crustal heat production. But this compensating effect may not hold when reconstructing past conditions, when heat production was higher than today. Although not the focus of this review, the mantle heat flux value determines lithospheric temperatures and thickness with implications for interpreting seismic velocity profiles and xenoliths thermo-barometry data. Reciprocally, xenoliths and seismic studies are useful to validate the thermal models of the lithosphere. Attractive as the concept of thermal isostasy might appear, it is difficult to apply in the tectonically active regions that provide a large part of the elevation signal owing to their transient thermal structures.

We have emphasized the effect of crustal differentiation and lower crustal heat produc-

tion on the thermal regime, strength and stability of the lithosphere. In addition, one should be aware that the crustal thickness should not be treated as a given but should rather be considered as resulting from a complex sequence of melting, intracrustal fractionation and deformation events.

High rates of crustal heat production have been found in several regions that experienced high temperature metamorphism in the past. For the examples examined in this study, crustal heat production is largely sufficient to explain such metamorphic events without calling for an external thermal perturbation. Likewise, the 20-100 My delay between tectonic events such as crustal accretion and compressional orogenies on the one hand and peak metamorphism on the other hand is consistent with crustal self-heating by radiogenic elements.

Table 4.1 Different estimates of heat production in the continental crust (in μW m^{-3}). For each crustal model with the exception of the North American cordillera, the first line lists the thicknesses of the crustal layers and the total crust thickness.

Model	Upper Crust	Middle Crust	Lower Crust	Bulk
Global Geochemical Models				
Rudnick and Gao (2014)	12 km	11 km	17 km	40 km
	1.6	0.96	0.18	0.89
Huang et al. (2013)	13 km	11 km	10 km	34 km
	1.6	0.73	0.17	0.94
Hacker et al. (2015) †	13.7 km	13 km	12.1 km	38.8 km
Model A	1.58	0.35	0.21	0.74
Model B	1.58	0.34	0.17	0.72
Model C	1.58	0.46	0.26	0.80
Model D	1.58	0.72	0.33	0.90
Exposed cross-sections				
North American Cordillera				
Lee et al. (2007) ‡	1.67	0.99	0.2	0.88
Kohistan, Pakistan				
Jagoutz and Schmidt (2012) §	/	/	$\approx$ 25 km	$\approx$ 55 km
Model 1	/	/	0.18	0.69
Model 2	/	/	0.11	0.50
Model 3	/	/	0.06	0.58
Heat Flow Data				
Jaupart and Mareschal (2014)				0.79-0.95

† Models A-D correspond to different end-member compositions that are compatible with geophysical characteristics.

‡ No thicknesses for the three crustal layers are reported.

§ Models 1-3 correspond to slightly different thicknesses and the inclusion or exclusion of the Chilas ultramafic-mafic complex.

Table 4.2 High heat production granites

Name	Heat Production (μW m^{-3})			reference
	Average	min	max	
Archean				
Cartier Batholith (Superior, Can)	4			(Meldrum et al., 1997)
Lac de Gras (Slave, Can)	8.1	4.9	15.9	(Thompson et al., 1995)
	6.4	5.3	8.1	(Thompson et al., 1995)
Bundelkhand craton (India)		4.0	4.8	(?)
Proterozoic				
Bohus (Norway)	6.4			(Landstrom et al., 1980)
Eastern Gawler Craton (Aus)	7.5	3.4	17.0	(Neumann et al., 2000)
Namaqua complex (South Af.)	3.7	0.86	46.0	(Andreoli et al., 2006)
Chottanagpur gneiss complex (India)		3.9	6.5	(?)
Phanerozoic				
Mount Painter Province (Aus)	16.1	4.5	60.1	(McLaren et al., 2006)
S W England batholith	4.7			(Tammemagi and Smith, 1975)
White Mountains (App, USA)	8.5			(Roy et al., 1968)

Table 4.3 Mean heat flow and surface heat production in different parts of the same geological province. The mean heat production is that of all the samples from the heat flow sites.

	Heat Flow ($\pm\sigma$) (mW m^{-2})	Heat Production ($\pm\sigma$) (μW m^{-3})	Reference
Accreted Terranes, Superior Province, Canada			
Wabigoon	42.5 ± 7.3	0.66 ± 0.51	(1)
Wawa	44.4 ± 8.0	0.85 ± 0.40	(1)
Abitibi (west of 77^{o}W)	43.3 ± 7.0	0.59 ± 0.52	(1)
Appalachians			
Canada part	56 ± 12	2.6 ± 2.0	(2)
U.S. part	58 ± 13	2.5 ± 1.9	(2)

References : (1) **?**, (2) Mareschal et al. (2000)

Table 4.4 Average crustal heat production range A and crustal heat flow component q_c calculated for a 40km thick crust *vs* crustal age group. From Jaupart and Mareschal (2014).

Age group	A μW m^{-3}	q_c mW m^{-2}	% Area †
Archean	0.56-0.73	23-30	9
Proterozoic	0.73-0.90	30-36	56
Phanerozoic	0.95-1.21	38-48	35
Total Continents	0.79-0.99	32-40	

†Fraction of total continental surface, from model 2 in Rudnick and Fountain (1995)

Table 4.5 Crustal Component of Heat Flow in high-T metamorphism provinces. Average surface heat flux, $\overline{q_o}$, mantle heat flux, q_m, crustal component, q_c.

Province	Age (Gy)	T, P conditions (^{o}C, GPa)	$\overline{q_o}$	q_m mW m^{-2}	q_c	q_c(past)	Reference
Superior, Can. (accreted belts)	2.7	725-810, 0.6-0.7	44	15	29	61	(1)
Namaqua, S. Africa	1.05	800-1000, 0.6-0.8	61	18	43	54	(2)
Mount Painter Province, Aus.	0.4	750-800, 0.6-0.7	92	15	80	85	(3)
Appalachians, N. Am.	0.4	1000, 1.0	57	18	39	43	(4)

References : (1) Heaman et al. (2011); Lévy et al. (2010); ?, (2) Jones (1987, 1992); Andreoli et al. (2006), (3) McLaren et al. (2006), (4) Ague et al. (2012); Lévy et al. (2010); Lévy and Jaupart (2011).

Table 4.6 Heat production of granulite facies terranes in different regions ranked by age and maximum pressure of granulite facies metamorphism.

Location	Age (Gy)	Pressure† (GPa)	Heat production (μW m^{-3})	Reference
Archean				
Vredefort (South Africa)	> 3.1	0.4 - 0.6	1.0	(1)
Western Dharwar craton (India)	2.7	0.5 - 0.7	0.65	(2)
Western Dharwar craton (India)	2.7	0.7 - 1.1	0.35	(2)
Eastern Dharwar craton (India)	2.7	0.5 - 0.7	0.35	(2)
Eastern Dhawar craton (India)	2.7	0.7 - 1.1	0.16	(2)
Kapuskasing (Superior, Canada)	2.65	1.0 - 1.1	0.40	(7)
Pikwitonei (Superior, Canada)	2.6	0.6 - 1.1 †	0.40	(3)
Varpaisjarvi (Finland)	2.6	0.8 - 1.1	0.57	(4)
Scourie (NW Scotland)	2.7	0.85 - 1.15	0.11	(5)
Proterozoic				
Turku (Finland)	1.82	0.4 - 0.6	2.24	(4)
Egersund (Norway)	1.0	0.4 - 0.6	0.40	(6)
Pielavesi (Finland)	1.89	0.45 - 0.65	0.96	(4)
Southern Estonia	1.83	0.6	1.35	(4)
Lapland (Finland)	2.0	0.6 - 0.7	1.0	(4)
Eastern Ghats (India)	1.0	0.8 - 1.2	0.26	(8)
Musgrave Range (Australia)	1.2	1.2	0.30	(9)
Phanerozoic				
Ivrea Zone (Italy)	0.3	0.6 - 0.9	0.40§	(10)
South Altay belt, NW China	0.35 - 0.30	9.1 - 9.3	0.97	(11)
Globaldataset				
31 terranes worlwide	/	/	0.68 ± 0.62	(12)

†Samples from several parts of the Pikwitonei with different metamorphic pressures. § Heat production value for a mixture of felsic and mafic lithologies (metapelites and stronalites on the one hand and a mafic complex on the other hand).

References : (1) Nicolaysen et al. (1981) ; (2) Kumar and Reddy (2004) ; (3) Fountain et al. (1987) ; (4) Joeleht and Kukkonen (1998) ; (5) Rollinson (2012) ; (6) Pinet and Jaupart (1987) ; (7) Ashwal et al. (1987) ; (8) Kumar et al. (2007) ; (9) Lambert and Heier (1967) ; (10) Galson (1983) ; (11) Yang et al. (2015) ; (12) Hasterok and Chapman (2011).

Table 4.7 Average surface heat flux, $\overline{q_o}$, average crustal heat production, $\overline{A}$, crustal thickness, h_m, and differentiation index, DI, (equation 4.11) for different provinces.

Province	Age (Gy)	$\overline{q_o} \pm \sigma$ (mW m^{-2})	$\overline{A} \pm \sigma$ (μW m^{-3})	h_m (km)	DI	Reference
Slave province, Can.	3.1	51	2.0	36	2.0	(1)
Superior craton core, Can.	> 2.7	31.8 ± 5.2	0.78 ± 0.37	40	2.0	(2)
Superior accreted terranes, Can.	2.7	41.0 ± 8.7	0.8 ± 0.8	40	1.0	(2)
Wawa subprovince, Superior, Can.	2.7	45.1 ± 8.0	0.85 ± 0.79	40	1.0	(3)
Abitibi subprovince (all), Superior, Can.	2.7	39.9 ± 7.0	0.5 ± 0.4	38	0.7	(3)
Trans-Hudson Orogen, Can.	2.1-1.8	42 ± 11	0.7 ± 0.5	40	1.1	(2)
Flin-Flon Snow Lake Belt (THO), Can.	1.9-1.8	40 ± 5	0.32 ± 0.2	40	0.5	(3)
Wopmay Orogen, Can.	1.8	90 ± 15	4.8	32	2.0	(3), (4)
Central Shield, Aust.	1.8	72 ± 24	3.6 ± 1.9	35	3.2	(5),(6)
Eastern Gawler craton, Aust.	1.6	78 ± 19	5.0	40	2.4	(5, (6)
Grenville, Can.	1.3-1.1.	41 ± 11	0.8	40	1.0	(3)
Namaqua, S. Africa	1.05	61 ± 11	2.3	43	2.0	(6) ,(7)
Appalachians, N. Am.	0.4	57 ± 13	2.6 ± 1.9	40	2.5	(3)

References : (1)Perry et al. (2006), (2) ?, (3) Perry et al. (2010), (4) Lewis et al. (2003), (5) Neumann et al. (2000), (6) Mareschal and Jaupart (2013), (7) Jones (1987, 1992).

Table 4.8 Heat Production Data for the Appalachians province, U.S.A.

	A (μW m^{-3})	Reference
Large-scale surface average	2.6 ± 0.3	(1)
Shales †	2.15 - 2.37	(2)
Syntectonic plutons‡(410-390 Ma)	1.8 - 2.2	(3),(4), (5)
Post-tectonic plutons§ (360 Ma)	4.0	(6)
Anorogenic granites & (*ca* 180 Ma)	8.6	(6)

†Sediments from the U.S. Atlantic continental margin (COST B-2 and B-3 boreholes).
‡New Hampshire plutonic suite (three major plutons : Kinsman, Spaulding and Bethlehem gneiss).
§ Concord two mica granites (several plutons scattered throughout New England).
& White Mountain plutonic series.
References : (1) Jaupart and Mareschal (2014), (2) Della Vedova and Von Herzen (1987), (3) Chamberlain and Sonder (1990), (4) Lyons (1964), (5) Jaupart et al. (1982), (6) Roy et al. (1968),

Table 4.9 Heat Production Data for the Lewisian-Scourie area, NW Scotland.

Rock type	U (ppm)	Th (ppm)	K (%)	A (present) (μW m^{-3})	A(2.7 Gy) (μW m^{-3})	Ref.
Loch Maree supracrustals †	3.19	11.1	2.1	1.83	3.46	(1)
Stoer mudstones ‡	3.2	8.2	2.3	1.64	3.30	(2)
Torridonian amphibolite gneisses	0.67	6.1	2.23	0.81	1.73	(3)
Scourie granulites	0.07	0.17	0.80	0.11	0.38	(3)

†Clastic metasediments derived partly from Archean basement of doubtful provenance (Park et al., 2001).

‡Clastic sediments derived from local Lewisian basement (Young, 1999; Kinnaird et al., 2007).

References : (1) Floyd et al. (1989), (2) Young (1999), (3) Rollinson (2012).

Table 4.10 Lowest surface heat flux measurements.

location	age (My)	heat flux (mW m^{-2})	Reference
West African Shield		18-22	(1)
Lynn Lake (Trans Hudson, Canada)	1800	22	(2)
Voisey Bay (Nain, Canada)	1600	22	(3)
LaGrande (Superior, Canada)	2700	22	(4)
Ukrainian Shield		20	(5)
Dharwar craton (India)	2700	23	(6)
Baltic Shield		18	(7)
Urals	400	20	(8)
Siberian platform		12	(9)

(1) Chapman and Pollack (1974), (2) Rolandone et al. (2002), (3) ?, (4) Lévy et al. (2010), (5) Kutas (1977), (6) Roy and Rao (2000), (7) ? (8) Kukkonen et al. (1997) (9) Duchkov (1991)

Table 4.11 Moho heat flux (q_m) in different regions

Location	Age (My)	q_m (mW m^{-2})	Reference
Kapuskasing (Superior, Canada)	1900	15	(1)
Abitibi subprovince (Superior, Canada)	2700	14	(2)
Grenville Province (Canada)	1100	14	(1)
Appalachians	400	18	(3)
Slave Province (Canada)	2700	11	(4) †
Dharwar craton (India)	2700	12-18	(5)
Baltic Shield	2700	12	(6), (7) †
Siberian platform		12	(8)
Altai-Sayan belt (Siberia)	450	10	(8)
Vredefort (South Africa)	2200	12-17	(9)
Kaapvaal (South Africa)		18-22	(10)†
Kaapvaal (South Africa)		14-18	(11)†
Sierra Nevada (USA)	200	<20	(12)
		10	(13)

† Estimated from surface heat flow and geothermobarometry on mantle xenoliths. References : (1) Pinet et al. (1991), (2) Guillou et al. (1994), (3) Lévy et al. (2010), (4) Russell et al. (2001), (5) Roy and Rao (2003), (6) Kukkonen and Jõeleht (1996), (7) Kukkonen and Peltonen (1999), (8) Duchkov (1991), (9)Nicolaysen et al. (1981), (10) Rudnick and Nyblade (1999), (11) Michaut et al. (2007), (12) Saltus and Lachenbruch (1991), (13) Brady et al. (2006)

Table 4.12 Creep parameters for lithospheric materials used in calculating the strength of the lithosphere (Ranalli, 1995; Carter and Tsenn, 1987).

	A ($MPa^{-n}s^{-1}$)	n	E ($kJ\ mol^{-1}$)	ρ ($kg\ m^{-3}$)
upper crust (dry granite)	1.0×10^{-7}	3.2	144	2700
lower crust (mafic granulites)	1.4×10^{4}	4.2	445	2700
mantle (dry dunite)	3.0×10^{4}	3.6	535	3300

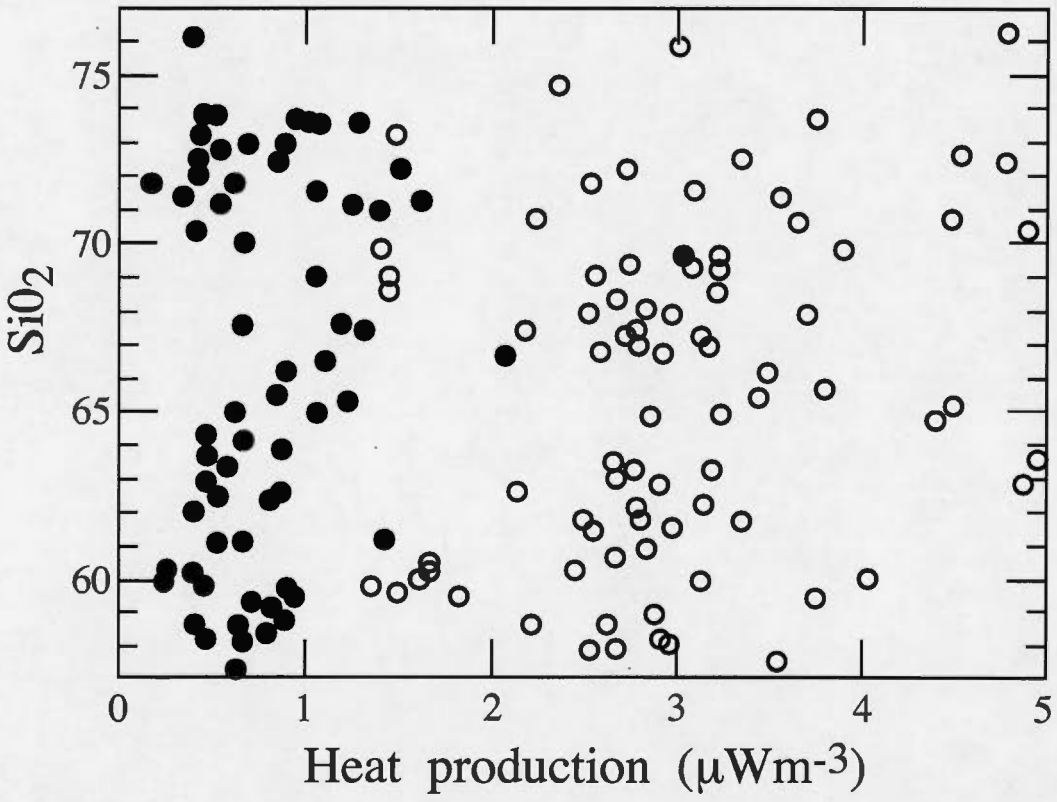

Figure 4.1 Radiogenic heat production rate as a function of SiO_2 content in the Sierra Nevada batholith, from data in Sawka and Chappell (1988). Filled circles : western foothills tonalites-trondhjemites. Open circles : granitoids from the central and eastern parts of the batholith.

Figures

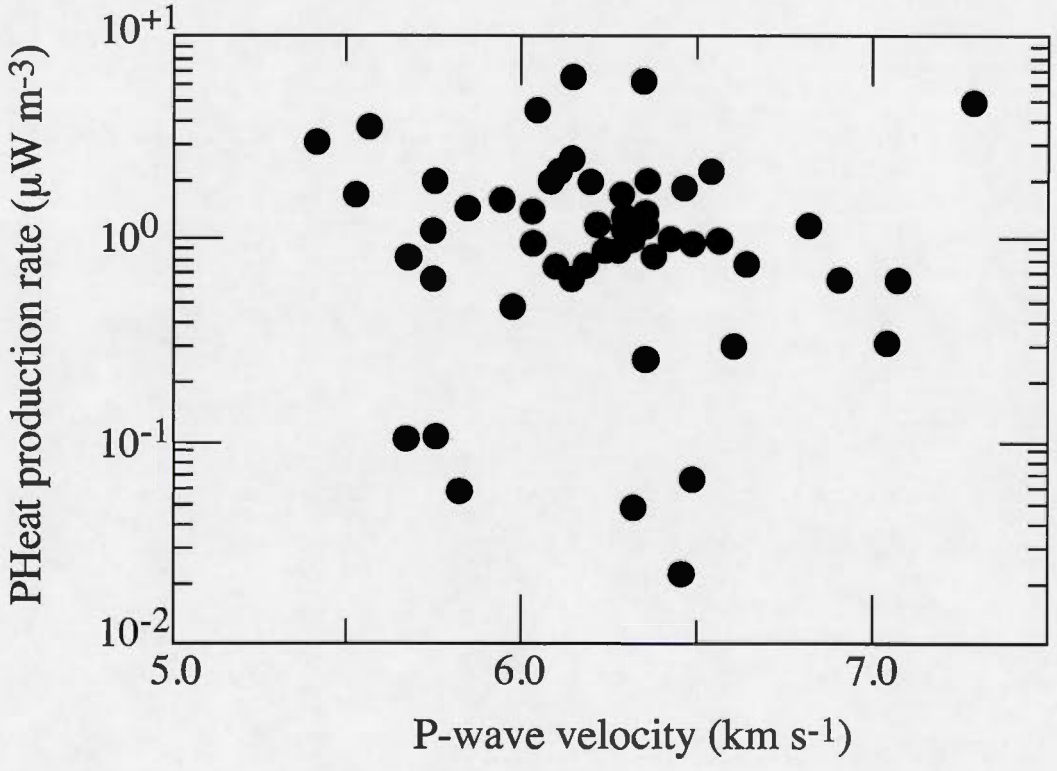

Figure 4.2 Radiogenic heat production rate as a function of P-wave velocity in Precambrian granulite-facies rocks from Finland and Estonia, from data in Joeleht and Kukkonen (1998).

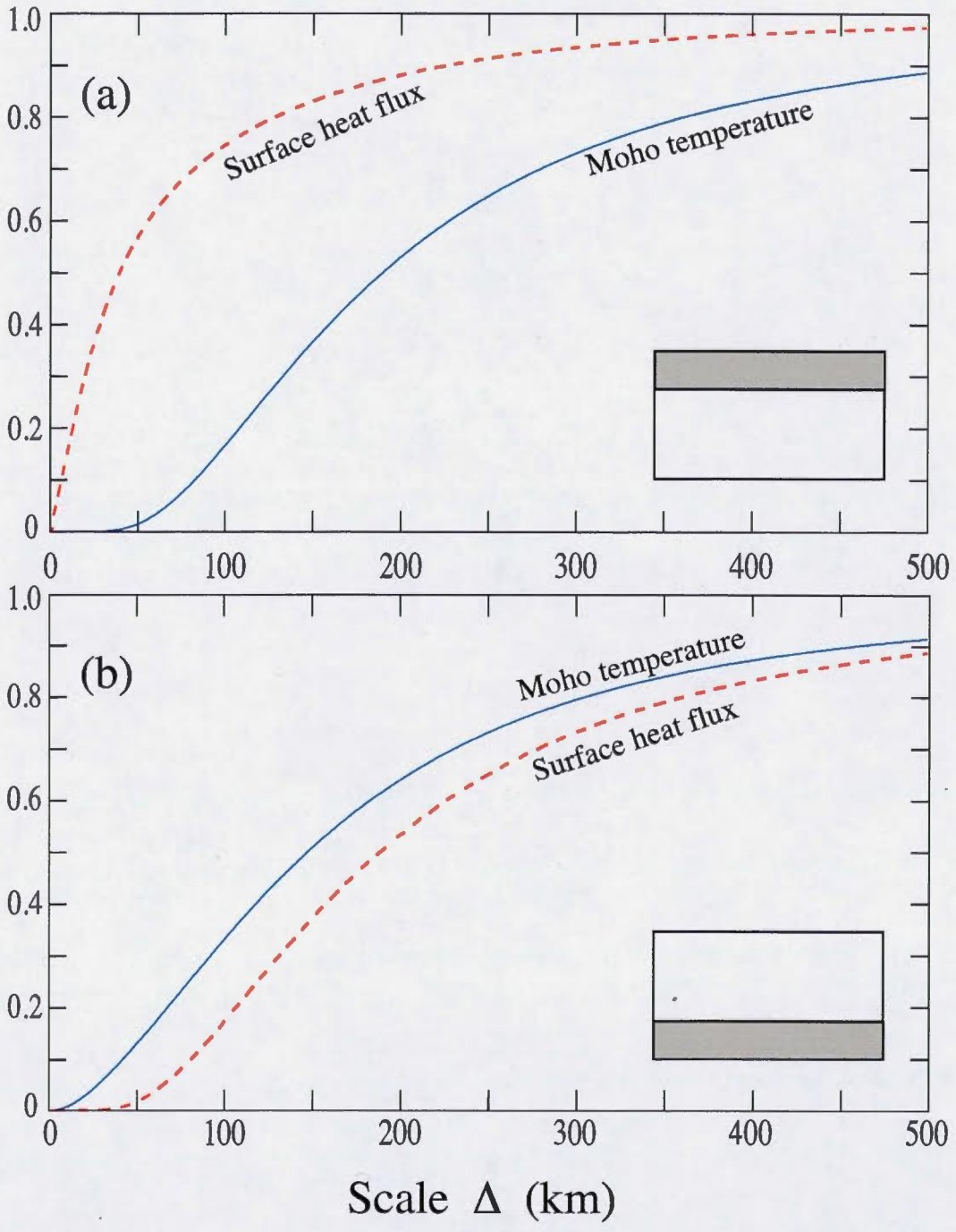

Figure 4.3 Amplitude of variations of the surface heat flow and the Moho temperature due to heat production variations in a 10-km thick crustal layer as a function of horizontal scale. Amplitudes are scaled to their values for an infinitely large scale, corresponding to purely vertical heat transport with negligible lateral diffusion. (a) Results for an upper crustal layer. (b) Results for a lower crustal layer located just above the Moho.

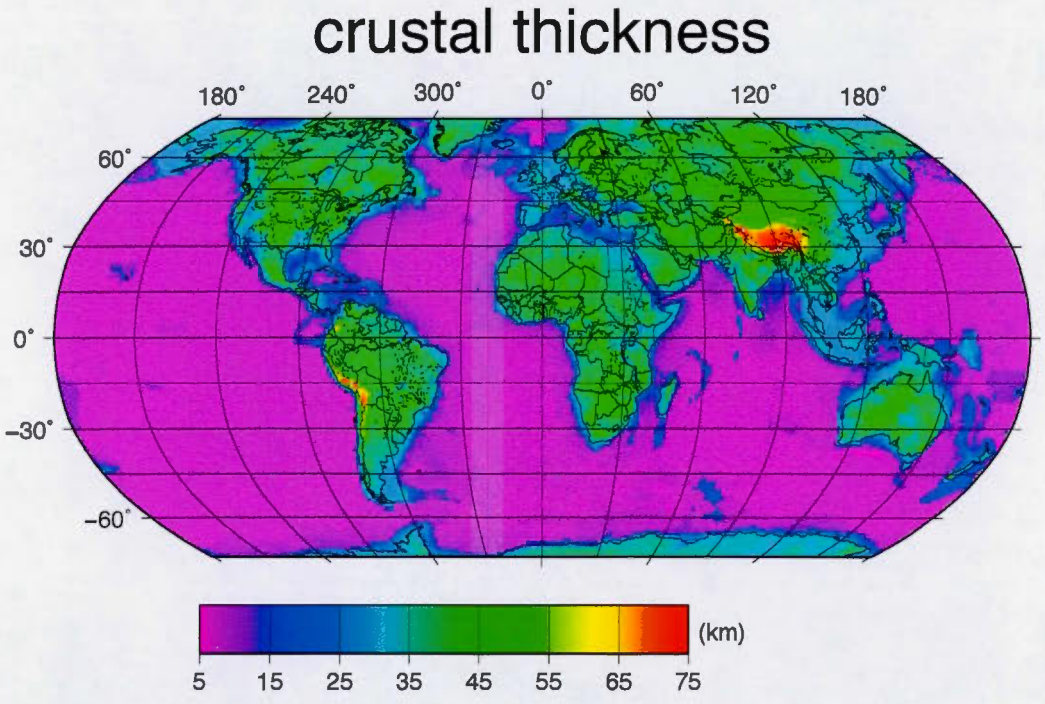

Figure 4.4 Map of crustal thickness based on the CRUST1.0 model on a $1^{o} \times 1^{o}$ grid (Laske et al., 2013). For many cells without seismic data, the values for the crustal thickness are based on geological type.

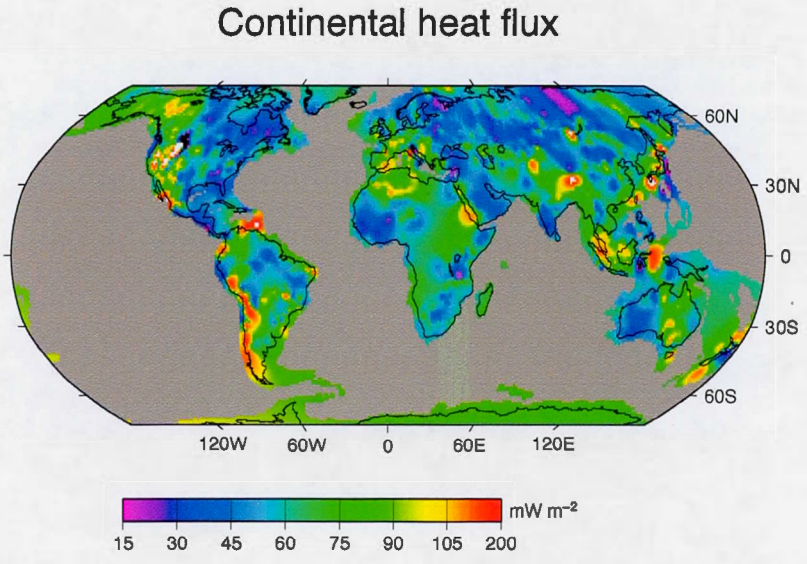

Figure 4.5 Map of continental heat flux based on ≈ 35,000 unevenly distributed continental heat flow measurements. For tectonic active regions, the heat flow is not in steady state and includes a transient perturbation on top of crustal heat production ; in tectonically stable regions with a steady state thermal regime, variations in surface heat flux directly reflect variations in crustal heat production. Note the higher variability of the heat flux compared with crustal thickness.

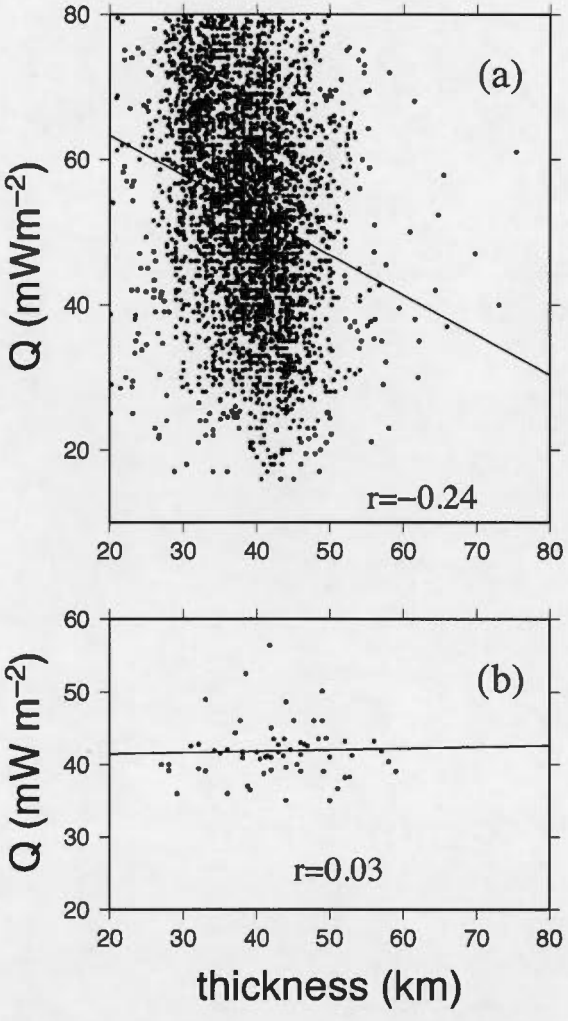

Figure 4.6 Scatter plot of heat flux and crustal thickness.
(a) Global data set comparing heat flux averaged over $1^o \times 1^o$cells *vs* crustal thickness from CRUST1.0. The solid line represents the best linear "fit" to the cloud of points (with a correlation coefficient r=-0.24).
(b) Data from eastern Canada. Heat flux data have been averaged over $1^o \times 1^o$cells and their values are plotted against the corresponding crustal thickness values from Lithoprobe (Perry et al., 2002) and recent receiver function studies (Fiona Darbyshire, pers. comm.). The plot shows no trend and the correlation coefficient between the two data sets r=0.03.

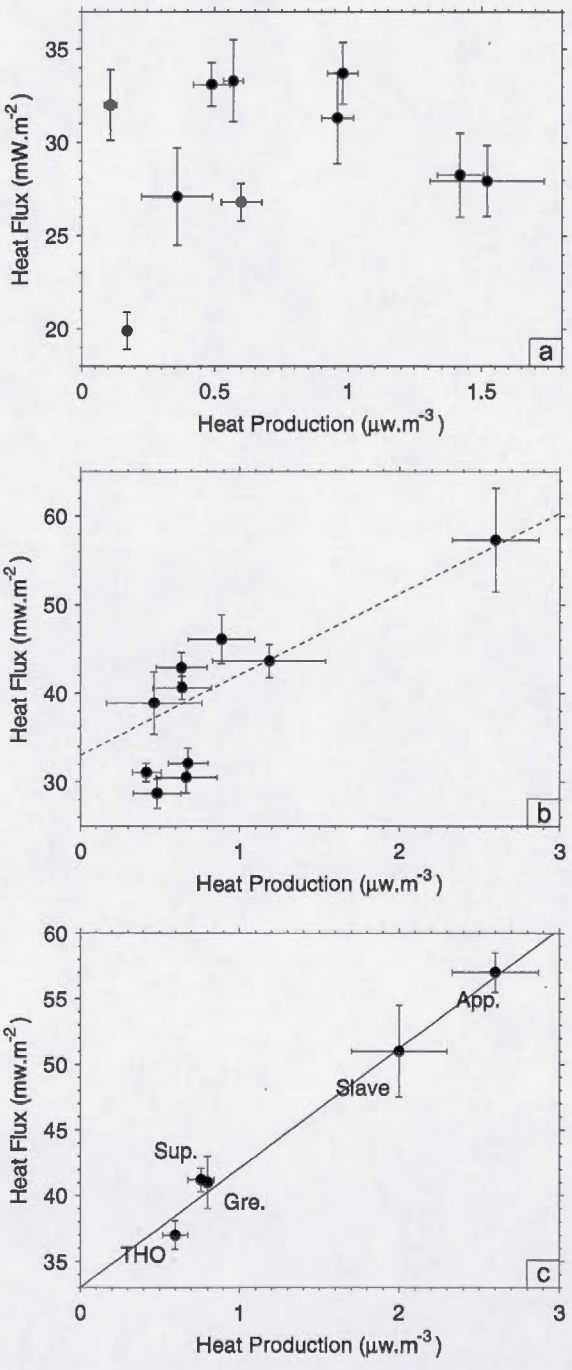

Figure 4.7 Plot of surface heat flow as a function of surface heat production for three different scales in the Canadian Shield and the Appalachians, from Lévy et al. (2010). (a) Local values in the northern part of the Superior province, Canada. (b) Average values for ten 250 × 250 km windows with a large number of measurements. The dashed line is the best-fit linear relationship to values at the largest scale. (c) Average values for the five main geological provinces of North America, the Archean Slave and Superior provinces, the Proterozoic Trans-Hudson Orogen (THO) and Grenville provinces and the Phanerozoic Appalachians province.

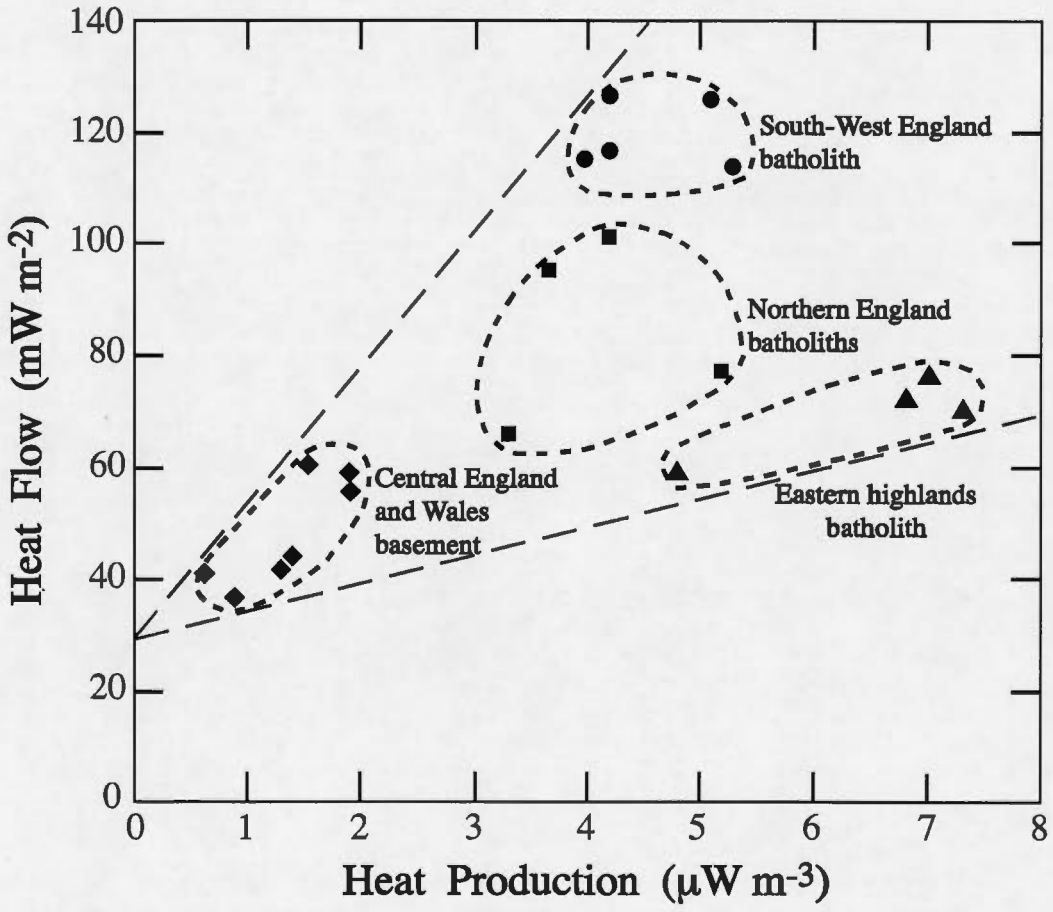

Figure 4.8 Relationship between heat flow and heat production in the United Kingdom, from Webb et al. (1987). The data are grouped in four domains according to location and geological type (short-dashed outlines). The two long-dashed lines have slopes of about 5 and 24 km, and indicate the thicknesses of enriched rocks that are required to account for the heat flow variations between the different domains.

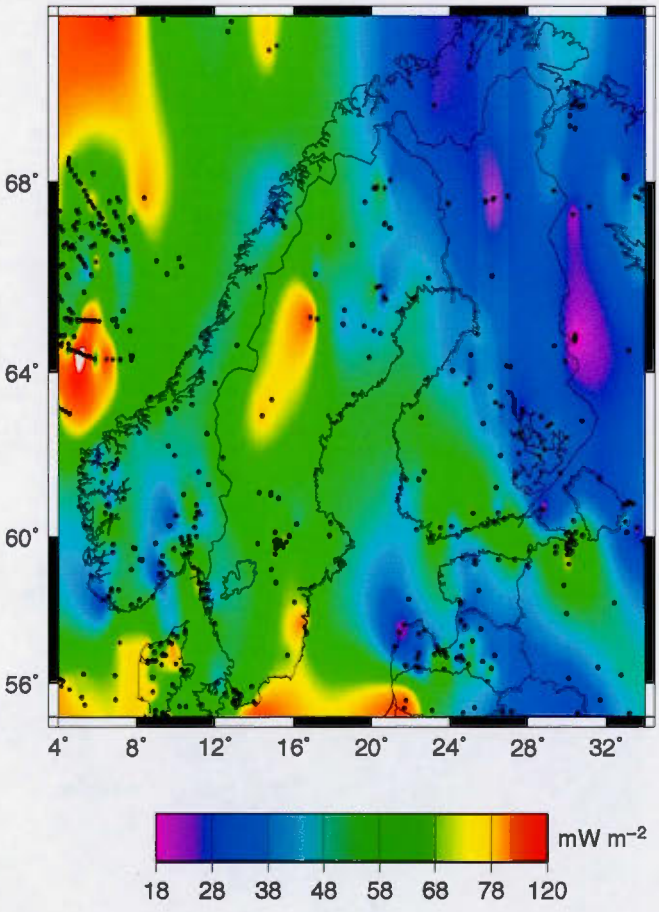

Figure 4.9 Heat flow map of Fennoscandia, from data in Slagstad et al. (2009). Heat flow decreases markedly towards the Archean Baltic Shield to the East. Several intermediate-scale ($\approx$ 120km) heat flow anomalies are generated by enriched or depleted rocks.

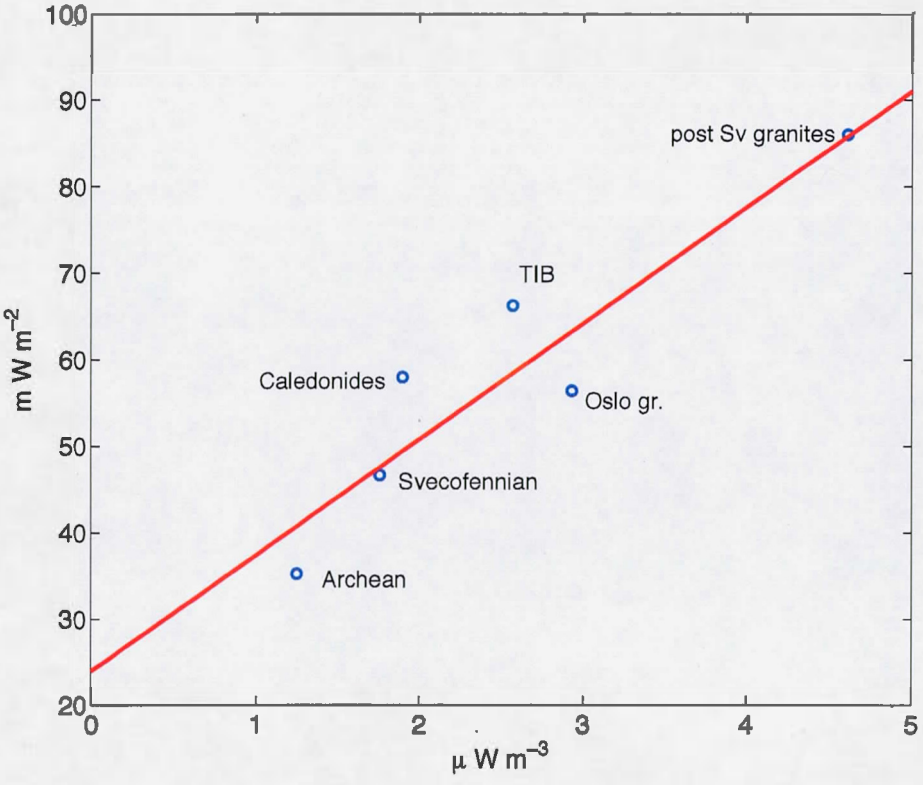

Figure 4.10 Relationship between heat flow and heat production in Fennoscandinavia, from Slagstad (2008). The data are averaged over 6 regions according to location and geological type. The best fitting line is $\overline{Q} = 24.5 + 13.4\overline{A}$. TIB is the TransScandinavian igneous belt.

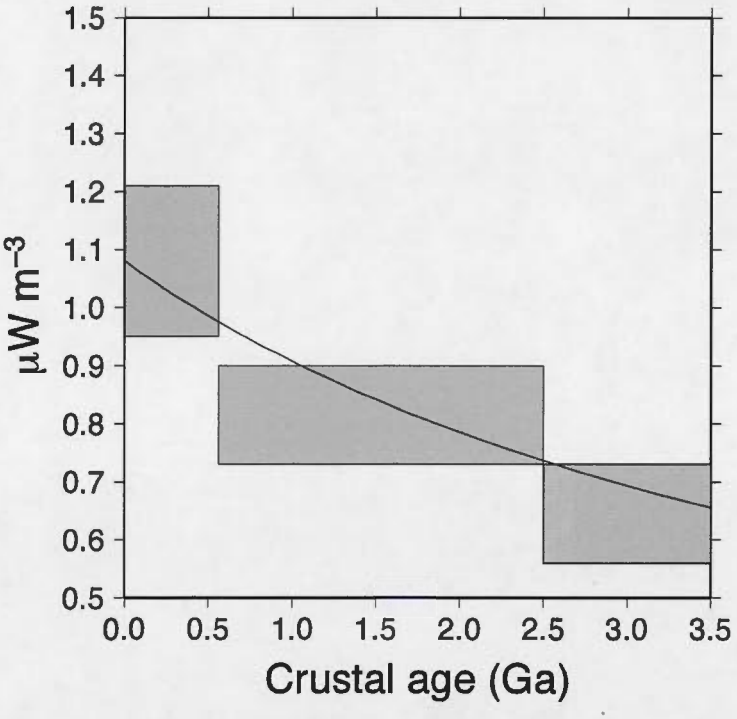

Figure 4.11 Average crustal heat production as a function of age, from Jaupart and Mareschal (2014). The large width of the age groups is due to the large spread of heat production values at any given age, which does not allow a fine scale separation. The thick curve illustrates the rundown of heat producing elements due to radioactive decay. After correction for this rundown, the crustal heat production at the time of crustal stabilization is essentially constant.

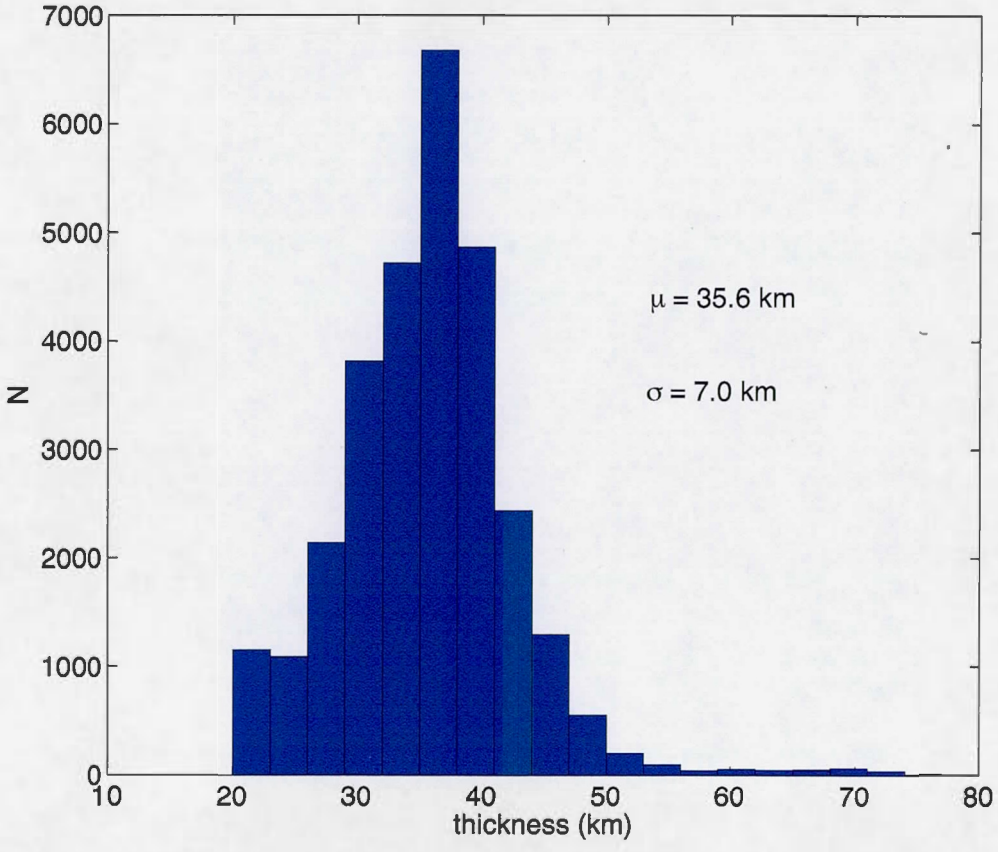

Figure 4.12 Histogram of continental crust thicknesses sampled at $1^o \times 1^o$ from Laske et al. (2013). Most of values >50km or <30km are in active regions.

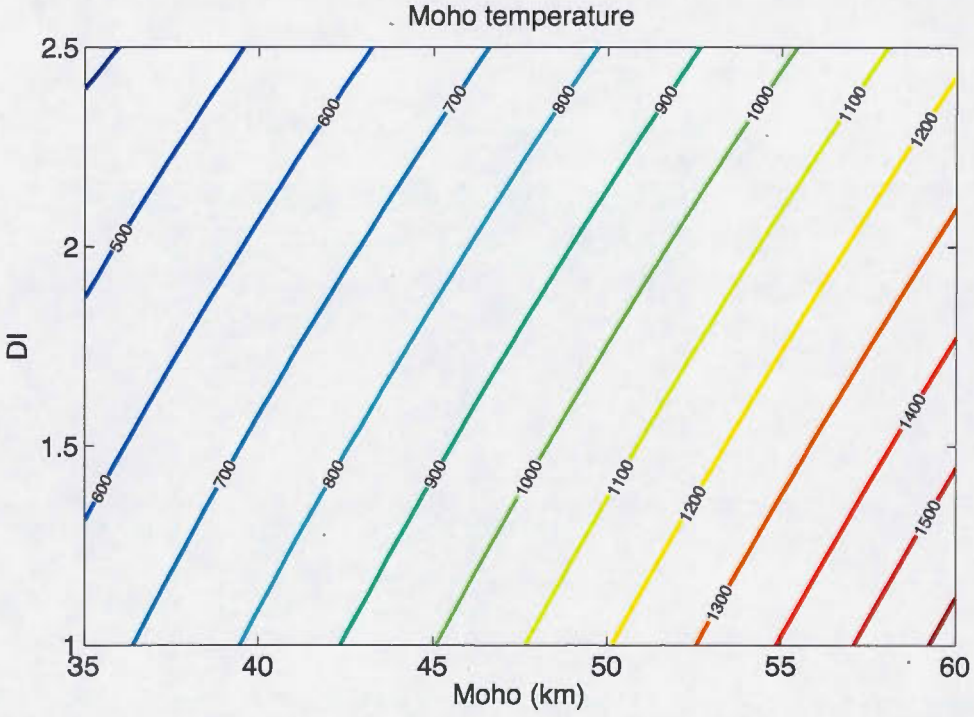

Figure 4.13 Moho temperature variations in function of crustal thickness and differentiation index DI for a mean crustal heat production 1.5 μW m^{-3} representing Archean conditions.

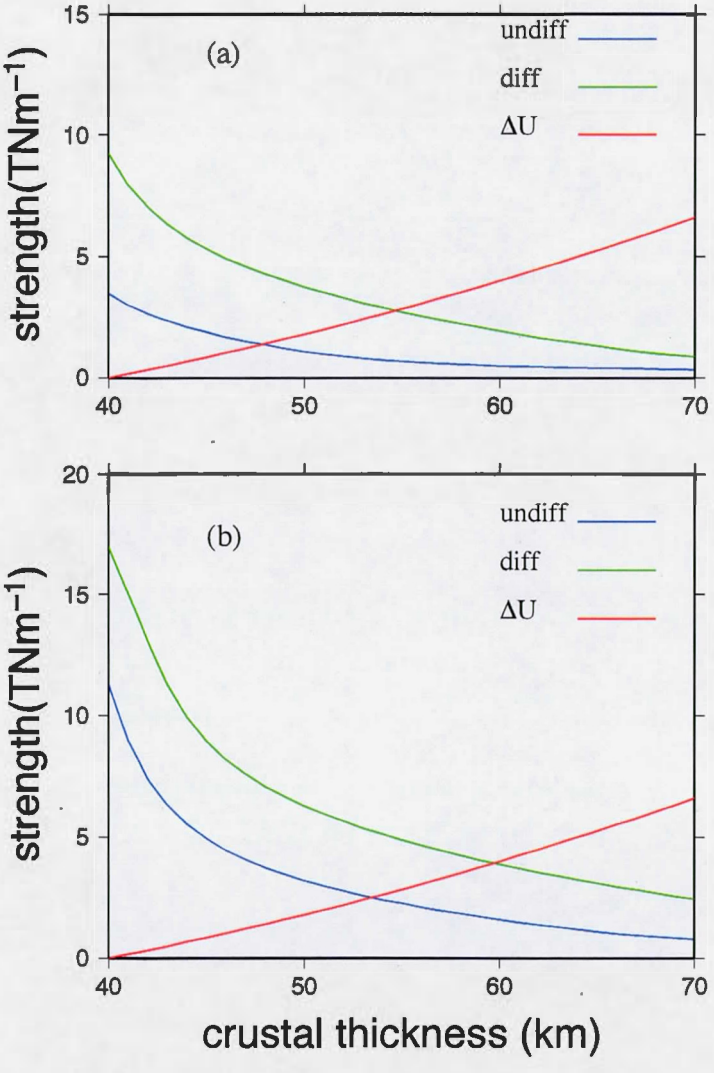

Figure 4.14 Total strength of lithosphere *vs* crustal thickness. The strength is calculated for $DI = 1$ (undifferentiated) and $DI = 2.5$ (differentiated crust). The potential energy difference (relative to 40 km thick crust) is given for comparison.
(a)The average crustal heat production is 1.5μW m^{-3} (i.e., the average heat production in cratons at the end of Archean).
(b)The average crustal heat production is 1.1μW m^{-3} (i.e., the average heat production of the Appalachians at the time of the orogeny).

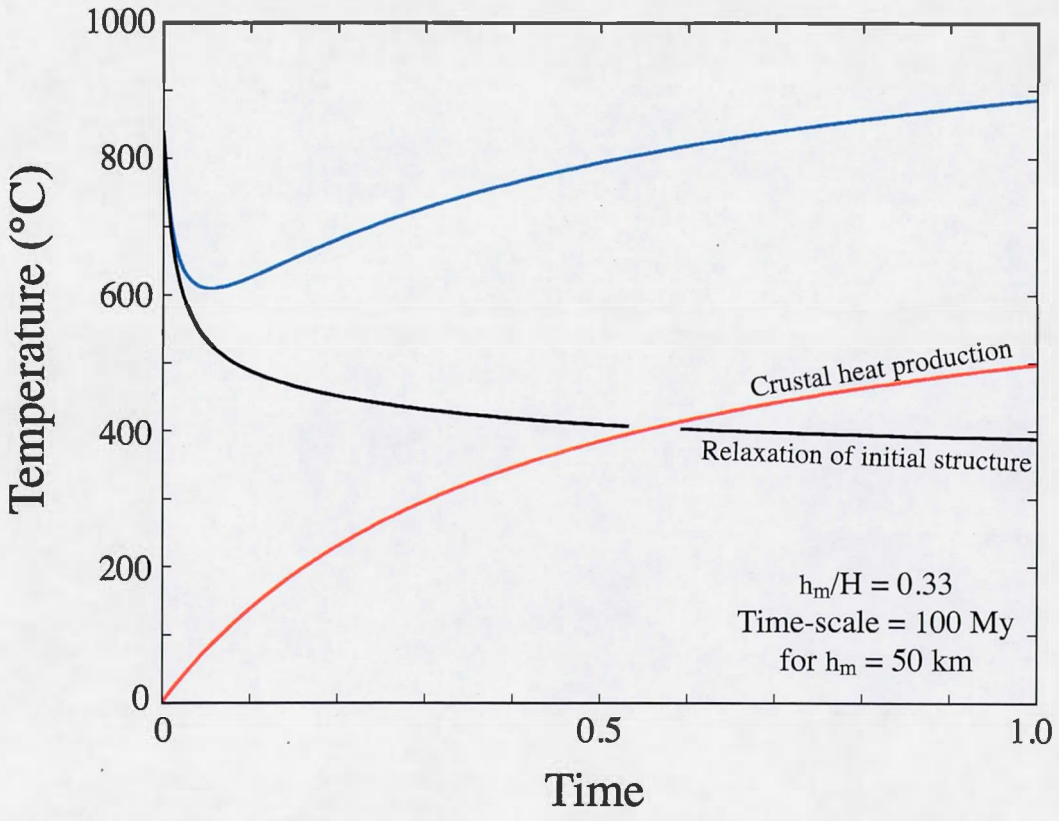

Figure 4.15 Post-accretion thermal evolution of crust with an initial temperature anomaly confined to a lower crustal layer. Results are given for the lower crust ($z = 0.8 \times h_m$). The two temperature components T_i and T_r (equation 4.15) are also shown. Crustal thickness h_m= 50 km, lithospheric thickness H=150 km. The initial thermal structure is characterized by a deep crustal anomaly with a temperature of 850^0C between depths of 35 km and 50 km (base of the crust). The time-lag between the end of accretion and high-temperature metamorphism (T≈850^{o}C) is ≈ 60 My.

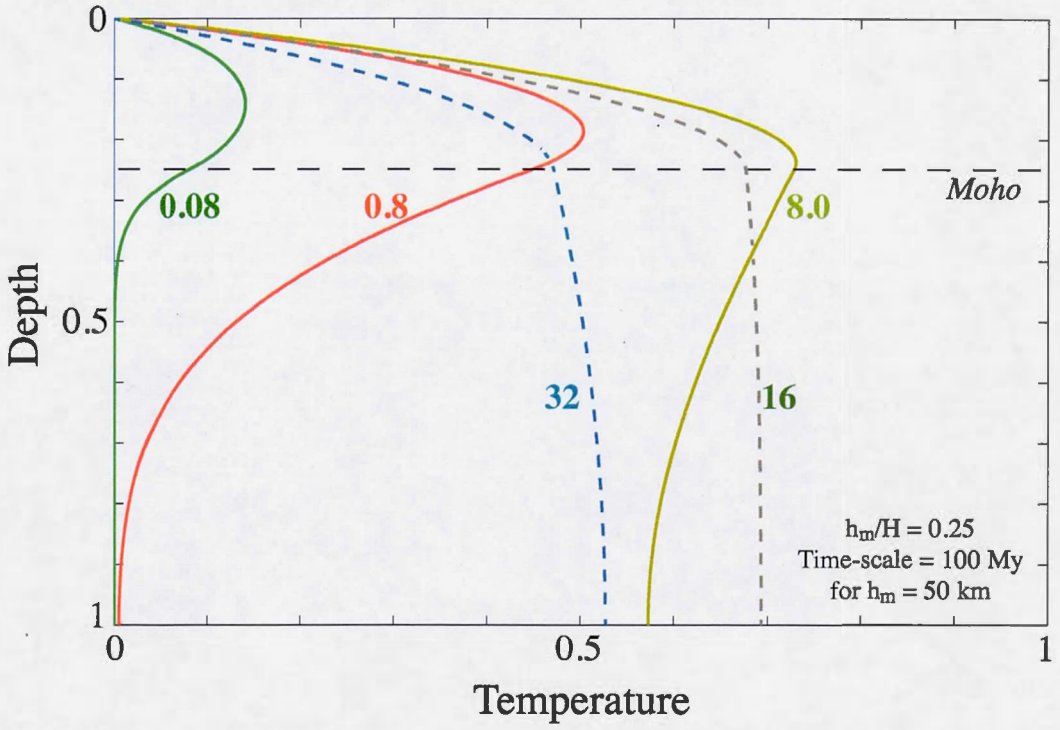

Figure 4.16 Vertical temperature profiles illustrating the heating of the crust and lithosphere by crustal heat sources. Heat production decays according to the $A(t) = A_o \exp(-t/\tau_r)$, where $\tau_r = 3.4$ Gy. Temperature has been scaled to $A_o h_m^2/(2\lambda)$, which is the Moho temperature for a uniform and steady crustal heat production equal to A_o. The labels by the curves refer to times scaled to the crustal diffusive time-scale, $\approx$ 100 My for 50 km thick crust. The thermal evolution can be split in two different phases. In an initial phase, temperatures increase everywhere, with the lithospheric mantle lagging behind the radioactive crust. As a consequence, the maximum temperature is reached in the lower crust and not at the Moho. In a second phase, with profiles shown as dashed lines, the whole lithospheric mantle has been heated up but the decay of heat production induces generalized secular cooling.

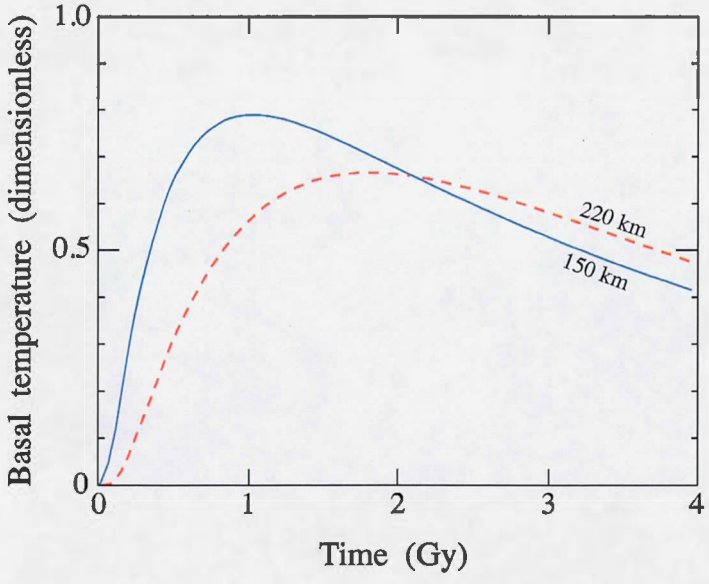

Figure 4.17 Variation of temperature at the base of the lithosphere due to crustal heat production for two different values of the lithosphere thickness, 150 and 220 km. The true basal temperature also includes a transient component that is due to the thermal relaxation of the lithosphere-forming event (not shown here). Heat production decays according to the $A(t) = A_o \exp(-t/\tau_{radio})$, where $\tau_{radio} = 3.4$ Gy. Temperature has been scaled to $A_o h_m^2/(2\lambda)$, which is the Moho temperature for a uniform and steady crustal heat production equal to A_o.

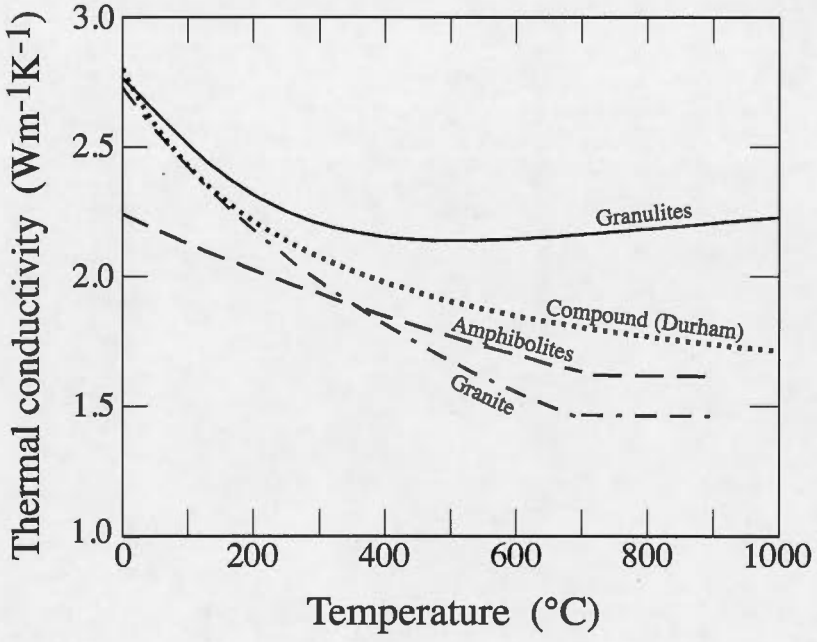

Figure 4.18 Variation of the lattice component of thermal conductivity as a function of temperature for several representative crustal rocks. The dotted line corresponds to empirical relationship 4.16 for a conductivity value of 2.8 W m^{-1} K^{-1}at room temperature. This relationship was derived from a best-fit analysis of seven different rock samples from the Archean Superior province (Durham et al., 1987). The data for amphibolites and granite samples are from Miao et al. (2014). For these two samples, the measurements do not resolve any significant variations of thermal conductivity in the 700-900°C range. The granulite data are from Merriman et al. (2013).

4.11 Appendix

4.11.1 Thermal conductivity

According to the metamorphic and plutonic records, the temperatures of crustal rocks may vary within a very large range of $\approx 0-1000^{o}$C. Over this temperature range, phonons are the main energy carriers and the contribution of photons is expected to be small. The variation of lattice conductivity with temperature has been determined for a number of minerals and rocks with different techniques (Durham et al., 1987; Merriman et al., 2013; Miao et al., 2014). The inherent heterogeneity of natural rocks is responsible for large variations of conductivity, even for a single rock type.

Measurements on a suite of rock samples from the Canadian Shield over a ($\approx 0-400^{o}$C) temperature range by Durham et al. (1987) can be accounted for by relationship of the following form :

$$\lambda = 2.264 - \frac{618.2}{T} + \lambda_0 \times (\frac{355.576}{T} - 0.30247) \tag{4.16}$$

where T is the absolute temperature in Kelvins and λ_0 is the thermal conductivity at 0^{o}C. According to this equation, the lattice conductivity decreases with increasing temperature and tends to a constant value at high temperatures, which has been confirmed by more recent measurements (Merriman et al., 2013; Miao et al., 2014).

According to Merriman et al. (2013), the lattice conductivities of several crustal rock types, including granulite, greenstone and tonalite-trondhjemite-granodiorite (TTG), are confined to a small 1.9-2.2 W m^{-1} K^{-1}range at temperatures larger than 700^{o}C. In the same high-T limit, Miao et al. (2014) report a much lower range of 1.26-1.55 W m^{-1} $K^{-1}$for granite, granodiorite, gabbro and garnet amphibolite samples. This discrepancy may be

due to anomalous samples. For example, Merriman et al. (2013) report a value of 4.5 W m^{-1} $K^{-1}$for a TTG sample at room temperature, which is far above the range of previously published values for similar rocks. Similarly, Miao et al. (2014) quote a room temperature value of 1.92 W m^{-1} $K^{-1}$for a granodiorite sample, which is this time significantly lower than all the measurements that are known to us on similar rocks. It may also be compared to the Merriman et al. (2013) value for a TTG sample, because both rocks belong to the same group. We have therefore excluded the data for these two particular samples. For the two suites of crustal rocks that were studied by these two groups, the range of conductivity values, which may be as high as 70% at room temperature, is only about 20% for $300 < T < 1000^{o}$C. As a result, thermal calculations are weakly sensitive to the choice of a representative crustal rock type.

Miao et al. (2014) have derived best-fit relationships to their conductivity data of the form $\lambda = (\alpha + \beta T)^{-1}$, where α and β depend on rock type and T is temperature in Kelvins. For $T > 700^{o}$C, the measurements do not resolve any significant change of conductivity and this relationship should not be used. Merriman et al. (2013) list empirical equations for both diffusivity and heat capacity which lead to more complicated expressions for conductivity.

The continental crust is a complex assemblage of different rock types in both the horizontal and vertical directions and this must be accounted for in the choice of a representative thermal conductivity. We find that equation (4.16) represents a good compromise. It is very close to all the Durham et al. (1987) data by construction. For $\lambda_0 = 2.8$W m^{-1} K^{-1}, it predicts conductivity values that are within 20% of those of Miao et al. (2014) and Merriman et al. (2013) in the $0 - 900^{o}$C range (Figure 4.18). Using this equation, we have calculated the mean thermal conductivity of the crust for a set of representative temperature profiles and found that the mean thermal conductivity varies between 1.9 and 2.2 W m^{-1} K^{-1}. We have also compared the "exact" Moho temperatures for the variable thermal conductivity to that obtained with the mean thermal thermal conductivity and found that, in most cases, they differ by less than 10K. We thus conclude that using a mean

thermal conductivity of 2.1 W m^{-1} $K^{-1}$for the crust results in negligible errors on the calculated Moho temperatures.

4.11.2 Moho Heat Flux

The first heat flow measurements were made on the continents, well before the advent of plate tectonics. It is therefore not surprising that early interpretations were focused mostly on crustal heat production. For example, Birch (1950) concluded from very imperfect heat flow, heat production, and gravity data that heat flow variations are due to changes in crustal structure and composition. He estimated that the heat flux at the base of the crust is $\approx$ 12mW m^{-2} which, as we shall see, was not far off the mark. Estimates of the Moho heat flux in continental regions are based on heat flow and heat production data, systematic geochemical sampling, geothermobarometric studies on mantle xenoliths, as well as studies of crustal and lithospheric structure with seismic and electromagnetic methods.

An obvious constraint on Moho heat flux is that it must be less than the lowest value that is measured at the surface. Values as low as 18-22mW m^{-2} have been measured in several Shield areas (Table 4.10). A value of 22mW m^{-2} has been found in three widely separated regions in the Canadian Shield : in the *ca* 2800Ma LaGrande belt of the Superior Province, in the LynnLake belt of the *ca* 1800Ma Trans Hudson Orogen and at Voisey Bay in the *ca* 1650Ma Nain plutonic Province. Because the heat production rate at these sites is not negligible, the Moho heat flux must be less than these values. In a rather extreme model, we consider that heat production in the whole crust beneath the masurement sites is consistently at the smallest value observed on crustal rocks, which is 0.10 μW m^{-3} (Tables 4.1 and 4.6). For crust of average thickness (40 km), therefore, the Moho heat flux must be less than 14-18mW m^{-2} . Similarly low values of Moho heat flux have been reported in other continents (Table 4.11).

The contribution of crustal heat sources can be estimated from crustal sections where

deep crustal levels are exposed at the surface. For example, this is the situation of Kapuskasing structural zone in the Superior Province of the Canadian Shield where the crust is exposed to paleo-pressures up to 1 GPa (Percival and West, 1994). The surface heat flux measured in the region where the metamorphic grade is highest is 33mW m^{-2} and the measured heat production of the granulites is 0.4μW m^{-3} (Table 4.6). The crustal thickness was estimated to be 50km from the seismic reflection and refraction surveys conducted by the LITHOPROBE program. Assuming that the granulites at the surface are representative of the present-day lower crust, we calculate a mantle heat flux of 13mW m^{-2} . This result has been checked in different ways. The Kapuskasing structure lies at the western termination of the Abitibi subprovince where seismic reflection and refraction profiles as well as gravity data are available, and where many heat flow data have been collected. Using the physical properties of the main rock types of the province, Guillou et al. (1994) used a Monte-Carlo method to find crustal models that fit the heat flux, gravity, and crustal thickness variations between eastern, western, and southernmost parts of the Abitibi. They found that the range of Moho heat flux values is narrow (11-18mW m^{-2}) and strongly peaked at 14mW m^{-2} .

The total crustal heat production and the mantle heat flux have also been estimated in the Vredefort structure in the Kaapvaal craton, South-Africa (Nicolaysen et al., 1981) where a section of the entire crust has been exposed by the rebound following a meteorite impact *ca* 2100Ma. Nicolaysen et al. (1981) sampled a transect across the structure and estimated the total crustal heat production to be between 29 and 34mW m^{-2} and the Moho heat flux to be 12-17mW m^{-2} .

Mantle temperature-depth profiles can be calculated from geothermobarometry studies of xenoliths brought to the surface by kimberlite eruptions. Studies based on the same thermobarometers yield consistent temperature gradients in the mantle (Grütter, 2009). Unfortunately, many authors still try to obtain a qualitative fit of the P-T data to a "reference surface heat flow geotherm" such as proposed by **?**, rather than directly estimate the mantle heat flux from the temperature gradient and thermal conductivity. The limitations

of such a procedure is made evident when the entire P-T array cannot be fit by the same "reference geotherm" but is intersected by different geotherms at different depths (see for instance Sand et al., 2009). When the mantle heat flux has been calculated, its values in cratonic areas range between 10 and 20mW m^{-2} (Table 4.11). The slightly higher values (15-22mW m^{-2}) that have been obtained for South Africa (Rudnick and Nyblade, 1999; Michaut et al., 2007) are consistent with the range of 12-17mW m^{-2} that was derived from surface heat flux and crustal heat production.

The crustal heat production models (and values of the Moho heat flux) have also been tested against P_n seismic velocity obtained from the LITHOPROBE seismic refraction profiles in the western Superior Province in Canada. Perry et al. (2006) calculated Moho temperatures and P_n velocities for different mantle compositions. They found a best fit between 12mW m^{-2} and 15mW m^{-2} depending on the amount of mantle depletion. On a larger scale, Lévy et al. (2010) narrowed down to 12-18mW m^{-2} the range of mantle heat flux values beneath central and eastern Canada using a combination of heat flux and shear wave vertical travel time delays calculated from surface wave tomography models (Bedle and van der Lee, 2009).

4.11.3 Horizontal Variations in Heat Sources

We assume that the horizontal distribution of heat production remains the same over some thickness h, and use calculations for elementary periodic distributions in the horizontal plane. These distributions are characterized by function $f(x,y)$ such that :

$$\nabla_H^2 f(x,y) = \frac{\partial^2 f}{\partial x^2} + \frac{\partial^2 f}{\partial y^2} = -k^2 f \tag{4.17}$$

where k is the equivalent of a wavenumber. Functions f that are solutions of equation 4.17 are such that their horizontal average is zero and can be understood as components of the

2-D Fourier transform in x and y of the heat production distribution $\delta A(x,y,z)$. They allow a wide range of periodic tesselations of the plane, including equally spaced parallel lines, squares and hexagons. For simplicity, we shall refer to a single scale or wavelength Δ such that :

$$k = \frac{2\pi}{\Delta} \tag{4.18}$$

For the heat equation with constant thermal conductivity, which is linear in T and A, we need only solve the problem for a layer that extends from the surface to depth h in a crust of total thickness h_m. Results for a layer located between depths z_T and z_B can be obtained by subtracting the solution for $h = z_T$ from that for $h = z_B$. For an elementary heat production distribution $\delta A = A_o f(x,y)$, solutions can be obtained in the form of $T(x,y,z) = \theta(z) f(x,y)$, such that :

$$\frac{d^2\theta}{dz^2} - k^2\theta + \frac{A_o}{\lambda} = 0 \tag{4.19}$$

where A_o is set to zero below the layer of thickness h. For this problem, which deals with fluctuations of heat production around the horizontal mean, the following boundary conditions must be satisfied :

$$\begin{aligned} \theta(0) &= 0, \text{ zero surface temperature} \\ \frac{d\theta}{dz}(z = h_m) &= 0, \text{ zero heat flux at the Moho} \end{aligned} \tag{4.20}$$

Solutions are derived using standard mathematical methods. The surface heat flux is :

$$\delta q_o = A_o h \, \frac{\sinh(kh) + [1 - \cosh(kh)]\tanh(kh_m)}{kh} \tag{4.21}$$

For simplicity, it is useful to scale the heat flux with the value for a layer of constant heat

production, *i.e.* $A_o h$. The Moho temperature is :

$$\delta T_m = \frac{A_o h^2}{\lambda} \frac{\cosh(kh) - 1}{k^2 h^2 \cosh(kh_m)} \tag{4.22}$$

As above, the Moho temperature will be scaled to the value for a layer of constant heat production, $(A_o h^2)/2\lambda$.

4.11.4 Rheology and strength of the lithosphere

Crustal rocks deform by power law creep (Ranalli, 1995)

$$\dot{\varepsilon} = A\sigma^n \exp(-(E + PV^*)/RT) \tag{4.23}$$

where $\dot{\varepsilon}$ is the strain rate, σ the deviatoric stress, A and n are constants characteristic of the material, E is the activation energy, V^* the activation volume, R the gas constant, P is pressure, and T temperature. In general, the strength is defined as the stress required to maintain a fixed rate of deformation $\dot{\varepsilon}$, typically 10^{-15} s^{-1}, which is a value commonly observed for tectonic deformations.

$$\sigma = \frac{\dot{\varepsilon}^{1/n}}{A^{1/n}} \exp((E + PV^*)/nRT) \tag{4.24}$$

We use parameters that correspond to dry rheologies for the crust and mantle (Table 4.12).

In the upper crust, deformation occurs by frictional sliding on randomly oriented fractures, leading to a linear increase in deviatoric stress with depth known as Byerlee's Law (Byerlee, 1978; Brace and Kohlstedt, 1980). The shear stress τ to overcome friction is

proportional to the stress normal to the plane of fracture :

$$|\tau| = f\sigma_n \tag{4.25}$$

where f is the coefficient of friction, σ_n the effective normal stress is the lithostatic less the fluid pore pressure (usually assumed to be hydrostatic). It gives

$$|\tau| = f(\rho_c - \rho_w)gz \tag{4.26}$$

where ρ_c is the density of rock and ρ_w that of water. Byerlee's experimental data show that :

$$\tau = 0.85\sigma_n \qquad \sigma_n < 200\text{MPa} \tag{4.27}$$

$$\tau = 50 + 0.6\sigma_n \qquad \sigma_n > 200\text{MPa} \tag{4.28}$$

In horizontal compression, where the maximum principal stress is horizontal σ_h, and the minimum σ_v is vertical, we have :

$$\sigma_h = 5\sigma_v \qquad \sigma_n < 200\text{MPa} \tag{4.29}$$

$$\sigma_h = 3.1\sigma_v + 175 \qquad \sigma_n > 200\text{MPa} \tag{4.30}$$

The strength of the crust in the brittle regime is the difference in principal stress components necessary to overcome friction :

$$\sigma = \sigma_h - \sigma_v \tag{4.31}$$

GENERAL CONCLUSIONS

We used a global crustal thickness model to estimate heat flux and compare it to data where they are available. Doing so on both local and global scale, we find large discrepancies particularly in areas of low heat production. The model heat flow maps resembling more to the crustal thickness maps than to maps based on heat flow data. When comparing the geoneutrino flux from data to the model alone, the discrepancies remain as large as 25 TNU even when we adjust the heat production of each separate crustal layer to minimize the differences with the data. Improving the calculation method and accuracy does not reduce the discrepancies.

We have shown the relevance of heat flow studies to optimize the use of the very limited geoneutrino observation data. The location of current geoneutrino observatories have not been selected based on heat flow analyses. Hence there are many limitations in our ability to accurately estimate the crustal heat production in their vicinity. More interesting locations for geoneutrino observatories are : oceanic plates, the Siberian and Scandinavian cratons and near James Bay in Northeastern Canada.

Heat producing elements (HPE) from the crust fit poorly in the crystalline network of minerals. High temperature events such as metamorphism, melts and partial melts lead to an upward redistribution of the radioactive elements. Crustal thickening increases the Moho temperature thus resulting in an upward redistribution of HPE. This increase of the differentiation index (DI) leads to a significantly more effective cooling. The crustal thickness it thus limited to the maximal thickness at which the radioactive heating starts melting or weakening the crust.

Small scale variations in the surface heat flow are due to variation in crustal heat production because the Moho flux varies only over scales of 500km. HPE alone can be sufficient to explain metamorphic events as mentioned above. Tectonic events like accretion and compressional orogenies are followed by metamorphism after 20-100 My. This delay

is consistent with the timescale of heating of the crust by the radiogenic elements therein.

BIBLIOGRAPHY

Abe, Y., Sep. 1993. Physical state of the very early Earth. Lithos 30 (3-4), 223–235.

Abe, Y., 1997. Thermal and chemical evolution of the terrestrial magma ocean. Phys. Earth Planet. Inter. 100, 27–39.

Ague, J. J., Eckert, J. O., Chu, X., Baxter, E. F., Chamberlain, C. P., 2012. Discovery of ultrahigh-temperature metamorphism in the Acadian orogen, Connecticut, USA. Geology 41, 271–274.

Allègre, C., Lewin, E., Dupré, B., 1988. A coherent crust-mantle model for the uranium-thorium-lead isotopic system. Chem. Geol. 70, 211–234.

Andreoli, M. A. G., Hart, R. G., Ashwal, L. D., Coetzee, H., 2006. Correlations between U, Th Content and Metamorphic Grade in the Western Namaqualand Belt, South Africa, with Implications for Radioactive Heating of the Crust. J. Petrol. 47, 1095–1118.

Artemieva, I., Mooney, W., 2001. Thermal thickness and evolution of Precambrian lithosphere : A global study. J. Geophys. Res. (Solid Earth) 106, 16,387–16,414.

Ashwal, L. D., Morgan, P., Kelley, S. A., Percival, J., 1987. Heat production in an Archean crustal profile and implications for heat flow and mobilization of heat producing elements. Earth Planet. Sci. Lett. 85, 439–450.

Bassin, C., Laske, G., Masters, G., 2000. The Current Limits of Resolution for Surface Wave Tomography in North America. EOS Trans. Am. Geophys. Union 81, F897.

Beaumont, C., Jamieson, R. A., Nguyen, M. H., Medvedev, S., 2004. Crustal channel flows : 1. Numerical models with applications to the tectonics of the Himalayan-Tibetan orogen. Journal of Geophysical Research (Solid Earth) 109, B06406.

Bedle, H., van der Lee, S., Jul. 2009. S velocity variations beneath North America. Journal of Geophysical Research (Solid Earth) 114, B07308.

Birch, F., 1950. Flow of heat from the front range, Colorado. Geol. Soc. Amer. Bull. 61, 567–630.

Birch, F., Roy, R. F., Decker, E. R., 1968. Heat flow and thermal history in New England and New York. In : An-Zen, E. (Ed.), Studies of Appalachian Geology. Wiley-Interscience, New York, pp. 437–451.

Bodorkos, S., Sandiford, M., Minty, B. R., Blewett, R. S., 2004. A high-resolution, calibrated airborne radiometric dataset applied to the estimation of crustal heat production in the Archaean northern Pilbara Craton, Western Australia. Precambrian Research 128 (1), 57–82.

Boerner, D., Milkereit, B., Davidson, A., 2000. Geoscience impact : a synthesis of studies of the sudbury structure. Can. J. Earth Sc. 37, 477–501.

Borexino collaboration group, 2010. Observation of geo-neutrinos. Phys. Lett. B 687, 299–304.

Borexino collaboration group, 2013. Measurement of geo-neutrinos from 1353 days of Borexino. Phys. Lett. B 722, 295–300.

Brace, W. F., Kohlstedt, D. L., 1980. Limits on lithospheric stress imposed by laboratory experiments. J. Geophys. Res. 85, 6248–6252.

Brady, R. J., Ducea, M. N., Kidder, S. B., Saleeby, J. B., 2006. The distribution of radiogenic heat production as a function of depth in the Sierra Nevada batholith, California. Lithos 86, 229–244.

Burke, K., Kidd, W., 1978. Were archean continental geothermal gradients much steeper than those of today ? Nature 272, 240–241.

Byerlee, J. D., 1978. Friction of rocks. Pure. Appl. Geophys. 116, 615–626.

Cameron, A. G. W., Jan. 2001. From interstellar gas to the Earth-Moon system. Meteoritics and Planetary Science 36 (1), 9–22.

Canup, R. M., April 2004. Simulations of a late lunar-forming impact. Icarus 168, 433–456.

Carter, N. L., Tsenn, M. C., 1987. Flow properties of continental lithosphere. Tectonophysics 136, 27–63.

Chamberlain, C. P., Sonder, L. J., 1990. Heat-producing elements and the thermal and baric patterns of metamorphic belts. Science 250, 763–769.

Chapman, D., Pollack, H., 1974. 'Cold Spot' in West Africa anchoring the African plate. Nature 250, 477–478.

Christensen, U. R., Mar. 1985. Thermal evolution models for the earth. J. Geophys. Res. (Solid Earth) 90, 2995–3007.

Clark, A., Fitzsimons, C., Healy, D., Harley, S., 2011. How does the continental crust get really hot. Elements 7, 235–240.

Davaille, A., Jaupart, C., Aug. 1993. Transient high-Rayleigh-number thermal convection with large viscosity variations. J. Fluid Mech. 253, 141–166.

Davies, G., 1999. Dynamic Earth : Plates, plumes, and mantle convection. Cambridge University Press, New-York.

Davies, G. F., 1980. Review of oceanic and global heat flow estimates. Rev. Geophys. Space Phys. 18, 718–722.

Davies, G. F., 1988. Ocean bathymetry and mantle convection 1. Large-scale flow and hotspots. J. Geophys. Res. (Solid Earth) 93, 10467–10480.

Davies, G. F., Oct. 1993. Cooling the core and mantle by plume and plate flows. Geophys. J. Int. 115, 132–146.

Davies, G. F., Richards, M. A., Mar. 1992. Mantle Convection. Journal of Geology 100, 151–206.

Davies, J. H., Davies, D. R., Feb. 2010. Earth's surface heat flux. Solid Earth 1, 5–24.

Della Vedova, B., Von Herzen, R. P., 1987. Geothermal heat flux at the cost b-2 and b-3 wells, u.s. atlantic continental margin. Tech. Rep. WHOI-87-27, Woods Hole Oceanog. Inst. Tech. Rept.

Dhuime, B., Hawkesworth, C. J., Cawood, P. A., Storey, C. D., Mar. 2012. A Change in the Geodynamics of Continental Growth 3 Billion Years Ago. Science 335, 1334–.

Duchkov, A. D., 1991. Review of Siberian heat flow data. In : Cermak, V., Rybach, L. (Eds.), Terrestrial heat flow and the Lithosphere structure. Springer-Verlag, Berlin, pp. 426–443.

Durham, W. B., Mirkovich, V. V., Heard, H. C., 1987. Thermal diffusivity of igneous rocks at elevated pressure and temperature. J. Geophys. Res. (Solid Earth) 92, 11615–11634.

Dye, S. T., Mar. 2009. Geo-Neutrinos. Nuclear Physics B Proceedings Supplements 188, 133–135.

Dye, S. T., Guillian, E., Learned, J. G., Maricic, J., Matsuno, S., Pakvasa, S., Varner, G., Wilcox, M., Dec. 2006. Earth Radioactivity Measurements with a Deep Ocean Anti-neutrino Observatory. Earth Moon and Planets 99, 241–252.

Eade, K. E., Fahrig, W. F., 1971. Geochemical evolutionary trends of continental plates : A preliminary study of the Canadian shield. Geol. Surv. Can. Bull. 179, 51 pp.

England, P. C., Bickle, M. J., 1984. Continental thermal and tectonic regimes during the Archean. J. Geol. 92, 353–367.

England, P. C., Thompson, A. B., 1984. Pressure-temperature-time paths of regional metamorphism. I. Heat transfer during the evolution of regions of thickened continental crust. J. Petrol. 25, 894–928.

Fiorentini, G., Lissia, M., Mantovani, F., Vannucci, R., Sep. 2005. Geo-neutrinos : A new probe of Earth's interior [rapid communication]. Earth Planet. Sci. Lett. 238, 235–247.

Flasar, F. M., Birch, F., 1973. Energetics of core formation : a correction. J. Geophys. Res. (Solid Earth) 78, 6101–6103.

Floyd, P. A., Winchester, J. A., Park, R. G., 1989. Geochemistry and tectonic setting of Lewisian clastic metasediments from the early Proterozoic Loch Maree group of Gairloch, NW Scotland 45, 203–214.

Foland, K. A., Allen, J. C., 1991. Magma sources for Mesozoic anorogenic granites of the White Mountain magma series, New England USA. Contrib. Mineral. Petrol. 109, 195–211.

Fountain, D. M., 1986. Is there a relationship between seismic velocity and heat production for crustal rocks ? Earth Planet. Sci. Lett. 79, 145–150.

Fountain, D. M., Salisbury, M. H., 1981. Exposed cross-sections through the continental crust : implications for crustal structure, petrology, and evolution. Earth Planet. Sci. Lett. 56, 263–277.

Fountain, D. M., Salisbury, M. H., Furlong, K. P., 1987. Heat production and thermal conductivity of rocks from the Pikwitonei-Sachigo continental cross-section, central Manitoba : Implications for the thermal structure of Archean crust. Can. J. Earth Sci. 24, 1583–1594.

Fourier, J. B. J., 1820. Extrait d'un mémoire sur le refroidissement du globe terrestre. Bull. Sci. par la Société philomatique de Paris.

Fourier, J. B. J., 1824. Remarques générales sur les températures du globe terrestre et des espaces planétaires. Ann. Chim. Phy 27, 136–167.

Furukawa, Y., Shinjoe, H., 1997. Distribution of radiogenic heat generation in the arc's crust of the Hokkaido island, Japan. Geophys. Res. Lett. 24, 1279–1282.

Galson, D., 1983. Heat production in the Ivrea and Strona Ceneri zones. Ph.D. thesis Univ. Cambridge, Cambridge, U.K., 200 pp.

Gao, S., Luo, T., Zhang, B., Zhang, H., Han, Y., Zhao, Z., Hu, Y., 1998. Chemical composition of the continental crust as revealed by studies in East China. Geochim. Cosmochim. Acta 62, 1959–1975.

Gaudemer, Y., Tapponnier, P., Jaupart, C., 1988. Thermal control on post-orogenic extension in collision belts. Earth and Planetary Science Letters 89, 48–62.

Gomi, H., Ohta, K., Hirose, K., Labrosse, S., Caracas, R., Verstraete, M. J., Hernlund, J. W., Nov. 2013. The high conductivity of iron and thermal evolution of the Earth's core. Phys. Earth Planet. Inter. 224, 88–103.

Grieve, R. A. F., Stoeffler, D., Deutsch, A., Dec. 1991. The Sudbury Structure - Controversial or misunderstood ? J. Geophys. Res. (Solid Earth) 96, 22,753–22,764.

Grütter, H. S., 2009. Pyroxene xenocryst geotherms : Techniques and application. Lithos 112, 1167–1178.

Guillou, L., Mareschal, J. C., Jaupart, C., Gariépy, C., Bienfait, G., Lapointe, R., 1994. Heat flow and gravity structure of the Abitibi belt, Superior Province, Canada. Earth Planet. Sci. Lett. 122, 447–460.

Gupta, M., Sundar, A., Sharma, S., 1991. Heat flow and heat generation in the Archaean Dharwar cratons and implications for the Southern Indian Shield geotherm and lithospheric thickness. Tectonophys. 194, 107–122.

Hacker, B. R., Kelemen, P. B., Behn, M. D., 2011. Differentiation of the continental crust by relamination. Earth Planet. Sci. Lett. 307, 501–516.

Hacker, B. R., Kelemen, P. B., Behn, M. D., 2015. Continental lower crust. Annu. Rev. Earth Planet. Sci. 43, 6.1–6.39.

Hacker, B. R., Mehl, L., Kelemen, P. B., Rioux, M., Behn, M. D., Luffi, P., 2008. Reconstruction of the Talkeetna intraoceanic arc of Alaska through thermobarometry. J. Geophys. Res. (Solid Earth) 113 (B3), B03204.

Hajnal, Z., Lewry, J., White, D., Ashton, K., Clowes, R., Stauffer, M., Gyorfi, I., Takacs, E., 2005. The Sask Craton and Hearne Province margin : seismic reflection studies in the western Trans-Hudson Orogen. Canadian Journal of Earth Sciences 42, 403–419.

Hart, S. R., Zindler, A., 1986. In search of a bulk-Earth composition. Chem. Geol. 57, 247–267.

Hasterok, D., Chapman, D. S., 2011. Heat production and geotherms for the continental lithosphere. Earth and Planetary Science Letters 307, 59–70.

Heaman, L. M., Bohm, C. O., Machado, N., Krogh, T. E., Weber, W., Corkery, M. T., 2011. The Pikwitonei Granulite Domain, Manitoba : a giant Neoarchean high-grade terrane in the northwest Superior Province. Can. J. Earth Sci. 48, 205–245.

Herzberg, C., Asimow, P. D., Arndt, N., Niu, Y., Lesher, C. M., Fitton, J. G., Cheadle, M. J., Saunders, A. D., Feb. 2007. Temperatures in ambient mantle and plumes : Constraints from basalts, picrites, and komatiites. Geochemistry, Geophysics, Geosystems 8, 2006.

Herzberg, C., Condie, K., Korenaga, J., Mar. 2010. Thermal history of the Earth and its petrological expression. Earth Planet. Sci. Lett. 292, 79–88.

Herzberg, C., Zhang, J., Apr. 1996. Melting experiments on anhydrous peridotite KLB-1 : Compositions of magmas in the upper mantle and transition zone. J. Geophys. Res. (Solid Earth) 101, 8271–8295.

Holmes, A., 1915a. Radioactivity and the earth's thermal history : Part 1. The concentration of radioactive elements in the earth's crust. Geol. Mag. 2, 60–71.

Holmes, A., 1915b. Radioactivity and the earth's thermal history : Part 2. Radioactivity and the earth as a cooling body. Geol. Mag. 2, 102–112.

Holmes, A., Jan. 1931. Radioaktivität und die thermische Geschichte der Erde. Naturwissenschaften 19, 73–79.

Huang, Y., Chubakov, V., Mantovani, F., Rudnick, R. L., McDonough, W. F., 2013. A reference Earth model for the heat-producing elements and associated geoneutrino flux. Geochemistry, Geophysics, Geosystems 14, 2003–2029.

Hyndman, R. D., 2010. The consequences of Canadian Cordillera thermal regime in recent tectonics and elevation : a review. Canadian Journal of Earth Sciences 47, 621–632.

Iarotsky, L., Mareschal, J., Jaupart, C., 2015b. A global perspective on the composition of the continental crust from the distribution of heat producing elements : Comparison between heat flow data and seismological crustal models. AGU Fall meeting, San Francisco, CA.

Jackson, M. G., Jellinek, M. A., 2013. Major and trace element composition of the high 3He/4He mantle : Implications for the composition of a nonchonditic earth. Geochem. Geophys. Geosyst. 14 (8), 2954–2976.

Jagoutz, O. E., Sep. 2010. Construction of the granitoid crust of an island arc. Part II : a quantitative petrogenetic model. Contributions to Mineralogy and Petrology 160, 359–381.

Jagoutz, O. E., Schmidt, M., 2012. The formation and bulk composition of modern juvenile continental crust : the Kohistan arc. Chem. Geol. 298-299, 79–96.

Jaupart, C., 1983. Horizontal heat transfer due to radioactivity contrasts : Causes and consequences of the linear heat flow-heat production relationship. Geophys. J. R. Astr. Soc. 75, 411–435.

Jaupart, C., Labrosse, S., Lucazeau, F., Mareschal, J. C., 2015. Temperatures, heat and energy in the mantle of the earth. In : Bercovici, D. (Ed.), Treatise on Geophysics, The Mantle. Vol. 7. Elsevier, New York, pp. 223–270.

Jaupart, C., Mann, J. R., Simmons, G., 1982. A detailed study of the distribution of heat flow and radioactivity in New Hampshire (U.S.A.). Earth Planet. Sci. Lett. 59, 267–287.

Jaupart, C., Mareschal, J. C., 1999. The thermal structure and thickness of continental roots. Lithos 48, 93–114.

Jaupart, C., Mareschal, J. C., 2008. Heat flow and thermal structure of the lithosphere. In : Watts, A. B. (Ed.), Treatise on Geophysics, vol 6, The lithosphere, 2nd Edition. Elsevier.

Jaupart, C., Mareschal, J. C., 2011. Heat generation and Transport in the Earth. Cambridge University Press, Cambridge (U.K.).

Jaupart, C., Mareschal, J. C., 2014. Constraints on crustal heat production from heat flow data. In : Rudnick, R. L. (Ed.), Treatise on Geochemistry, The Crust, 2nd Edition. Vol. 4. Elsevier, New York, pp. 53–73.

Jaupart, C., Mareschal, J. C., 2015a. Heat flow and thermal structure of the lithosphere. In : Watts, A. B. (Ed.), Treatise on Geophysics, vol 6, The lithosphere, 2nd Edition. Elsevier, pp. 217–253.

Jaupart, C., Mareschal, J.-C., 2015. Post-orogenic thermal evolution of newborn Archean continents. Earth and Planetary Science Letters 432, 36–45.

Jaupart, C., Mareschal, J.-C., Bouquerel, H., Phaneuf, C., Dec. 2014a. The building and stabilization of an Archean Craton in the Superior Province, Canada, from a heat flow perspective. Journal of Geophysical Research (Solid Earth) 119, 9130–9155.

Jaupart, C., Mareschal, J. C., Guillou-Frottier, L., Davaille, A., 1998. Heat flow and thickness of the lithosphere in the Canadian Shield. J. Geophys. Res. (Solid Earth) 103, 15269–15286.

Javoy, M., 1999. Chemical earth models. C. R. Acad. Sci. Paris 329, 537–555.

Jeffreys, H., 1936. On the Radioactivities of Rocks . Beitrage zur geophysik 47, 149–170.

Joeleht, T. H., Kukkonen, I. T., 1998. Thermal properties of granulite facies rocks in the Precambrian basement of Finland and Estonia. Tectonophys. 291, 195–203.

Johnson, T., White, R., 2011. Phase equilibrium constraints on conditions of granulite facies metamorphism at Scourie, NW scotland. J. Geol. Soc. London 168, 147–158.

Joly, J., 1909. Radioactivity and Geology. Constable, London.

Jones, M. Q. W., 1987. Heat flow and heat production in the Namaqua mobile belt, South Africa. J. Geophys. Res. (Solid Earth) 92, 6273–6289.

Jones, M. Q. W., 1988. Heat flow in the Witwatersrand Basin and environs and its significance for the South African Shield geotherm and lithosphere thickness. J. Geophys. Res. (Solid Earth) 93, 3243–3260.

Jones, M. Q. W., 1992. Heat flow anomaly in Lesotho : implications for the southern boundary of the Kaapvaal craton. Geophys. Res. Lett. 19, 2031–2034.

Kaminski, E., Javoy, M., 2013. A two-stage scenario for the formation of the Earth's mantle and core. Earth Planet. Sci. Lett. 365, 97–107.

Kamland collaboration, Jul. 2005. Experimental investigation of geologically produced antineutrinos with KamLAND. Nature 436, 499–503.

Kamland collaboration, 2011. Partial radiogenic heat model for Earth revealed by geoneutrino measurements. Nature Geosciences 4, 647–651.

Kamland collaboration, 2013. Reactor on-off antineutrino measurement with KamLAND. Phys. Rev. D 88, 033001.

Kelemen, P., Hanghoj, K., Greene, A., 2014. One view of the geochemistry of subduction-related magmatic arcs, with an emphasis on primitive andesite and lower crust. In : Rudnick, R. L. (Ed.), The Crust, Treatise on Geochemistry 2nd Edition, 2nd Edition. Vol. 4. Elsevier-Permagon, Oxford, pp. 749–805.

Kinnaird, T., Prave, A. R., Kirkland, C., Horstwood, M., Parrish, R., Batchelor, R., 2007. The late Mesoproterozoic - early Neoproterozoic tectonostratigraphic evolution of NW Scotland : the Torridonian revisited. J. Geol. Soc. London 164, 541–551.

Korenaga, J., Apr. 2003. Energetics of mantle convection and the fate of fossil heat. Geophys. Res. Lett. 30, 1437.

Korenaga, J., Jun. 2008. Urey ratio and the structure and evolution of Earth's mantle. Rev. Geophys. 46, 2007.

Kramers, J., Kreissig, K., Jones, M., 2001. Crustal heat production and style of metamorphism : a comparison between two high-grade provinces in the Limpopo Belt, South Africa 112, 149–163.

Krogh, T. E., 1993. High precision U-Pb ages for granulite metamorphism and deformation in the Archean Kapuskasing structural zone, Ontario : implications for structure and development of the lower crust. Earth Planet. Sci. Lett. 119, 1–18.

Kukkonen, I., Joehlet, A., Apr. 1996. Geothermal modelling of the lithosphere in the central Baltic Shield and its southern slope. Tectonophysics 255, 25–45.

Kukkonen, I., Peltoniemi, S., 1998. Relationships between thermal and other petrophysical properties of rocks in Finland. Phys. Earth Planet. Inter. 23, 341–349.

Kukkonen, I. T., 1989a. Terrestrial heat flow and radiogenic heat production in Finland, the central Baltic Shield. Tectonophys. 164, 219–230.

Kukkonen, I. T., Golovanova, Y. V., Druzhinin, V. S., Kosarev, A. M., Schapov, V. A., 1997. Low geothermal heat flow of the Urals fold belt : Implication of low heat production, fluid circulation or paleoclimate. Tectonophys. 276, 63–85.

Kukkonen, I. T., Jõeleht, A., 1996. Geothermal modelling of the lithosphere in the central Baltic Shield and its southern slope. Tectonophysics 255, 25–45.

Kukkonen, I. T., Peltonen, P., 1999. Xenolith-controlled geotherm for the central Fennoscandian shield : implications for lithosphere-asthenosphere relations. Tectonophys. 304, 301–315.

Kumar, P. S., Menon, R., Reddy, G. K., 2007. The role of radiogenic heat production in the thermal evolution of a Proterozoic granulite-facies orogenic belt : Eastern Ghats, Indian Shield. Earth Planet. Sci. Lett. 254, 39–54.

Kumar, P. S., Reddy, G. K., 2004. Radioelements and heat production of an exposed Archaean crustal cross-section, Dharwar craton, south India. Earth Planet. Sci. Lett. 224, 309–324.

Kutas, R. I., 1977. Investigation of heat flow in the territory of the Ukraine. Tectonophysics 41, 139–145.

Labrosse, S., May 2002. Hotspots, mantle plumes and core heat loss. Earth Planet. Sci. Lett. 199, 147–156.

Lambert, I. B., Heier, K. S., 1967. The vertical distribution of uranium, thorium, and potassium in the continental crust. Geochim. Cosmochim. Acta 31, 377–390.

Landstrom, O., Larson, S. A., Lind, G., Malmqvist, D., 1980. Geothermal investigations in the Bohus granite area in southwestern Sweden. Tectonophys. 64, 131–162.

Langmuir, C. H., Goldstein, S. L., Donnelly, K., Su, Y. K., 2005. Origins of enriched and depleted mantle reservoirs. In : Suppl., F. M. (Ed.), Eos Trans. Vol. 86. American Geophysical Union, Abstract V23D-02, p. 1.

Laske, G., Masters, G., Ma, Z., Pasyanos, M., 2013. Update on CRUST1.0 - a 1-degree global model of Earth's crust. In : Geophys. Res. Abstracts, 15. EGU.

Lee, C.-T. A., Morton, D., Kistler, R. W., Baird, A. K., 2007. Petrology and tectonics of Phanerozoic continent formation : From island arcs to accretion and continental arc magmatism. Earth Planet. Sci. Lett. 263, 370–387.

Lévy, F., Jaupart, C., 2011. Temperature and rheological properties of the mantle beneath the North American craton from an analysis of heat flux and seismic data. J. Geophys. Res. (Solid Earth) 116 (B15), BO1408.

Lévy, F., Jaupart, C., Mareschal, J., Bienfait, G., Limare, A., 2010. Low heat flux and large variations of lithospheric thickness in the Canadian Shield. J. Geophys. Res. (Solid Earth) 115, BO6404.

Lewis, T. J., Hyndman, R. D., Fluck, P., 2003. Heat flow, heat generation and crustal temperatures in the northern Canadian Cordillera : Thermal control on tectonics. J. Geophys. Res. (Solid Earth) 108, 2316.

Lister, C., 1977. Estimators for heat flow and deep rock properties based on boundary layer theory. Tectonophys. 41, 157–171.

Lister, C. R. B., Sclater, J. G., Nagihara, S., Davis, E. E., Villinger, H., Sep. 1990. Heat flow maintained in ocean basins of great age - Investigations in the north-equatorial West Pacific. Geophys. J. Int. 102, 603–630.

Litasov, K., Ohtani, E., Nov. 2002. Phase relations and melt compositions in CMAS-pyrolite-H_2O system up to 25 GPa. Phys. Earth Planet. Inter. 134, 105–127.

Lyons, J. B., 1964. Distribution of thorium, uranium in three early Paleozoic plutonic suites of New Hamphsire. Tech. Rep. 1144-F, U.S. Geol. Surv. Bull.

Lyubetskaya, T., Korenaga, J., Nov. 2007. Chemical composition of Earth's primitive mantle and its variance : 1. Method and results. J. Geophys. Res. (Solid Earth) 112, BO3211.

Mareschal, J., 1985. Inversion of potential field data in Fourier transform domain. Geophys. 50, 685–691.

Mareschal, J. C., Jaupart, C., 2004a. Variations of surface heat flow and lithospheric thermal structure beneath the North American craton. Earth Planet. Sci. Lett. 223, 65–77.

Mareschal, J. C., Jaupart, C., 2006. Archean thermal regime and stabilization of the cratons. In : Benn, K., Condie, K., Mareschal, J. C. (Eds.), Archean Geodynamic Processes. AGU, Washington (DC), pp. 61–73.

Mareschal, J.-C., Jaupart, C., 2013. Radiogenic heat production, thermal regime and evolution of continental crust. Tectonophysics 609, 524–534.

Mareschal, J. C., Jaupart, C., Gariépy, C., Cheng, L. Z., Guillou-Frottier, L., Bienfait, G., Lapointe, R., 2000. Heat flow and deep thermal structure near the southeastern edge of the Canadian Shield. Can. J. Earth Sci. 37, 399–414.

Mareschal, J.-C., Jaupart, C., Phaneuf, C., Perry, C., Mar. 2012. Geoneutrinos and the energy budget of the Earth. Journal of Geodynamics 54, 43–54.

Mareschal, J. C., Jaupart, C., Rolandone, F., Gariépy, C., Fowler, C. M. R., Bienfait, G., Carbonne, C., Lapointe, R., 2005. Heat flow, thermal regime, and elastic thickness of the lithosphere in the Trans-Hudson Orogen. Can. J. Earth Sci. 42, 517–532.

Mareschal, J. C., Poirier, A., Rolandone, F., Bienfait, G., Gariépy, C., Lapointe, R., Jaupart, C., 2000a. Low mantle heat flow at the edge of the North American continent, Voisey Bay, Labrador. Geophys. Res. Lett. 27, 823–826.

McDonough, W. F., Sun, S. S., 1995. The composition of the Earth. Chem. Geol. 120, 223–253.

McKenzie, D., Jackson, J., Priestley, K., 2005. Thermal structure of oceanic and continental lithosphere. Earth Planet. Sci. Lett. 233, 337–349.

McKenzie, D., Priestley, K., 2016. Speculations on the formation of cratons and cratonic basins. Earth and Planetary Science Letters 435, 94–104.

McKenzie, D. P., Dec. 1967. Some remarks on heat flow and gravity anomalies. J. Geophys. Res. (Solid Earth) 72, 6261–6273.

McLaren, S., Sandiford, M., Hand, M., Neumann, N., Wyborn, L., Bastrakova, I., 2003. The hot southern continent : heat flow and heat production in Australian Proterozoic terranes. In : Evolution and Dynamics of the Australian plate. Vol. 22. Geological society of Australia Special Publications, Ch. 12, pp. 151–161.

McLaren, S., Sandiford, M., Powell, R., Neumann, N., Woodhead, J., 2006. Palaeozoic intraplate crustal anatexis in the Mount Painter Province, South Australia : timing, thermal budgets and the role of crustal heat production. Journal of Petrology 47 (12), 2281–2302.

McLennan, S. M., Taylor, S. R., 1996. Heat flow and the chemical composition of continental crust. The Journal of Geology 104, 377–396.

Meldrum, A., Abdel-Rahman, A. F. M., Martin, R., Wodicka, N., 1997. The nature, age and petrogenesis of the Cartier Batholith, northern flank of the Sudbury Structure, Ontario, Canada Precam. Res. 82, 165–285.

Menke, W., 2012. Geophysical Data Analysis : Discrete Inverse Theory, Third Edition : MATLAB Edition (International Geophysics Series), 3rd Edition. Academic Press.

Merriman, J. D., Li, A. G. W., Hofmeister, A. M., Nabelek, P. I., Benn, K., 2013. Thermal transport properties of major Archean rock types to high temperature and implications for cratonic geotherms Precambrian Research 233, 358–372.

Mezger, K., Bohlen, S., Hanson, G. N., 1990. Metamorphic history of the Archean Pikwitonei granulite domain and the Cross Lake subprovince, Superior Province, Manitoba, Canada. J. Petrol. 32, 483–517.

Miao, S. Q., Li, H. P., Chen, G., 2014. Temperature dependence of thermal diffusivity, specific heat capacity and thermal conductivity for several types of rocks. J. Therm. Anal. Calorim. 115, 1057–1063.

Michaut, C., Jaupart, C., 2007. Secular cooling and thermal structure of continental lithosphere. Earth and Planetary Science Letters 257, 83–96.

Michaut, C., Jaupart, C., Bell, D. R., Apr. 2007. Transient geotherms in Archean continental lithosphere : New constraints on thickness and heat production of the subcontinental lithospheric mantle. J. Geophys. Res. (Solid Earth) 112, BO4408.

Michaut, C., Jaupart, C., Mareschal, J. C., 2009. Thermal evolution of cratonic roots. Lithos 109, 47–60.

Mooney, W. D., Laske, G., Guy Masters, T., Jan. 1998. CRUST 5.1 : A global crustal model at $5^{o} \times 5^{o}$. J. Geophys. Res. (Solid Earth) 103, 727–748.

Morgan, P., 1985. Crustal radiogenic heat production and the selective survival of ancient continental crust. J. Geophys. Res. (Solid Earth) 90, C561–C570.

Morse, P. M., Feshbach, H., 1953. Methods of Theoretical Physics. McGraw-Hill, New-York.

Müller, R. D., Sdrolias, M., Gaina, C., Roest, W. R., 2008. Age, spreading rates, and spreading asymmetry of the world's ocean crust. Geochem. Geophys. Geosyst. 9, QO4006.

Musacchio, G., White, D. J., Asudeh, I., Thomson, C. J., 2004. Lithospheric structure and composition of the Archean western Superior Province from seismic refraction/wide-angle reflection and gravity modeling. Journal of Geophysical Research (Solid Earth) 109, B03304.

Neumann, N., Sandiford, M., Foden, J., 2000. Regional geochemistry and continental heat flow : implications for the origin of the South Australian heat flow anomaly. Earth Planet. Sci. Lett. 183, 107–120.

Nicolaysen, L. O., Hart, R. J., Gale, N. H., 1981. The Vredefort radioelement profile extended to supracrustal strata at Carletonville, with implications for continental heat flow. J. Geophys. Res. (Solid Earth) 86, 10653–10662.

Nielsen, S. B., 1987. Steady state heat flow in a random medium and the linear heat flow-heat production relationship. Geophys. Res. Lett. 14, 318–322.

Nyblade, A. A., Pollack, H. N., 1993. A global analysis of heat flow from Precambrian terrains - Implications for the thermal structure of Archean and Proterozoic lithosphere. J. Geophys. Res. (Solid Earth) 98, 12207–12218.

O'Nions, R. K., Evensen, N. M., Hamilton, P. J., Oct. 1979. Geochemical modeling of mantle differentiation and crustal growth. J. Geophys. Res. (Solid Earth) 84, 6091–6101.

Oxburgh, E. R., Turcotte, D. L., Apr. 1968. Mid-ocean ridges and geotherm distribution during mantle convection. J. Geophys. Res. (Solid Earth) 73, 2643–2661.

Palme, H., O'Neill, H. S. C., 2003. Cosmochemical estimates of mantle composition : Mantle and Core. In : Holland, H., Turekian, K. K. (Eds.), Treatise on Geochemistry. Vol. 2. Elsevier, New York, pp. 1–38.

Park, R. G., Tarney, J., Connelly, J. N., 2001. The Loch Maree Group : Palaeoproterozoic subduction accretion complex in the Lewisian of NW Scotland Precambrian Research 105, 205–226.

Percival, J. A., West, G. F., 1994. The Kapuskasing uplift : a geological and geophysical synthesis. Canadian Journal of Earth Sciences 31, 1256–1286.

Perry, H., Rosieanu, C., Mareschal, J. C., Jaupart, C., 2010. Thermal regime of the lithosphere in Canada. Can. J. Earth Sci. 47, 389–408.

Perry, H. K. C., Eaton, D. W. S., Forte, A. M., 2002. LITH5.0 : A revised crustal model for Canada based on Lithoprobe results. Geophys. J. Int. 150, 285–294.

Perry, H. K. C., Jaupart, C., Mareschal, J. C., Bienfait, G., 2006. Crustal heat production in the Superior Province, Canadian Shield, and in North America inferred from heat flow data. J. Geophys. Res. (Solid Earth) 111, B04401.

Perry, H. K. C., Jaupart, C., Mareschal, J.-C., Shapiro, N. M., 2006. Upper mantle velocity-temperature conversion and composition determined from seismic refraction and heat flow. Journal of Geophysical Research (Solid Earth) 111, B07301.

Perry, H. K. C., Mareschal, J., Jaupart, C., 2009. Enhanced crustal geo-neutrino production near the Sudbury Neutrino Observatory, Ontario, Canada. Earth Planet. Sci. Lett. 288, 301–308.

Phaneuf, C., Mareschal, J., 2014. Estimating concentrations of heat producing elements in the crust near the Sudbury Neutrino Observatory, Ontario, Canada. Tectonophys. 622, 135–144.

Pinet, C., Jaupart, C., 1987. The vertical distribution of radiogenic heat production in the Precambrian crust of Norway and Sweden : Geothermal implications. Geophys. Res. Lett. 14, 260–263.

Pinet, C., Jaupart, C., Mareschal, J.-C., Gariepy, C., Bienfait, G., Lapointe, R., 1991. Heat flow and structure of the lithosphere in the eastern Canadian shield. J. Geophys. Res. (Solid Earth) 96, 19941–19963.

Pollack, H. N., Chapman, D. S., 1977a. On the regional variation of heat flow, geotherms and thickness of the lithosphere. Tectonophys. 38, 279–296.

Pollack, H. N., Hurter, S. J., Johnston, J. R., 1993. Heat flow from the Earth's interior : analysis of the global data set. Rev. Geophys. 31, 267–280.

Pozzo, M., Davies, C., Gubbins, D., Alfé, D., 2012. Thermal and electrical conductivity of iron at Earth's core conditions. Nature 485, 355–358.

Pujol, M., Marty, B., Burgess, R., Aug. 2011. Chondritic-like xenon trapped in Archean rocks : A possible signature of the ancient atmosphere. Earth Planet. Sci. Lett. 308, 298–306.

Putirka, K. D., May 2005. Mantle potential temperatures at Hawaii, Iceland, and the mid-ocean ridge system, as inferred from olivine phenocrysts : Evidence for thermally driven mantle plumes. Geochemistry, Geophysics, Geosystems 6, 5 Q05L08.

Ranalli, G., 1995. Rheology of the Earth, 2nd Edition. Chapman Hall, London.

Rogers, J. J. W., Adams, J. A. S., Gatlin, B., 1965. Distribution of thorium, uranium and potassium in three cores from the Conway granite, New Hampshire. Amer. J. Sci. 263, 817–822.

Rolandone, F., Jaupart, C., Mareschal, J. C., Gariépy, C., Bienfait, G., Carbonne, C., Lapointe, R., 2002. Surface heat flow, crustal temperatures and mantle heat flow in the Proterozoic Trans-Hudson Orogen, Canadian Shield. J. Geophys. Res. (Solid Earth) 107, 2314.

Rollinson, H., 2012. Geochemical constraints on the composition of Archean lower continental crust : Partial melting in the Lewisian granulites. Earth Planet. Sci. Lett. 351-352, 1–12.

Roy, R. F., Blackwell, D. D., Birch, F., 1968. Heat generation of plutonic rocks and continental heat flow provinces. Earth and Planetary Science Letters 5, 1–12.

Roy, S., Rao, R. U. M., 2000. Heat flow in the Indian shield. J. Geophys. Res. (Solid Earth) 105, 25587–25604.

Roy, S., Rao, R. U. M., 2003. Towards a crustal thermal model for the Archean Dharwar craton, southern India. Physics and Chemistry of the Earth 28, 361–373.

Rudnick, R., Taylor, S., 1987. The composition and petrogenesis of the lower crust : a xenolith study. Journal of Geophysical Research : Solid Earth 92 (B13), 13981–14005.

Rudnick, R. L., Fountain, D. M., 1995. Nature and composition of the continental crust : A lower crustal perspective. Rev. Geophys. 33, 267–310.

Rudnick, R. L., Gao, S., 2003. Composition of the continental crust. In : Rudnick, R. L. (Ed.), Treatise on Geochemistry, The Crust. Vol. 3. Permagon, New York, pp. 1–64.

Rudnick, R. L., Gao, S., 2014. Composition of the Continental Crust. Treatise on Geochemistry (2nd edition), Volume 4. Editor : Roberta L. Rudnick, 1–51.

Rudnick, R. L., Nyblade, A. A., 1999. The thickness of Archean lithosphere : constraints from xenolith thermobarometry and surface heat flow. In : Fei, Y., Bertka, C. M., Mysen, B. O. (Eds.), Mantle Petrology ; Field Observations and High Pressure Experimentation : A Tribute to Francis R. (Joe) Boyd. Geochemical Society, Kansas-City (MO), pp. 3–11.

Russell, J. K., Dipple, G. M., Kopylova, M. G., 2001. Heat production and heat flow in the mantle lithosphere, Slave craton, Canada. Phys. Earth Planet. Inter. 123, 27–44.

Saltus, R. W., Lachenbruch, A. H., 1991. Thermal evolution of the Sierra Nevada : Tectonic implications of new heat flow data. Tectonics 10, 325–344.

Sand, K. K., Waight, T. E., Pearson, D. G., Nielsen, T. F., Makovicky, E., Hutchison, M. T., 2009. The lithospheric mantle below southern West Greenland : A geothermobarometric approach to diamond potential and mantle stratigraphy. Lithos 112, 1155–1166.

Sandiford, M., McLaren, S., 2002. Tectonic feedback and the ordering of heat producing elements within the continental lithosphere. Earth Planet. Sci. Lett. 204, 133–150.

Sandiford, M., McLaren, S., Neuman, N., 2002. Long term thermal consequences of the redistribution of heat producing elements associated with large-scale granitic complexes. J. metamorphic Geol. 20, 87–98.

Sawka, W. N., Chappell, B. W., 1988. Fractionation of uranium, thorium and trace elements in a vertically zoned granidiorite : implications for heat production distributions in the Sierra Nevada batholith, California, U.S.A. Geochim. Cosmochim. Acta 52, 1131–1143.

Schneider, R. V., Roy, R. F., Smith, A. R., 1987. Investigations and interpretations of the vertical distribution of U, TH, and K : South Africa and Canada. Geophys. Res. Lett. 14, 264–267.

Sclater, J. G., Francheteau, J., Sep. 1970. The Implications of Terrestrial Heat Flow Observations on Current Tectonic and Geochemical Models of the Crust and Upper Mantle of the Earth. Geophys. J. R. Astr. Soc. 20, 509–542.

Sclater, J. G., Jaupart, C., Galson, D., 1980. The heat flow through oceanic and continental crust and the heat loss from the earth. Rev. Geophys. 18, 269–311.

Shaw, D., Cramer, J., Higgins, M., Truscott, M., 1986. Composition of the Canadian Precambrian shield and the continental crust of the earth. In : et al., J. D. (Ed.), Nature of the Lower Continental Crust. Geol. Soc. London., pp. 257–282.

Slagstad, T., 2008. Radiogenic heat production of Archean to Permian geological provinces in Norway. Norwegian J. Geology 88, 149–166.

Slagstad, T., Balling, N., Elvebakk, H., Midttømme, K., Olesen, O., Olsen, L., Pascal, C., 2009. Heat-flow measurements in Late Palaeoproterozoic to Permian geological provinces in south and central Norway and a new heat-flow map of Fennoscandia and the Norwegian-Greenland Sea. Tectonophysics 473, 341–361.

Solomatov, V. S., Stevenson, D. J., 1993. Nonfractional Crystallization of a Terrestrial Magma Ocean. J. Geophys. Res. (Solid Earth) 98, 5391–5406.

Stacey, F. D., Davis, P. M., 2008. Physics of the Earth, 4th Edition. Cambridge University Press.

Stein, C. A., Stein, S., 1994. Constraints on hydrothermal heat flux through the oceanic lithosphere from global heat flow. J. Geophys. Res. 99, 3081–3095.

Strutt, R. J., 1906. On the distribution of radium in the earth's crust and on internal heat. Proc. Roy. Soc. Ser. A 77, 472–485.

Su, Y. J., 2000. Mid-ocean ridge basalt trace element systematics : Constraints from database management, icpms analysis, global data compilation and petrologic modeling. Unpub. Ph.D. thesis, Columbia University, New York 1, 569 pp.

Swanberg, C., Chessman, M., Simmons, G., Smithson, S., Gronlie, G., Heier, K., 1974. Heat-flow – heat-generation studies in Norway. Tectonophys. 23, 31–48.

Tammemagi, S. R., Smith, N., 1975. A radiogeologic study of the granites of SW England. J. geol. Soc. Lond. 131, 415–427.

Tarantola, A., 1987. Inverse Problem Theory. Elsevier, Amsterdam.

Taylor, S. R., McLennan, S. M., 1995. The continental crust : Its composition and evolution. Blackwell, 6582885.

Tenzer, R., Hamayun, K., Vajda, P., May 2009. Global maps of the CRUST 2.0 crustal components stripped gravity disturbances. Journal of Geophysical Research (Solid Earth) 114, 5408.

Thompson, P. H., Judge, A. S., Lewis, T. J., 1995. Thermal parameters in rock units of the Winter Lake-Lac de Gras area, central Slave Province, Northwest Territories–Implications for diamond genesis. Curr. Res. 1995-E, 125–135.

Thomson, W., 1864. On the secular cooling of the earth. Trans. Roy. Soc. Edinburgh 23, 295–311.

Šrámek, O., McDonough, W. F., Kite, E. S., Lekić, V., Dye, S. T., Zhong, S., Jan. 2013. Geophysical and geochemical constraints on geoneutrino fluxes from Earth's mantle. Earth Planet. Sci. Lett. 361, 356–366.

Vasseur, G., Singh, R. N., 1986. Effects of random horizontal variations in radiogenic heat source distribution on its relationship with heat flow. J. Geophys. Res. (Solid Earth) 91, 10397–10404.

Wasson, J. T., Kallemeyn, G. W., Jul. 1988. Compositions of chondrites. Royal Society of London Philosophical Transactions Series A 325, 535–544.

Weaver, B. L., Tarney, J., 1984. Empirical approach to estimating the composition of the continental crust Nature 310, 575–577.

Webb, P. C., Lee, M. K., Brown, G. C., 1987. Heat flow - heat production relationships in the UK and the vertical distribution of heat production in granite batholiths. Geophys. Res. Lett. 14, 279–282.

Wedepohl, K. H., 1995. The composition of the continental crust. Geochim Cosmochim. Acta 59, 1217–1239.

Williams, D. L., von Herzen, R. P., 1974. Heat Loss from the Earth : New Estimate. Geology 2, 327–330.

Workman, R., Hart, S., 2005. Major and trace element composition of the depleted MORB mantle (DMM). Earth Planet. Sci. Lett. 231, 53–72.

Wurm, M., Beacom, J. F., Bezrukov, L. B., Bick, D., Blümer, J., Choubey, S., Ciemniak, C., D'Angelo, D., Dasgupta, B., Derbin, A., Dighe, A., Domogatsky, G., Dye, S., Eliseev, S., Enqvist, T., Erykalov, A., von Feilitzsch, F., Fiorentini, G., Fischer, T., Göger-Neff, M., Grabmayr, P., Hagner, C., Hellgartner, D., Hissa, J., Horiuchi, S., Janka, H.-T., Jaupart, C., Jochum, J., Kalliokoski, T., Kayunov, A., Kuusiniemi, P., Lachenmaier, T., Lazanu, I., Learned, J. G., Lewke, T., Lombardi, P., Lorenz, S., Lubsandorzhiev, B., Ludhova, L., Loo, K., Maalampi, J., Mantovani, F., Marafini, M., Maricic, J., Marrodán Undagoitia, T., McDonough, W. F., Miramonti, L., Mirizzi, A., Meindl, Q., Mena, O., Möllenberg, R., Muratova, V., Nahnhauer, R., Nesterenko, D., Novikov, Y. N., Nuijten, G., Oberauer, L., Pakvasa, S., Palomares-Ruiz, S., Pallavicini, M., Pascoli, S., Patzak, T., Peltoniemi,

J., Potzel, W., Räihä, T., Raffelt, G. G., Ranucci, G., Razzaque, S., Rummukainen, K., Sarkamo, J., Sinev, V., Spiering, C., Stahl, A., Thorne, F., Tippmann, M., Tonazzo, A., Trzaska, W. H., Vergados, J. D., Wiebusch, C., Winter, J., Jun. 2012. The next-generation liquid-scintillator neutrino observatory LENA. Astroparticle Physics 35, 685–732.

Yang, X., Li, Z., Wang, H., Chen, H., Li, Y., Xiao, W., 2015. Petrology and geochemistry of ultrahigh-temperature granulites from the South Altay origenic belt, northwestern China : Implications for metamorphic evolution and protolith composition. Island Arc 24, 169–187.

Young, G. M., 1999. Some aspects of the geochemistry, provenance and paleoclimatology of the Torridonian of NWScotland. J. Geol. Soc. London 156, 1097–1111.

Zhang, P., Cohen, R., Haule, K., 2015. Effects of electron correlations on transport properties of iron at Earth's core conditions. Nature 517, 605–607.

Appendices

Annexe A

Important equations

In this appendix, we summarieze the equations that we have used for some of the calculations in the Annexes A and B.

A.1 Horizontal variations in Heat Sources

In space domain, we can use the logarithmic potential to find temperature due to a point heat source in two dimensions (*i.e.* a line source in three dimensions). For a unit point heat source A in x', z', the temperature at x, z such that $T(x, z = 0) = 0$ is given by (Morse and Feshbach, 1953, p.1180)

$$T(x,z) = \frac{1}{4\pi\lambda} \log \frac{(x-x')^2 + (z-z')^2}{(x-x')^2 + (z+z')^2} \tag{A.1}$$

Where λ is thermal conductivity. For a uniform source distribution of width 2W and thickness H, the temperature is obtained as

$$T(x,z) = \frac{A}{4\pi\lambda}\int_{-W}^{W} dx' \int_{0}^{H} dz' \log\frac{(x-x')^2+(z-z')^2}{(x-x')^2+(z+z')^2} \tag{A.2}$$

where A is heat production rate. This equation can be integrated numerically.

The temperature at Moho depth ($z = H$) can be obtained in closed form after very tedious calculations :

$$T(x,z) = \frac{A}{4\pi\lambda}\int_{-W}^{W} dx' \int_{0}^{H} dz' \log\frac{(x'-x)^2+(z'-H)^2}{(x-x')^2+(z'+H)^2} \tag{A.3}$$

Changing variables $v = (x'-x)/H$, $u = (z'-H)/H$, and $u' = (z'+H)/H$

$$T(x,z) = \frac{AH^2}{4\pi\lambda}\left[\int_{w-}^{w+} dv \int_{0}^{1} du \log(u^2+v^2) - \int_{w-}^{w+} dv \int_{1}^{2} du' \log(u'^2+v^2)\right] \tag{A.4}$$

with $w+ = (W-x)/H$ and $w- = -(W+x)/H$

$$T(x,H) = \frac{AH^2}{4\pi\lambda} \times \ldots$$
$$\left[4atan(\frac{v}{2}) - 2atan(v) + 2v\log\frac{4+v^2}{1+v^2} - 2v^2 acot(v) + v^2 acot(\frac{v}{2})\right]_{w-}^{w+} \tag{A.5}$$

We shall find the effect of horizontal variations in heat production rate in the Fourier

domain. The Fourier transform of the heat equation is

$$\left(\frac{\partial^2}{\partial z^2} - k^2\right) T(k,z) = \frac{-H(k,z)}{\lambda}$$
$$H(k,z) = S(k) \quad z < b \tag{A.6}$$
$$H(k,z) = 0 \quad z > b$$

where $H(k,z)$ is Fourier transform of heat production rate, k is horizontal wavenumber, and b the thickness ofthe heat producing layer (which could be equal to crustal thickness). The formal solution can be be written as (Mareschal, 1985) :

$$T(k,z) = \frac{S(k)}{2|k|\lambda} \int_0^b dz' \left(\exp(-|k||z-z'|) - \exp(-|k||z+z'|)\right) \tag{A.7}$$

We find

$$T(k,z) = \frac{S(k)}{k^2\lambda}(1 - \exp(-|k|z) - \exp(-|k|b)\sinh(|k|z)) \quad z < b$$
$$T(k,z) = \frac{S(k)}{k^2\lambda}\exp(-|k|z)(\cosh(|k|b) - 1) \quad z > b \tag{A.8}$$

The temperature at Moho ($z = b$) is given by :

$$T(k,b) = \frac{S(k)}{2k^2\lambda}(1 - \exp(-|k|b))^2 \tag{A.9}$$

We can check that for an infinite layer with uniform heat source distribution ($k \to 0$)

$$T(b) = \frac{S(0)}{2k^2\lambda}(kb)^2(1 + ...) = \frac{S(0)b^2}{2\lambda} \tag{A.10}$$

A.2 Transient effects

A.2.1 Heating by heat production 1-D

Heat equation

$$\frac{1}{\kappa}\frac{\partial T}{\partial t} = \frac{\partial^2 T}{\partial z^2} + \frac{H}{\lambda};\quad 0 < z < b$$
$$\frac{1}{\kappa}\frac{\partial T}{\partial t} = \frac{\partial^2 T}{\partial z^2};\quad b < z \tag{A.11}$$

Boundary conditions

$$T = 0 \quad z = 0$$
$$T = 0 \quad z = \infty \tag{A.12}$$
$$T \text{ and } \frac{\partial T}{\partial z} \text{continuous at } z = b$$

Initial conditions

$$T(z, t = 0) = 0 \tag{A.13}$$

Laplace transform

$$\frac{s}{\kappa}T = \frac{\partial^2 T}{\partial z^2} + \frac{H}{s\lambda}\quad 0 < z < b$$
$$\frac{s}{\kappa}T = \frac{\partial^2 T}{\partial z^2}\quad b < z \tag{A.14}$$

General solution

$$T(s,z) = A\exp(\sqrt{\frac{s}{\kappa}}z) + B\exp(-\sqrt{\frac{s}{\kappa}}z) + \frac{\kappa H}{\lambda s^2} \quad 0 < z < b$$
$$T(s,z) = C\exp(-\sqrt{\frac{s}{\kappa}}z) \quad b < z \tag{A.15}$$

Boundary conditions

$$A + B + \frac{\kappa H}{\lambda s^2} = 0$$
$$A\exp(\sqrt{\frac{s}{\kappa}}b) + B\exp(-\sqrt{\frac{s}{\kappa}}b) + \frac{\kappa H}{\lambda s^2} = C\exp(-\sqrt{\frac{s}{\kappa}}b) \tag{A.16}$$
$$A\exp(\sqrt{\frac{s}{\kappa}}b) - B\exp(-\sqrt{\frac{s}{\kappa}}b) = -C\exp(-\sqrt{\frac{s}{\kappa}}b)$$

$$A = \frac{-\kappa H}{2\lambda s^2}\exp(-\sqrt{\frac{s}{\kappa}}b)$$
$$B = \frac{\kappa H}{2\lambda s^2}(\exp(-\sqrt{\frac{s}{\kappa}}b) - 2) \tag{A.17}$$

$$T(s,z) = \frac{\kappa H b^2}{2\lambda s^2} \ldots.$$
$$\ldots. \times \left[2 - 2\exp(-\sqrt{\frac{s}{\kappa}}z) - \exp(\sqrt{\frac{s}{\kappa}}(z-b)) + \exp(-\sqrt{\frac{s}{\kappa}}(z+b))\right] \tag{A.18}$$
$$= \frac{Hb^2}{\lambda}\frac{\kappa}{s^2b^2}\left[1 - \exp(-\sqrt{\frac{s}{\kappa}}z) - \exp(-\sqrt{\frac{s}{\kappa}}b)\sinh(\sqrt{\frac{s}{\kappa}}z)\right]$$

Note similarity with Fourier transform equation C8. Check that transform yields the steady

state solution for $t \to \infty$. OK.

$$\lim_{s\to 0} sT(s,z) = \lim_{t\to\infty} T(s,t) = \frac{Hb^2}{\lambda}\frac{z}{b}(1-\frac{z}{2b})+... \tag{A.19}$$

Inverse Laplace transform (using transform 10 in Carslaw and Jaeger).

$$\begin{aligned}\frac{T(z,t)}{Hb^2/\lambda} &= \frac{t}{\tau} - [(\frac{t}{\tau}+\frac{z^2}{2b^2})\text{erfc}(\frac{z}{2b}\sqrt{\frac{\tau}{t}}) - \frac{z}{b}\sqrt{\frac{t}{\pi\tau}}\exp(\frac{-z^2\tau}{4b^2t})] \\ &+\frac{1}{2}[(\frac{t}{\tau}+\frac{(z+b)^2}{2b^2})\text{erfc}(\frac{z+b}{2b}\sqrt{\frac{\tau}{t}}) - \frac{z+b}{b}\sqrt{\frac{t}{\pi\tau}}\exp(\frac{-(z+b)^2\tau}{4b^2t})] \\ &-\frac{1}{2}[(\frac{t}{\tau}+\frac{(b-z)^2}{2b^2})\text{erfc}(\frac{b-z}{2b}\sqrt{\frac{\tau}{t}}) - \frac{b-z}{b}\sqrt{\frac{t}{\pi\tau}}\exp(\frac{-(b-z)^2\tau}{4b^2t})]\end{aligned} \tag{A.20}$$

Limit for $t \to \infty$ checks.

A.3 Transients 2-D

The Laplace and Fourier transform of the solution is obtained as :

$$T(s,k,z) = \frac{H}{\lambda}\frac{\kappa}{s(s+\kappa k^2)}[1-\exp(-\sqrt{\frac{s}{\kappa}+k^2}z) - \exp(-\sqrt{\frac{s}{\kappa}+k^2}b)\sinh(\sqrt{\frac{s}{\kappa}+k^2}z)] \tag{A.21}$$

$\lim_{s\to 0} = sT(s,k,z)$ yields equation C8. OK